AD-A195 334 DRUM CENTRIFUGE STUDY OF THE TRANSPORT OF LEACHATES FROM LANDFILL SITES(U) CAMBRIDGE UNIV (ENGLAND) DEPT OF ENGINEERING J R GRONOW ET AL. 05 MAY 88 1/2

UNCLASSIFIED CUED/D-SOILS/TR214 DAJA45-86-C-0021 F/G 24/3 NL

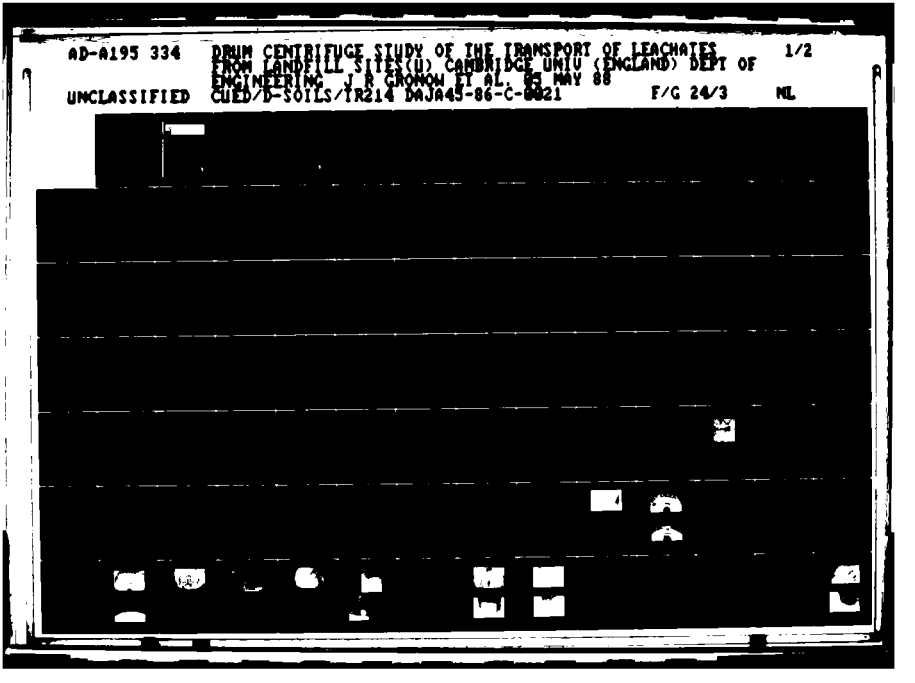

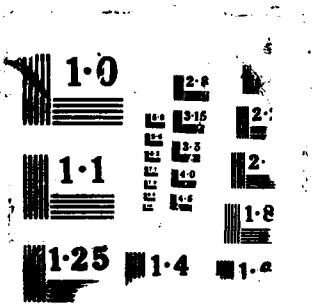
1·0
1·1
1·25
1·4
1·8

2

CAMBRIDGE UNIVERSITY

DRUM CENTRIFUGE STUDY OF THE TRANSPORT OF LEACHATES FROM LANDFILL SITES.

J.R.Gronow, R.I.Edwards and A.N.Schofield

CUED/D-SOILS/TR214 1988

Engineering Department

Unclassified
SECURITY CLASSIFICATION OF THIS PAGE

REPORT DOCUMENTATION PAGE

Form Approved OMB No 0704-0188 Exp Date: Jun 30, 1986

1a REPORT SECURITY CLASSIFICATION: Unclassified	1b. RESTRICTIVE MARKINGS
2a. SECURITY CLASSIFICATION AUTHORITY	3. DISTRIBUTION/AVAILABILITY OF REPORT: Approved for public release; distribution unlimited.
2b. DECLASSIFICATION/DOWNGRADING SCHEDULE	
4. PERFORMING ORGANIZATION REPORT NUMBER(S): CUED/D-SOILS/TR214	5. MONITORING ORGANIZATION REPORT NUMBER(S): R&D 5400-EN-01
6a. NAME OF PERFORMING ORGANIZATION: University of Cambridge; 6b. OFFICE SYMBOL (If applicable): Engineering Dept.	7a. NAME OF MONITORING ORGANIZATION: USARDSG-UK
6c. ADDRESS (City, State, and ZIP Code): Trumpington Street, Cambridge CB2 1PZ, UK	7b. ADDRESS (City, State, and ZIP Code): Box 65, FPO NY 09510-1500
8a. NAME OF FUNDING/SPONSORING ORGANIZATION: U.S. Army Construction Eng. Research Lab; 8b. OFFICE SYMBOL (If applicable): CERL	9. PROCUREMENT INSTRUMENT IDENTIFICATION NUMBER: DAJA45-86-C-0021
8c. ADDRESS (City, State, and ZIP Code): P.O. Box 4005, Champaign, IL 61820	10. SOURCE OF FUNDING NUMBERS: PROGRAM ELEMENT NO. 61102A; PROJECT NO. 1161102BH57; TASK NO. 01; WORK UNIT ACCESSION NO

11. TITLE (Include Security Classification): (U) Migration of Leachates from Landfill Sites

12. PERSONAL AUTHOR(S): Janet R Gronow, Ruth I Edwaeds and Andrew N Schofield

13a. TYPE OF REPORT	13b. TIME COVERED	14. DATE OF REPORT (Year, Month, Day)	15. PAGE COUNT
Final	FROM April 86 TO April 88	1988 May 5th	119

16. SUPPLEMENTARY NOTATION

17. COSATI CODES			18. SUBJECT TERMS (Continue on reverse if necessary and identify by block number)
FIELD	GROUP	SUB-GROUP	
13	02		

19. ABSTRACT (Continue on reverse if necessary and identify by block number)

This report gives the results of a feasibility study of drum centrifuge modelling of transport phenomena. A discussion of the modelling of transport processes in general is included, together with a description of the scaling of accelerated physical models and the verification of scaling assumptions. This is followed by a description of the laboratory and 1g experiments to determine the physical properties of the model medium and pollutant used and to estimate the sorption, diffusion and dispersion coefficients required in the modelling of transport processes.

Details are given of the construction of the two drum centrifuge models used, together with the results of the second centrifuge test. These results were obtained both in flight and from analysis of cores and from ultra-violet photography after the test. These are discussed in the context of the role of geotechnical centrifuge modelling in the verification of numerical models of porous media transport.

20 DISTRIBUTION/AVAILABILITY OF ABSTRACT	21. ABSTRACT SECURITY CLASSIFICATION	
☒ UNCLASSIFIED/UNLIMITED ☐ SAME AS RPT ☒ OTIC USERS	Unclassified	
22a. NAME OF RESPONSIBLE INDIVIDUAL: Jerry C. Comati	22b TELEPHONE (Include Area Code): 01-402-7331	22c. OFFICE SYMBOL: AMXEN-RE

DD FORM 1473, 84 MAR — 83 APR edition may be used until exhausted. All other editions are obsolete

SECURITY CLASSIFICATION OF THIS PAGE: Unclassified

2

DRUM CENTRIFUGE STUDY OF THE TRANSPORT OF LEACHATES FROM LANDFILL SITES.

J.R.Gronow, R.I.Edwards

and A.N.Schofield

CUED/D-SOILS/TR214 1988

Soil Mechanics Group,

Cambridge University Engineering Department,

Trumpington Street, Cambridge, CB2 1PZ. U.K.

A report to the U.S.Army Development and Standardization Group (U.K.)

SUMMARY

This report gives the results of a feasibility study of drum centrifuge modelling of transport phenomena. A discussion of the modelling of transport processes in general is included, together with a description of the scaling of accelerated physical models and the verification of scaling assumptions. This is followed by a description of the laboratory and 1g experiments to determine the physical properties of the model medium and pollutant used and to estimate the sorption, diffusion and dispersion coefficients required in the modelling of transport processes.

Details are given of the construction of the two drum centrifuge models used, together with the results of the second centrifuge test. These results were obtained both in flight and from analysis of cores and from ultra-violet photography after the test. These are discussed in the context of the role of geotechnical centrifuge modelling in the verification of numerical models of porous media transport.

Acknowledgements

This work was funded by the Environmental Branch of the European Research Office of the U.S. Army Research, Development and Standardization Group (U.K). It could not have been completed without the proficient and determined support of the group's electronics engineer, Mr N.H. Baker, to whom we are most grateful. We are also indebted to Mr C.W. Hooper, Mr P.Ford, Mr S.G. Chandler, Mr C.H. Collison, Mr J. Docherty, Mr W. Gwizdala, and many other members of the Soil Mechanics Group and the Electronics Development Laboratory at Cambridge University Engineering Department, who have helped in the development, construction and instrumentation of the models.

ICI Fibres Ltd., Pontypool, supplied the geotextiles for the models free of charge and gave valued advice on the handling and use of the materials. The conductivity meter and fluorimeter were on loan from Cambridge Life Sciences plc, who also provided the spectral analysis of the 8-hydroxy-1,3,6-pyrenetrisulphonic acid trisodium salt.

LIST OF CONTENTS page

LIST OF FIGURES

LIST OF TABLES page

DRUM CENTRIFUGE MODEL STUDY OF THE TRANSPORT OF LEACHATES FROM LANDFILL SITES.

J.R.GRONOW, R.I.EDWARDS and A.N.SCHOFIELD.

Soil Mechanics Group,

Cambridge University Engineering Department,

Trumpington Street, Cambridge, CB2 1PZ. U.K.

INTRODUCTION

Landfilling of waste has been a common practice in Europe and the United States for many years. It has appeared to be a cheap and simple way of disposing of waste, but recently we have become aware of the existence of many badly managed disposal sites.

The clean-up costs of improper waste disposal practices have proved to be astronomical and we now realise that landfilling may not necessarily be quite as cheap and effective as first thought. To achieve a safe repository, several expensive measures must be undertaken. Firstly a full and costly hydrological investigation of the site must be carried out. If proved to be satisfactory this must then be followed by careful site preparation procedures which must be carried out under strict quality control. The actual emplacement of the waste must also be closely managed and monitored. None of these essential measures is cheap, but used together they guarantee against much costlier remedial measures. In contrast to other methods of disposal, carefully controlled landfilling is still the cheapest form of waste disposal and will continue to be used in the forseeable future, despite opposition from

the public, especially in the United States.

Despite our recent awareness of the necessity for hydrological investigations and careful construction and monitoring, we have a legacy of inadequate landfills to deal with. Apart from the undesirable conditions which may prevail in the vicinity of a site and the danger of gas explosion, by far the greatest problem associated with landfilling of waste is the pollution of groundwater. This work is part of a study of the way in which pollutants will migrate away from such sites and how they may cause pollution of the surrounding environment, and also of what measures can be undertaken to remedy such situations.

OBJECTIVES

To establish a new methodology of study of physical models of hazardous waste migration, which will in the future, firstly provide data for the verification of numerical analysis and secondly allow direct physical modelling of specific problems.

TECHNICAL APPROACH

The work was carried out in two parts. Firstly laboratory experiments at 1g which identified the dominant factors involved in transport through porous media and which were of importance to the physical modelling process and also the determination of parameters required in the modelling of transport phenomena. Secondly, two drum centrifuge models were built and tested. The first showed the feasibility of this physical modelling technique. The second was to gather data which could be used to verify numerical models of pollution migration, and to indicate the effect of remedial measures which may prevent

or slow the migration of a pollution plume, once developed, from spreading to a nearby aquifer.

MODELLING OF TRANSPORT PROCESSES

Contaminant transport in porous media is often described by a form of an equation referred to as the advection-dispersion equation (Anderson, 1984). The equation is derived from a combination of mass balance with an expression for the gradient of mass flux. The advection-dispersion equation in its most general one dimensional form is written

$$\frac{\partial}{\partial x}\left[\phi D_x^* \frac{\partial C}{\partial x}\right] - \frac{\partial}{\partial x}(V_x \phi C) - C'W + \phi \sum_{k=1}^{s} R_k = \phi \frac{\partial C}{\partial t} \qquad [1]$$

where and ϕ is the effective porosity of the medium. This factor may not actually be the total porosity of the sample, i.e. the total void space per volume of sediment, but may be the ratio of the volume of interconnected water to the total volume of the sediment. This may include only interconnected water space and not isolated fluid filled pores. C' is the concentration of a solute in a source or sink fluid (mass per unit volume of fluid [ML^{-3}]). C is the concentration of a solute at a given point (mass per unit volume of pore fluid [ML^{-3}]). W is the volume flow rate of the source or sink fluid [T^{-1}]. The chemical reaction term, R_k is the rate of production of solute in reaction k of s different reactions [$ML^{-3}T^{-1}$]. D^* is the coefficient of hydrodynamic dispersion [L^2T^{-1}] This is given by:

$$D^* = D_d^* + D_m$$

where D_d^* is the coefficient of molecular diffusion in the porous medium. D_m

is the coefficient of mechanical dispersion which is a function of the mean interstitial velocity. Hydrodynamic dispersion is a non-steady irreversible process wich can be regarded as the development of a transition or mixing zone in the migrating front of a water miscible pollutant which increases with the distance travelled by the front. Much of the modelling of transport in porous media is concerned with the definition of this zone.

Hydrodynamic dispersion denotes spreading on the macroscopic scale and has two components, firstly molecular diffusion which is migration on the microscopic scale of a solute species in the direction of and in response to a gradient in chemical potential of that species. This is independent of the velocity but depends on time and so will be most significant at low fluid flow velocities. Except for systems in which groundwater velocities are very low, the coefficient of diffusion will generally will be one or more orders of magnitude less than the mechanical dispersion coefficient.

The coefficient of diffusion in a porous medium, D_d^* (often called the effective diffusion coefficient) is generally taken to be the product of the free diffusion coefficient of the ion in water (D_d) and a tortuosity factor. This factor has a value of less than one and is required to correct for the obstructing effect of the porous medium. Effective diffusion coefficients are generally around 10^{-6} cm^2/s.

The second component of hydrodynamic dispersion is mechanical dispersion which is the spreading of the mixing zone due to velocity variations in both magnitude and direction within the pores on the microscopic level. Mechanical dispersion describes flux caused by deviations of microscopic fluid velocity from its macroscopic average. So mechanical dispersion is a process of mixing which occurs because of variations in fluid velocity both within pores due to

laminar flow and between pores due to differences in pore size and possible path lengths within the porous system. The coefficient of mechanical dispersion can be shown to be given by (Bear and Verruijt, 1987):-

$$D_m = a \bar{V} f(Pe,\delta)$$

where Pe is the Peclet number of molecular diffusion given by $L\bar{V}/D_d$, where L is a length characterizing the microscopic structure of the porous medium (the pore length, often taken as the mean particle diameter) δ is the ratio of the length characterizing an individual channel of the porous medium to its hydraulic radius, $\bar{V}$ is the average linear flow velocity. $f(Pe,\delta)$ is a function which introduces the effect of transport by molecular diffusion between adjacent streamlines at a microscopic level, a is a parameter known as the dispersivity [L], which is commonly and somewhat vaguely referred to as a characteristic mixing length. Dispersivity represents a length scale characteristic of heterogeneity at the microscopic level, typically 10^{-3} m.

It has been shown (Bear and Bachmat, 1967) that if B is the conductance of an elementary medium channel, BT^* is an oriented conductance of a channel, $\bar{T}^*$ is the tortuosity of of the medium, and ϕ is the porosity of the medium, then the permeability of the medium is given by $\phi\bar{B}\bar{T}^*$ and is therefore related to the average, $\bar{B}\bar{T}^*$ of BT^*, while the dispersivity is related to the variance of BT^*.

In addition to hydrodynamic dispersion other phenomena may contribute to the distribution of concentration of the pollutant during transport through a porous medium. The pollutant may react with the surface of the porous medium to produce sorption, precipitation, redox reactions, dissolution of the solid phase and simple or complex ion exchange reactions. Radioactive decay and

reactions within the liquid phase itself will also contribute to changes in solute concentration. Such changes may affect the density and viscosity of the fluid phase and hence change the velocity distribution within the medium. It must be noted that we have not taken account of any such changes in density or viscosity in the current study.

Difficulties in quantifying dispersion are related to the fact that field studies of flow through porous media are conducted at a macro rather than microscopic level. For example, Darcy's Law [2], the fundamental equation for describing flow through porous media is a macroscopic equation.

$$\bar{V} = \frac{K\ I}{\phi} \qquad [2]$$

where $\bar{V}$ is the average linear velocity of the groundwater, K is the hydraulic conductivity of the medium [L T^{-1}] and I is the hydraulic gradient. K,I and ϕ are measured in some representative elementary volume (REV) and their values are assumed to represent an average value of K,I and ϕ within the elementary volume. So at the basis of dispersion theory, is a measurement problem. It is argued that it is a reasonable approximation to use an average linear velocity $\bar{V}$, as given by Darcy's Law [2] because it is not possible to measure the velocity field any more accurately.

The key assumption in deriving a term to evaluate dispersion is that dispersion can be represented by an expression analogous to Fick's second law of diffusion, i.e. The mass transport due to dispersion in direction x,

$$J_{Dx} = \frac{\partial}{\partial x}\left[\phi\ D_x^*\ \frac{\partial C}{\partial x}\right]dA \qquad [3]$$

Now the mass transport due to advection, $J_{Ax} = \bar{V}_x \phi C dA$, where advection refers to transport of the pollutant at the same rate as the average linear velocity of the groundwater and A is the cross sectional area.

The total mass transport in direction x (mass per unit cross sectional area of total sediment per unit time) $J_x = J_{Dx} + J_{Ax}$, then

$$\frac{\partial(\phi C)}{\partial t} = - \frac{\partial Jx}{\partial x} + \phi \sum_{k=1}^{s} R_k - C'W \qquad [4]$$

The advection-dispersion equation shows transport to be a Fickian type process which applies to laboratory-scale experiments using homogeneous porous materials. The heterogeneity of such a medium on the microscopic scale cannot be measured and so the material is modelled as a homogeneous medium, the parameters of which are spatially averaged over some representative elementary volume (REV) to provide values on the macroscopic scale. At this scale, transport occurs by advection at the average linear pore velocity and by hydrodynamic dispersion. It has been shown that much larger values of dispersivity are required when modelling field situations, and so the advection-dispersion equation as it stands is not necessarily applicable to the field situation (Abriola, 1987). It has been found that the value of dispersivity required to obtain acceptable fit increases over the distance travelled by the pollutant (Matheron and de Marsily, 1980) and so the phenomenon can not always be described by a Fickian type relationship.

Studies have shown that for long times or large transport distances the dispersion component of the advection dispersion equation can be obtained by a Fickian type expression and that this will accurately represent transport in a

porous medium, provided that dispersivity can be quantified in a meaningful way. At present the most successful attempts to do this have been to represent the velocity field in detail by defining hydraulic conductivity in a stochastic manner and so to simulate the effects of macroscopic dispersion directly (Smith and Schwartz, 1980, 1981a, 1981b).

THE SCALING OF ACCELERATED PHYSICAL MODELS OF TRANSPORT PHENOMENA

The soil mechanics group of the Engineering Department at Cambridge has used centrifuge modelling for several years for the investigation of geotechnical problems because many important soil parameters are highly stress dependent. The stress distribution in a 1/N scale model which experiences a relative centrifugal field of Ng will represent the stress distribution in the prototype very closely and is therefore much more suitable for geotechnical investigations than is a scale model at 1g.

It can be shown that the seepage velocity within a 1/N scale model flying at N gravities will be increased by a factor N with respect to the prototype and that the time for seepage between any two points in the model will be N^2 times less than between similar points in the protoype (see Appendix I). This gives us the other important advantage of accelerated modelling, that we are able to observe up to 30 years prototype migration in as many hours on a centrifuge, flying at 100g and we shall be able to observe 5,000 years migration in a week of continuous running on the drum centrifuge at 500g.

The scaling laws for centrifuge modelling are derived by either dimensional or inspectional analysis and they are usually verified by the modelling of models, where models of different scale are built and flown in the relevant relative centrifugal field and, if all is well, then similarity

between models is observed.

The study of processes within a prototype situation by means of modelling requires mathematical similarity of equations describing the processes within the prototype and model. The analysis of dispersion phenomena was carried out by Bachmat (1967) using modified inspectional analysis. He gave nineteen scale factors which define the problem and thirteen relationships between the factors. These relationships define the non dimensional criteria for the scaling of dispersion phenomena in general.
These criteria are:

Geometric similarity of the model and prototype. That is the ratios between all corresponding lengths in the protoype and model must be the same.

Kinematic similarity of solution motion requires that the flownets in prototype and model are geometrically similar.
The ratio $(\bar{V}t/L)$ must remain invariant, where $\bar{V}$ is the interstitial flow velocity, t is the time and L is any linear quantity.

Dynamic similarity of fluid motion
The criterion for this is that the Reynolds number remains invariant. That is that the ratio between the inertial forces and viscous forces in a fluid remains invariant. The Reynolds number, Re is given by

$$\frac{\bar{V}\rho L}{\eta}$$

where ρ is the density of the fluid, η is the viscosity of the fluid and L is a characteristic length. In this case, the Reynolds number can be expressed

as:

$$Re = \frac{\bar{V}}{\phi_T^2}\left[\frac{\kappa}{a}\right]\frac{\rho}{\eta}$$

where the characteristic length is replaced by a combined parameter consisting of a component of the permeability of the medium (κ) and the dispersivity (a). The factor $\phi_T\eta/\rho$ represents a macroscopic coefficient of viscous diffusivity of the solution in an isotropic porous medium.

Physicochemical similarity of the solutions

This condition is that the ratio of $(\upsilon/\upsilon_o)_r$ and $(C/C_o)_r$ remain invariant, i.e. the ratio of viscosities and also of concentrations between the prototype and model remain invariant.

Similarity of dispersion mechanisms

This criterion requires that the Peclet number remains invariant in prototype and model. The Peclet number represents the ratio of the transport by mechanical dispersion to that by molecular diffusion and is given by,

$$Pe = \frac{\bar{V}L}{D_d}$$

In this case the characteristic length of convective dispersion can be represented by the dispersivity and the macroscopic molecular diffusivity is $\phi_T D_d$, to give

$$Pe = \frac{q\ a}{\phi_T D_d}$$

where q is the Darcy velocity.

It can be shown that in the case of accelerated physical modelling just two of these criteria do not always hold and that two dimensionless groups,

the Reynolds number and the Peclet number do not always remain invariant since both of these numbers scale with fluid velocity. However in most problems encountered in groundwater flow, the inertial forces are negligible in comparison with viscous resistance. When this is the case the condition that the Reynolds number remains invariant can be ignored and flow can be described in a straightforward manner by Darcy's Law.

Similarly with the Peclet number, it has been shown that there is only a linear relationshop between D_m and $\bar{V}$ when the groundwater velocity is sufficiently low that the Peclet number is less than 1. Much experimental and laboratory work has shown the relationship given in figure 1 between dispersion and velocity. In region I, where molecular diffusion dominates, the Peclet number is independent of velocity. So in this region, under the conditions of low Pe and low Re, there is perfect similarity between prototype and model and transport can be shown to scale satisfactorily on the centrifuge. At higher Peclet numbers dispersion will be velocity dependent. Even so, a centrifuge model test with average interstitial flow velocities sufficiently large to produce higher Peclet numbers can be regarded as an independent geotechnical event producing data under repeatable laboratory controlled conditions where the processes of advection, dispersion and, in some cases, sorption occur in two and three dimensional situations and can be used to validate numerical analyses, provided the boundary conditions are carefully controlled.

CONCLUSIONS ON MODELLING

It has been recognised that the failure of the classical transport model is rooted in small scale heterogeneities of the medium on the macroscopic level.

However neither the theoretical nor practical problems associated with field scale dispersivities have been resolved. Even in the region where the scaling laws are completely valid, there still exists the problem of simulating field heterogeneities and coping with the problem of scale dependent dispersivities. For this reason, one may conclude that, at present, accelerated physical modelling is of most value in the validation of numerical models, and that like the numerical models themselves, physical models suffer from the uncertainties of translation to the field situation.

THE VERIFICATION OF SCALE EFFECTS

The modelling of models required for the validation of the assumptions made in the investigation of transport phenomena has not been attempted at Cambridge as similar work has recently been conducted at the University of California at Davis by Arulanandan et al. (1988). They concluded that the scaling laws were valid in models where the grain size of the porous medium was sufficiently small that the Peclet number remained below 1.

LABORATORY AND 1G EXPERIMENTS

a) Choice of model pollutant

The characterization of landfill leachate poses an enormous problem. The leachate depends on the geohydrological setting of a site, which will control such factors as the degree of saturation of the surrounding environment and the spatial variation in redox potential within the site, which will in turn affect the pathway and degree of breakdown of the organic component of the leachate and the mobility of heavy metals and other redox sensitive species. The permeability and homogeneity of the geological formations in which the

site is constructed, the geochemistry of those formations and of the groundwater percolating through them and the amount of precipitation and infiltration are totally site specific.

For this reason it did not seem necessary to attempt to model a general leachate (e.g. Campbell et al., 1983) so the work was carried out using two solution components only, a 0.5M NaCl solution or a 100ppm solution of 8-hydroxy-1,3,6-pyrenetrisulphonic acid trisodium salt (pyranine, figure 2) and sometimes a mixture of the two. The salt solution was used as a conservative species (see next section). It was hoped that the migration of pyranine also was not subject to any attenuating processes. As will be shown in the next section all attempts to determine a sorption coefficient for pyranine on E Grade kaolin seemed to indicate that there was none. However it was shown both in diffusion and centrifuge tests that the migration of this tracer was considerably slower than that of the salt solution.

The chloride, where used, indicated the worst possible case for the migration of a small inorganic pollutant species, unaffected by attenuating processes. In all experimental work chloride concentration was determined using a Corning solid state chloride ion-selective electrode in conjuction with a double junction reference electrode containing a 1M KNO_3 bridge solution. Pyranine would be expected to represent the worst case for a small conservative organic molecule. The details of the fluorescence of pyranine and the determination of its concentration in solution are given in Appendix II. Figure 3 shows the characteristic excitation and emission spectra for the molecule.

It had been hoped that we might also use a non-aqueous-phase liquid (NAPL). The work in this area was initiated by the planning of a Part II

(Third year) undergraduate project to investigate small scale accelerated physical modelling of non-aqueous-phase fluid flow using a bench centrifuge. Unfortunately the timing of this project coincided with the second drum centrifuge test, and it was therefore not possible to help the student overcome the novel problems of modelling with NAPLs. He was forced to turn to a continuation of small scale modelling of aqueous-phase-liquids in order to complete a satisfactory piece of work for his degree.

A Part II project of this kind is an ideal starting point for studies of this type and it is recommended that it should be attempted again next year when closer supervision of the project could lead to a successful outcome. This is an important area of porous media transport and one which should model well under accelerated gravity.

It was hoped that we would be able to correct for the higher density of the chloride solutions by the addition of a lower density, water miscible fluid to them. However after an extensive data-base search, we were unable to find a suitable fluid which was both stable and which had a sufficiently high flash point to preclude a fire hazard during long periods of continuously running the centrifuge.

b) Choice of porous medium

Arulanandan et. al. (1988) have shown that simple ionic exchange reactions appear to scale satisfactorily in accelerated models. However in reactions in which the mechanisms or kinetics of the sorption/immobilization process may not be so straightforward, there may be significant problems to overcome in the modelling of the process. For this reason it was decided to use a simple kaolin clay as the porous medium. This clay has the platey morphology shown

in figure 4, the structure shown in figure 5 and the chemical composition given in table 1.

TABLE 1 Chemical composition of E Grade Kaolin

SiO_2	47.3%
Al_2O_3	37.2%
Fe_2O_3	1.01%
TiO_2	0.08%
CaO	0.10%
MgO	0.10%
K_2O	2.43%
Na_2O	0.07%
loss on ignition	11.70%

Kaolin has the relatively low cation exchange capacity of 3-15 mEq/100g (Yariv and Cross 1979), a specific surface area of 7 m^2/g (English China Clay Company, personal communication) and therefore shows relatively little affinity for dissolved species. A relatively coarse grade of kaolin was chosen which had the particle size distribution given in figure 6 and the hydraulic conductivities shown in figures 7 and 8.

The results of batch sorption tests to determine the sorption coefficient for pyranine on E Grade kaolin are given in figures 9, 10 and 11. The details of the experiments are given in Appendix III. The experiments were difficult to perform as significant sorption of pyranine onto the walls of the containers was observed. It was difficult to correct for this in an adequate manner using blank determinations (with no clay in the tubes) as there is then a considerable disparity in surface area available for sorption, and as sorption onto a surface is often a competitive process, blank corrections are not necessarily valid. More useful determinations of the sorption coefficent can sometimes be obtained during diffusion and permeability tests and are given in the section on diffusion coefficients below.

Batch sorption experiment using E Grade kaolin and sodium chloride were conducted in the same way as for pyranine and, as expected, showed there to be little or no sorption onto kaolin. The results of these experiments using 0.1M, 0.25M and 0.5M NaCl over 3, 5 and 11 days are given in table 2 and figure 12a and b.

TABLE 2 BATCH DETERMINATION OF CHLORIDE SORPTION COEFFICIENTS

$[Cl^-]$	K_d (cm^3g^{-1})		
	3 days	5 days	11 days
0.10 M	0.0	0.0	0.0
0.25 M	0.0	0.0	0.06
0.50 M	0.18	0.36	0.06

THE DETERMINATION OF DIFFUSION COEFFICIENTS

The effective diffusion coefficients of the migration of both pyranine and chloride through samples of kaolin were determined at similar effective stress levels as would be experienced on the centrifuge at 100g. The experimental details of this work are given in Appendix IV and the results are given in table 3 and figures 13 and 14a and b.

One diffusion experiment was conducted using a chloride solution of 0.6M. In this experiment there was no net flow of solution across the sample and the values of intrinsic diffusion coefficient and matrix capacity factor were calculated as given in Appendix IV. They confirm that there was no sorption of chloride onto E. Grade kaolin. It is considered that the matrix capacity factor (α) obtained in this case (and many other previous similar results obtained, where α was found to be less than the porosity (ϕ) obtained by drying) is a measure of the through-transport or effective porosity of the system.

In both of the pyranine diffusion experiments, the tracer took so long to migrate through the sample that it was impossible to prevent a small flow of fluid across the sample. Having calculated the advective flux across each sample, it is possible using equation [A.2] to obtain the intrinsic diffusion coefficient for the migration of pyranine through each sample. Then, provided that the measured concentration is much less than the source concentration,

$$C_t = \frac{F^* t C_o}{v} \qquad t > t_B$$

(Bradbury et al., 1986) where v is the volume of solution in the measurement cell and F^* is the volume flow rate through the sample. If t_B is the intercept on the time axis of the extrapolated linear portion of the curve of C_t against t then:

$$F^* t_B = \alpha V_s$$

where V_s is the volume of the sample. The values of the matrix capacity factor, α obtained from the two samples can be seen in table 3, together with the values of the effective diffusion coefficient for transport of pyranine through the sample. Despite disparities in ϕD_s and α between the two samples, there is agreement in the effective diffusion coefficient and confirmation that a small amount of pyranine attenuation occurs.

Using the expression $\alpha = (\phi + \rho_b k_d)$ values of the sorption coefficient, k_d were obtained and are also shown in table 3. It was thought initially that the slow migration of pyranine may have been attributable to the large size of the molecule, ~1.5 nm in comparison with the hydrated ionic diameter of a

chloride ion which is of the order of 0.37 nm. The values of the intrinsic diffusion coefficients obtained are, if anything slightly higher than that for chloride, indicating that this is not the case and that some other attenuation process, probably a small amount of sorption is occurring.

Bradbury et al. (1986) discussed the problems inherent in batch techniques for the determination of sorption coefficients and suggested that the method employed above may produce more realistic values of k_d. One must still ensure that the conditions under which the migration experiment are conducted relate closely to prototype conditions to be sure of accurate sorption data.

TABLE 3 DIFFUSION EXPERIMENT RESULTS

	chloride	**pyranine 1**	**pyranine 2**
sample length	3.54 cm	2.40 cm	3.28 cm
x sectional area	7.87 cm^2	7.87 cm^2	7.87 cm^2
C_o	0.6M	100ppm	100ppm
C_t volume	135 cm^3	165 cm^3	187.4 cm^3
porosity	0.52	0.48	0.51
bulk density	1.78 g cm^{-3}	1.83 g cm^{-3}	1.80 g cm^{-3}
Darcy velocity	0	$1.7x10^{-6}$cm s^{-1}	$7.5x10^{-7}$cm s^{-1}
volume flux	0.01097 cm^3 h^{-1}	0.0656 cm^3 h^{-1}	0.04133 cm^3h^{-1}
k_d	0	0.92 cm^3 g^{-1}	1.79 cm^3g^{-1}
ϕD_s	$1.32x10^{-6}cm^3s^{-1}$	$1.52x10^{-6}cm^3s^{-1}$	$2.56x10^{-6}cm^3s^{-1}$
α	0.42	2.16	3.73
D_A	$3.14x10^{-6}cm^2s^{-1}$	$7.04x10^{-7}cm^2s^{-1}$	$6.86x10^{-7}cm^2s^{-1}$

THE DETERMINATION OF DISPERSION COEFFICIENTS

There are three methods of attempting to estimate this parameter. The first is

to use a column technique as did Pfannkuch (1962). This has been attempted in the laboratory recently (Hensley, 1988) but preliminary results show that although the dependence of dispersion on interstitial velocity was as expected, the absolute values determined were not. It has been suggested that a modification to the column design now underway, might improve the accuracy of the results obtained.

The other two methods of assessing the dispersion coefficient are to fit the results of a diffusion type experiment in which some advection was known to occur to a numerical model, or to fit the observed results from centrifuge tests to a transport model. Both of these two methods have been attempted with varying degrees of success.

In the former case, the diffusion experiment data given in table 3 was used in POLLUTE, a one dimensional computer program designed to simulate pollutant migration through a non homogeneous soil deposit. Using the chloride diffusion data, a dispersion coefficient of $2.9 \times 10^{-6} cm^2 s^{-1}$ was indicated and with the pyranine data a dispersion coefficient of $1.4 \times 10^{-6} cm^2 s^{-1}$ appeared to produce a more realistic data fit. Both sets of results are in reasonable agreement with expected values in the light of the observed diffusion data.

In employing the observed results of the centrifuge test in POLLUTE, the results were less conclusive. However, as the calculated Peclet number remained below 1 for the duration of each centrifuge run, the values of dispersion coefficients obtained using the laboratory diffusion data should provide good approximations to those pertaining to the centrifuge runs. In practice however, it is likely that the non-uniform nature of the kaolin apparent during the centrifuge runs, produced deviations from the expected

values and this has precluded a satisfactory fit of this data up to the present time.

DRUM CENTRIFUGE MODELLING

a) aims

The main aim of this work was to develop the drum centrifuge for the modelling of transport phenomena in porous media and to investigate the feasiblity of the technique for the investigation of the migration of pollution plumes and similar hazardous waste management problems. Secondary to this was the gathering of data from such modelling experiments which could be used to verify numerical models of transport in porous media. Our second drum centrifuge test also showed the effect of the installation of pumping wells in an attempt to slow the migration of a pollution plume to an underlying aquifer.

The work consisted of a feasibilty study carried out in late Summer 1987 (test 1) and a longer second test, consisting of three runs, in early 1988 in which data were obtained which could be used to verify numerical models. In the two tests carried out, the models were essentially of similar design and so only details of the second test will be given here.

b) model construction

The drum centrifuge has a radius and height of one metre and was operated at a relative centrifugal field (RCF) of 100g in both tests. The models were constructed by lining the walls of the drum firstly with a layer of 9mm thick high density polyethylene sheeting, followed by a 6.5mm layer of Filtram (figure 15). This is a laminated filter drain produced by ICI Fibres Ltd.

which consists of a 100% polyethylene 'Netlon' structured core, bonded to and sandwiched between two sheets of permeable Terram 1000, a 67% polypropylene, 33% polyethylene non-woven filter membrane. The Netlon allows flow in both horizontal and vertical directions. The pore size distribution of the Terram is given in figure 16. Because of the open nature of the Netlon structure it was covered by a sheet of 2.5 mm thick Vyon F, a porous material with a maximum pore size of 90μm, made from 100-300μm diameter high density polyethylene spheres welded together. This high permeability layer formed the base of the model and was sealed to the top and the base of the drum with silicon adhesive (figures 17a and b).

In this permeable layer at points X and Y on the drum wall (the sites of the two drainage points in the base of the drum) 8mm OD stainless steel tubes, perforated along their length with 5 mm diameter holes, were laid from the top to the base of the drum (see figure 18a). One acted as a water supply to the permeable layer (Y), the other as a drain (X). The flow of water from the drum was controlled by gate valves at X and Y. The valve at X could be opened or closed and was connected directly to the drain in the permeable layer. The valve at Y was permanently open and was connected to a standpipe, the top of which stood 150 mm above the base of the model (the sides of the drum, see figure 18a). This standpipe controlled the surface water level in the model. It was also connected to a length of 8 mm OD flexible tubing (to which wells would later be connected) via a T piece and tap (see figure 19a). A Druck PDCR 81 miniature pore pressure transducer was attached to each of the stainless steel tubes, 500 mm from the base of the drum (half way up the wall) to monitor the water flow pattern in the permeable layer.

The water supply to the permeable layer was connected to the hydraulic

slip-ring of the centrifuge and was supplied via a flow meter and a 4m header tank. Surface water to the model and pollutant to the landfills was provided by supplying three concentric containers at the centre of the drum from variable speed peristaltic pumps, at known rates. A pore pressure transducer was attached to the surface water supply to monitor the water depth at that point. Water levels in the vicinity of the landfills were monitored using two-electrode resistivity probes situated inside and outside the landfills and by floats which were placed in the field of view of the two cameras mounted at the centre of the drum.

Three miniature pore pressure transducers were mounted on stalks at position B in the drum (see figure 18c and d) at varying heights from the base of the model to monitor the consolidation of the clay (figure 19b). Once the drum was plumbed and instrumented, a bag consisting of a tarpaulin base and Terram 4000 sides was fitted into the drum to line it and to protect the electronic circuitry (figure 20).

Transport of chloride from the landfill sites was monitored using four-electrode resistivity probes (figure 21a) constructed in-house. These were made by setting the four 1mm diameter silver pins in Araldite epoxy resin. The two outer pins of the probe supplied a 100μA a.c. current at a frequency of 49 Hz. The voltage across the centre two pins was amplified and recorded. An array of seven probes was placed at each landfill site to monitor the chloride transport beneath each site. Each array was mounted on a perspex framework (figure 21b) in the formation given in figure 21c.

The model was produced using two tonnes of E Grade kaolin slurry mixed to 100% moisture content with deionised water. It was obtained from a contractor in slurry form and transported in four 400L bulk containers. A Mono pump was

used to transfer the slurry to the drum while the centrifuge was revolving slowly at 70 rpm (~6g). Having transferred half of the clay, the drum was accelerated to 299 rpm (100g) and the clay was consolidated at this RCF for approximately 4 hours.

The model consisted of four landfill sites situated as shown in figures 18c and d. At this stage is was necessary to lay the plumbing for the pumping wells which were to be used in run 3 of the test. Three sets of two wells were installed at 60mm from the base of the model as shown in figure 18c. No well was situated at landfill 4 as this was to be the control site.

The wells were constructed from 20mm lengths of 50mm diameter perforated plastic tubing, fitted with discs of 2.5mm thick Vyon F at either end. The inside of each well was lined with filter paper and filled with 25/52 mesh sand. Each well was connected to the valve at Y via the standpipe. One of the wells at landfill 1, that furthest away from the drain at Y, contained a miniature pore pressure transducer to give an indication of the hydraulic head in this model. The wells and all of the tubing were filled with water, the tap at Y was closed and the remaining slurry added and consolidated for 10 hours.

Landfills 1 and 3 were sited next. The landfills were constructed using tubes, 150mm OD and 100mm long of 2.5mm thick Vyon F. The top 70mm of each was painted to make it impermeable. The unpainted end of each tube was inserted 40mm into the clay layer in the drum at approximately half drum height at the positions shown in figures 18c and d. The 40mm of clay inside the landfill was removed and the pollutant supply tube attached as shown in figure 22a. The landfill was then filled with Fontainbleau sand (figure 22b) to a height of 40mm in the case of landfill 1 and to 60mm in landfill 3. The

sides of landfill 3 were built up as shown in figure 22a. Level probes and floats were fitted as shown in figure 22c. A resistance thermometer was fitted at position A. A miniature pore pressure transducer was attached to the frame beneath landfill 1, 80mm from the base of the model (figure 23).

c) first run

The model simulated the siting of landfills in a relatively impermeable clay stratum in which there was a a small downward hydraulic gradient inducing a slow advective velocity towards an underlying aquifer in which there was a horizontal flow of groundwater.

The centrifuge was spun up to 100g, all water and pollutant supplies started and the centrifuge was run continuously until the pollutant had reached the permeable layer, approximately 34 hours. The pollutant was a 0.5M NaCl solution containing 100ppm pyranine. Pore pressure transducer and resistivity probe output was recorded at approximately hourly intervals. The centrifuge was then stopped and clay moisture contents were taken.

d) Second run

The procedure was repeated for landfills 2 and 4, leaving landfills 1 and 3 in place but no further pollutant was supplied to either of these two sites. This can be regarded as having the same effect as capping the two sites, thus preventing further infiltration to the sites and reducing the volume of leachate produced by them. The second run continued for 39 hours. During this time it was found that it was necessary to supply a great deal of water to the surface of the model and that even under such conditions it was not possible to keep the surface of the model flooded. On stopping the centrifuge

it was found that the surface of the model contained several fissures (figure 24) and that at one site in particular a large channel had formed (figure 25) from about half drum height, terminating at the top of the drum and that at this site water had been conducted to the base of the model, possibly causing a drying out of the surface. Moisture contents were again taken before run 3 was started.

e) third run

This was used to simulate the effects of remedial measures which attempted to slow the migration of the pollutant to the surrounding environment. The valve at X in the porous layer was closed, the tap at Y was opened inducing migration to the wells (figure 26) since they and the surface water standpipe were connected to the only drain in the model Two 1½ inch sand drains were bored through the whole depth of the clay at A and filled with coarse (14/25 mesh) sand, to provide continuity between the top and the base of the model. The drum was spun up to 100g again and the surface water supply and pollutant supply to landfills 2 and 4 restarted. Pore pressure transducer output and resistivity probe readings beneath landfills 2 and 4 were monitored at approximately hourly intervals. Run 3 was continued for 92 hours. After this time the water and pollutant supplies were stopped and the four sites photographed and sectioned. Having removed the landfills themselves, two cores were taken from the remaining 80mm of clay beneath each site (see figure 27) and 1cm sections of each core were weighed into weighed sample containers for moisture content, chloride and pyranine analyses.

f) Calibration of resistivity probes

After the main tests the landfill sites were sectioned and photographed. Each site was excavated sufficiently to accommodate a perspex box (see figures 28a and b) which was to be used for calibration purposes. It had been suggested in preliminary experiments that the probes might be sensitive to overburden stress and to position within the model. For this reason the results of the calibration were analysed statistically to see if there was any significant difference between readings obtained from probes at different levels in the model. It can be seen from figure 21c that in each box the centre five probes were all at the same level within the model, with the first and seventh, 20mm above and below them.

Each box containing the array of 7 probes together with one pore pressure transducer was filled with a 90% slurry of kaolin (figure 28c) made up in (1) deionised water, (2) 0.1M NaCl, 20ppm pyranine, (3) 0.3M NaCl, 60ppm pyranine, (4) 0.5M NaCl, 100ppm pyranine and consolidated at 100g for 5 hours. The surface liquid (figure 28d) was then removed from the boxes and further slurry added and reconsolidated until there was no further change in response from the pore pressure transducers (~12 hours). A set of resistivity probe readings was taken for each concentration at 100g.

OBSERVATIONS

a) first run

Table 4 summarises the details of the test. The plots of relative concentration against time are given in figures 29a-d. Figure 29a, for landfill 1 is a near-perfect example of the S shaped curve that would be expected from the model, the curves from probes 1 and 7, the upper and lower

members of the array, straddling those from the centre of the array. There was a 24% variation in relative concentrations registered at the five centre probes and although some of this was undoubtedly due to instrumentation, a large proportion must have been representative of fluid velocity variations and therefore presumably variations in hydraulic conductivity within the model.

The advective velocity here was calculated to be 1.3×10^{-4}cm/s, which is four times faster than was expected from the hydraulic gradient and the measured permeability. Figure 30 shows the pock marks which appeared in the clay during later stages of consolidation. It is possible that these provide pathways for fluid migration and that they may have been responsible for the higher than expected flow velocity and for some of the variations in permeabilty. Even so the Peclet number for chloride dispersion was calculated to be less than 0.04, indicating that the model would scale satisfactorily to a *prototype*.

The data provided by landfill 3 (figure 29b) is not so clear cut, there being a much greater variation in values of relative concentration between the centre probes. Channels 10 and 11 of the data transfer system were erratic and so affected the values obtained from both landfills 3 and 4. The statistical analysis described in the calibration section below, indicates that the data obtained from landfill 3 was not normally distributed and so there was probably a fault in probe 13 of that landfill. If this was the case, only channels 9 and 12 gave data representative of the central probes at this site. There was a 13% variation in relative concentrations between these two probes. The flow velocity was calculated to be slightly lower than that for landfill 1 at 1.2×10^{-4}cm/s. This landfill had been designed to have a

slightly higher hydraulic gradient than landfill 1 but it was not found practical to fill the landfill to the surface with pollutant without causing a breakout to the surrounding clay and so the hydraulic gradient was likely to have been of very similar value to that at landfill 1.

TABLE 4 DETAILS OF THE SECOND DRUM CENTRIFUGE TEST

Run 1	Landfills 1 and 3 supplied with pollutant. Landfill 3 built up 20mm above the general clay surface level. Advective velocity at landfill 1 of 1.3×10^{-4}cm/s. Advective velocity at landfill 2 of 1.2×10^{-4}cm/s Peclet number for chloride dispersion between 0.03 and 0.04. Duration 34 hours.
Run 2	Landfills 2 and 4 supplied with pollutant. Landfill 4 built up 20mm above clay level. Landfills 1 and 3 'capped'. Variable hydraulic gradient in the model due to channel formation. Average advective velocity estimated to be 1×10^{-4}cm/s at landfill 2 and 0.7×10^{-4}cm/s at landfill 4. Peclet no between 0.02 and 0.03. Duration 39 hours.
Run 3	Landfills 2 and 4 supplied with pollutant. Landfill 4 built up 20mm above the clay layer. Landfills 1 and 3 'capped'. Pumping wells installed in vicinity of landfills 1, 2, and 3. Flow induced as shown in figure 26, velocity undetermined. Peclet number >0.02. Duration 92 hours.

b) Second run

The problem of maintaining surface water on the model during run 2 was mentioned in the section on model construction above. The result of this loss of hydraulic gradient can be seen particularly in figure 29c and also in figure 29d and is most noticeable in the upper probes. There is a considerably greater spread of relative concentrations amongst the centre probes in this run (45%). The variable hydraulic gradient and the cracked and fissured nature of the clay in the model presumably were responsible for greater variations in advective velocity within this model in comparison with run 1, which was in all other aspects similar to this run The hydraulic gradient in the landfills themselves was not lost and so migration to the base through the sample was slowed during this time, presumably in preference for a spreading of the pollutant in a horizontal direction in the model. The average advective velocity at landfill 2 was calculated to be $1x10^{-4}$cm/s.

At landfill 4, as in run 1, channels 10 and 11 were not functioning correctly and in this run probe 9 was not responding, so again only the data from two out of the five centre probes was valid. There was a spread of 18% in the relative concentration values obtained from these two probes. As in run 1, landfill 4 was designed to have a higher hydraulic gradient than landfill 2 and, for the same reasons as in the first run, it was not filled. At no time during the run was pollutant observed at the surface of the landfill and the advective velocity at landfill 2 was calculated to be $0.7x10^{-4}$cm/s. This landfill did not seem to be so affected by the variations in hydraulic gradient across the rest of the model. Presumably this was related to the construction of the landfill. The response to fluctuations in

hydraulic gradient can be seen in figure 29d, probes 8, 12 and 13 but are not as marked as in landfill 2. The increase of 5% in the variation of realative concentraton values of the centre probes over those observed in the similar model of landfill 3 is possibly a result of the fissuring which was observed after the run.

c) Third run

The changes in relative concentration of chloride beneath landfills 2 and 4 are given in figure 31a and b, those beneath landfills 1 and 3 were not monitored during this run. Both of these landfills were supplied with pollutant during the run but landfill 4 had no wells associated with it.

There was a slow but constant loss of concentration at the lowest probe (7) beneath landfill 2 when compared with probe 14, below landfill 4. The upper probe (1) appeared unaffected by the presence of the wells, as did probe 5 of the centre array, which was closest to the well.

Figures 32a-d show the pattern of chloride and pyranine concentration in the clay beneath each landfill with depth, the origin on the x axis being the base of the model. Samples B were core at a greater distance from the wells than were those at D (see figure 27).

Firstly, from figures 32a-d, the slower migration of pyranine in comparison with the chloride is immediately obvious. Secondly the effect of 'capping' the two landfills 1 and 3 (figures 32a and b respectively) is more obvious in the clay closer to the surface; there appears to be no effect whatsoever at the base of the model.

On comparing the two 'capped' landfills 1 and 3 (figures 32a and b respectively) it appears that the effect of the wells in both cases was to

distort the plume towards the well in the vicinity of the well but to have only a small effect on the concentration at clay levels above or below the wells. Because landfill 3 was built up higher than 1, it is assumed that there was a larger residual volume of pollutant at that site to be dispersed and that this accounts for the rather different patterns observed at the two sites.

At landfill 1 (figure 32a) there appeared to be no preferential loss of concentration close to the landfill as seemed to occur at landfill 3 (figure 32b), although figure 33c, an ultra-violet illuminated photograph taken at the 60mm section of landfill 1, suggests that there may have been loss of concentration closer to the wells. Generally in figures 33a-e it is possible to detect the apparent slightly higher concentration of pyranine in the upper quadrants of the landfill suggested by figure 32a, but the effect is not very marked. However the graph actually suggests that the whole plume may have been pulled slightly towards the wells, but this is not at all evident from the photographs. Figure 32b suggests that there was a loss of pollutant in the vicinity of the wells in landfill 3 but the UV photos (figures 34a-d) show no indication of this, although they do show the general tendency for the site to have had a higher pollutant concentration in the lower quadrants.

A comparison of landfill 3 ('capped', figure 32b) and landfill 2 ('uncapped', figure 32c) shows that they followed a rather similar pattern, presumably because of the high residual pollutant volume in landfill 3. The concentration of the pollutant in the upper layers of the clay was obviously far higher in the 'uncapped' site, but both sites responded in a similar way to the presence of the wells as indicated by the suggested distortion of the plume at the relevant heights in the clay. Figure 32b suggests that in

landfill 3 the pollutant was affected in the vicinity of the landfill whereas figure 32c suggests that the whole plume may have distorted. The UV photos of landfill 3 are in agreement with figure 32b in as much as there appears to have been a higher concentration of pollutant in the lower quadrants of the site, but on the other hand they suggest that the plume had been pulled down slightly towards the wells as would be expected.

The UV photos of landfill 2, figure 35a-e suggest a higher concentration in the upper quadrants of the site that at the lower, in agreement with figure 32c. Figure 35b in particular shows the variation in pollutant concentrations at the base of the landfill which was so evident from the variations in relative chloride concentrations detected at the centre probes in figure 29c.

The effect of the presence of the wells was indicated by comparison of landfills 2 and 4 (figures 32c and d respectively and the photos in figures 35 and 36). The pollutant concentration in the upper layers beneath landfill 4 was generally higher than at 2 and the lowering of pollutant concentration beneath landfill 2 was absent in landfill 4. At both sites, the concentration of pollutant at B was greater than that at D, but was much more markedly so at site 2.

Comparison of the surface UV photos of site 2 (figure 35a) with that of site 4 (figure 36a) shows that the lack of hydraulic gradient at 4 caused a far greater spread of the pollutant over the surface of the model than at 2 and that this extended further from the site in the section at 80mm from the base (figures 35b and 36b) in landfill 4 than in landfill 2. Figures 36a-d show that there was generally a uniform pollutant concentration distribution over the whole site in contrast to the other sites, although it must be admitted that no trend in concentration pattern was very marked. This is

probably due to the fact that it was found that the pore pressure transducer in well 1a, gave considerably higer readings at ~30kPa than had been expected, indicating that the hydraulic gradient in the model was not as large as had been hoped and that the effect of the pumping wells was therefore not as marked as expected.

d) calibration of resistivity probes

For each box the values obtained from the centre five probes were subjected to the Kolmogorov-Smirnov normality test. The data from boxes 1, 2, and 4 proved to be normally distributed, those from box 3 were not. For normally distributed data the mean of the values obtained from the upper probe during calibration was compared with that from the lower probe using an unpaired two sample t test, to see if there was any significant difference between the two probes. For the non-normal data, median values were compared in the same way using a Mann-Whitney Rank-sum test. There was found to be no significant difference between upper and lower probes in boxes 1 and 2.

The mean of data from the centre probes was compared with that from upper or lower probes in the case of normally distributed data using a one sample t test and the median values were compared using the Wilcoxon Signed-rank test for non-normally distributed data.

The results of the statistical analysis are given in table 5. Although the results are not conclusive, none of them show significant differences between probes at each height within a site. In the two cases where it is suggested that there is a significant difference between the upper and lower probes, there is no significant difference between the centre probes and either an upper or lower probe 20mm distant from them. It is concluded that,

for the purpose of this test, there was no significant difference between values given by probes at different heights within the model.

TABLE 5 STATISTICAL ANALYSIS OF CALIBRATION DATA

	BOX 1	BOX 2	BOX 3	BOX 4
normal distribution	✓	✓	x	✓
upper & lower similar	✓	✓	x	x
upper & centre similar	x	x	✓	x
lower & centre similar	✓	✓	x	✓

CONCLUSIONS

This work has shown that the study of transport processes using accelerated physical modelling on the drum centrifuge is feasible. It is doubtful, however, that it is the most effective way to study the phenomenon. The physical problems encountered when building such large models are quite significant and it is suggested that the balanced arm centrifuge is a better tool for such work, unless the research is specifically directed towards a study of long-term pollutant transport through a low permeability medium.

Such a study is currently underway for the U.K. Department of the Environment. A model built in the drum centrifuge over a path length of 150cm around the drum circumference will take of the order of 12 days to complete and will represent over 7,000 years prototype migration. This would not be possible on the balanced arm centrifuge.

As it is not at present feasible to scale up such models to the field situation because of the problem of the scaling of dispersivities, the technique is of most value in the validation of numerical models. Again the balanced arm centrifuge is more suited to this task, as models can be

constructed with greater accuracy than in the drum and so the parameters required for the validation process are known with greater precision. The importance of obtaining this precision is demonstrated by the observation in this test of the significant effect of a relatively small sorption coefficient (k_d = 0.9-1.8cm^3g^{-1}) on the rate of pyranine migration . This highlights the significance, firstly, of being able to model such parameters correctly and, secondly, being able to determine them accurately and under conditions which are totally relevant to the field situation, before they can be of use in a predictive model.

References

Abriola, L.M. (1987) Modelling contaminant transport in the subsurface: An interdiciplinary challenge. Reviews in Geophysics, 25 (2) 125-134.

Anderson, M.P. (1984) Movement of contaminants in groundwater: groundwater transport - advection and dispersion. In Groundwater Contamination. Studies in Geophysics, National Research Council, National Academic Press, Washington D.C. 37-45.

Arulanandan, K., Thompson, P.Y., Kutter, B.L., Meegoda, N.J., Muraleetharan, S.M. and Yogachandran, C. (1988) Centrifuge modelling of transport processes for pollutants in soils. Am. Soc. Civil Eng., in press.

Bachmat, Y. (1967) On the similitude of dispersion phenomena in homogeneous isotropic porous mediums. Water Resources Research, 3(4), 1079-1083.

Bear, J. (1972) Dynamics of fluids in porous media. American Elsevier, New York. 764pp.

Bear, J. (1979) *Hydraulics of Groundwater.* McGraw Hill Inc., New York. 569pp.

Bear, J. and Bachmat, Y. (1967) A generalized theory on hydrodynamic dispersion in porous media. I.A.S.H. symposium on artificial recharge and management of aquifers. Haifa, israel. I.A.S.H. publication no 72, 7-16.

Bear, J. and Verruijt, A. (1987) Modelling groundwater flow and pollution. D. Reidel Publishing Co., Dordrecht, 414pp.

Bradbury, M.H., Green, A., Lever, D. and Stephen, I.G. (1986) Diffusion and permeability based sorption measurements in sandstone, anhydrite and upper magnesian limestone samples. Waste Disposal Studies Group, Chemistry Division, Harwell Laboratory Report AERE-R11995.

Bradbury, M.H. and Jefferies, N.L. (1985) Review of sorption data for site

assessment. Harwell Laboratory Report no. AERE-R-11881.

Campbell, D.J.V., Parker, A., Rees, J.F. and Ross, C.A.M. (1983) Attenuation of potential pollutants in landfill leachate by Lower Greensand. Waste Management Research, 1, 31-52.

Crank, J. (1970) The mathematics of diffusion. Clarendon Press, 347pp.

Deer, W.A., Howie, R.A. and Zussman, J. (1979) An introduction to the rock forming minerals. Longmans, London. 528pp.

Freeze, R.A. and Cherry, J.A. (1979) Groundwater. Prentice-Hall, Englewood Cliffs, N.J. 604pp.

Greenkorn, R.A. (1983) Flow phenomena in porous media. Marcel Dekker Inc., New York, 550pp.

Hensley, P.J. (1988) Geotechnical centrifuge modelling of hazardous waste migration. Forthcomming Ph.D. thesis, University of Cambridge.

Hillel, D. (1982) An introduction to soil physics. Academic Press Ltd., London, 364pp.

Lambe, T.W. and Whitman, R.V. (1979) Soil Mechanics. John Wiley and Son, New York, 553pp.

Lever, D., Bradbury M.H. and Hemmingway, S.J. (1983) Modelling the effect of diffusion into the rock matrix on radionuclide migration. Progress in Nuclear Energy, 12, 85-117.

Matheron, G. and de Marsily, G. (1980) Is transport in porous media always diffusive? A counter example. Water Resources Research, 16(5) 910-917.

Pfannkuch, H.O. (1963) Contribution à l'étude des déplacements de fluides miscibles dans un milieu poreux. Rev de l'Institut Francais du Pétrole, 18(2), 215-270.

Reynolds, E.R.C. (1966) The percolation of rainwater through soil. J. Soil Sci., 17, 127-132.

Rowe, R.K. and Booker, J.R. (1983) POLLUTE -1D Pollutant migration analysis program. SACDA Faculty of Engineering Science, University of Western Ontario, London, Ontario.

Saffmann, P.G. (1960) Dispersion due to molecular diffusion and macroscopic mixing in flow through a network of capilaries. J. Fluid Mechanics, 7(2), 194-208.

Smith, L. and Schwartz, F.W. (1980) Mass transport. 1. A stochastic analysis of macroscopic dispersion. Water Resources Research, 16(2) 303-313.

Ibid (1981a) Mass transport. 2. Analysis of uncertainty in prediction. Water Resources Research, 17(2) 351-369.

Ibid (1981b) Mass transport. 3. Role of hydraulic conductivity data in prediction. Water Resources Research, 17(5) 14663-1479.

Schofield, A.N., (1980) Cambridge geotechnical centrifuge operations. Twentieth Rankine Lecture. Geotechnique, 30, 227-260.

Walker, A.F. (1965) A comparison of the predictions of two stress/strain theories for clay with the results of stress-controlled triaxial tests on saturated remoulded kaolin. Ph.D. Thesis, University of Cambridge.

Yariv, S. and Cross, H. (1979) Geochemistry of colloid systems. Springer-Verlag, Berlin, 450pp.

APPENDIX I CENTRIFUGE MODELLING OF FLUID VELOCITY

If two identical soils form geometrically similar conformations where one is at full scale (the prototype) and the other is at 1/N scale; if the 1/N scale model is accelerated to a relative centrifugal field of Ng, then the stresses at corresponding points in the two systems are similar, if they are similar at the boundaries. So provided that care is taken to follow the same stress paths as in the prototype, in the initial consolidation of the 1/N scale model, there should be stress similarity between the two.

Water flow within soils is laminar, provided the value of Reynolds number does not exceed some value between 1 and 10 (Bear, 1972). The Reynolds number (Re) is given by

$$Re = \frac{2r\bar{V}\rho}{\eta} \qquad [A.1]$$

where r is the average particle radius [L], ρ is the density of the fluid [$ML^{-1}T^{-1}$], $\bar{V}$ is the average flow velocity [LT^{-1}] and η is the viscosity of the pore fluid [$ML^{-1}T^{-1}$]. Laminar flow occurs according to Darcy's Law,

$$q = Ki \qquad [A.2]$$

where K is the hydraulic conductivity of the the sediment [LT^{-1}] and where i is the hydraulic gradient [LL^{-1}] which is equal to H/L where H is the hydraulic head drop and L is the distance over which the drop occurs.

Hydraulic conductivity is a property of both the soil and the pore fluid. It is dependent on soil geometry and on the density and viscosity of the permeant, i.e.

$$K = \kappa f \qquad [A.3]$$

where k is the intrinsic permeability of the soil [L^2] and f is the fluidity of the pore fluid [$L^{-1}T^{-1}$], (see Hillel, 1982). where

$$f = \frac{\rho g}{\eta} \qquad [A.4]$$

so at 1g, flow velocity can be written as

$$\bar{V} = \frac{q}{\phi} = \frac{k\rho g i}{\eta} = \frac{k\gamma i}{\eta} \qquad [A.5]$$

where γ is the unit weight of the fluid and ϕ is the porosity.

If the model experiences an acceleration of Ng, then

$$\bar{V}_m = N\bar{V}_p \qquad [A.7]$$

where the subscript m and p denote the model and prototype respectively.

So the effect of increased acceleration on seepage flow within a model is to increase the flow velocity in the model by a factor N. This can be considered to be due to the increase in the self-weight of the pore fluid. The effect of the reduction of the dimensions of the model by 1/N compared with the prototype, reduces the time it takes the water to flow between geometrically similar points in the model by a further factor of N. That is the time for seepage between two geometrically similar points in the prototype (t_p) and model (t_m) is reduced by a factor N^2 in the reduced scale model experiencing a relative centrifugal field of Ng, i.e.

$$N^2 t_m = t_p \qquad [A.7]$$

APPENDIX II THE USE OF A FLUORESCENT TRACER

It would be possible to use a model polutant which might be present in a percentage of Department of the Army landfills. For example the selective herbicides 2,4-D and 2,4,5-T both exhibit fluorence to a certain extent. However centrifuge models require large volumes of leachate and it is not desirable to work with large quantities of toxic substances or to have to dispose of them after testing. Also the fluorescence yield of such substances is low in comparison with the chosen molecule, pyranine, which was shown to be suitable for this type of study by Reynolds (1966).

Fluorescence is useful in both the qualitative and quantitative studies of migration through porous media. Qualitatively it can indicate the migration of a pollutant plume within a body of soil and quantitatively it can be used as a very sensitive indicator of concentration in solution (down to 10^{-9} molar). If incident light is absorbed by a substance it is absorbed in quanta according to the relationship:

$$E = hc/\lambda$$

where E is the energy, λ is the wavelength, h is Plank's constant and c is the velocity of light. Photons in the visible and ultra-violet regions of the electromagnetic spectrum have energies of 35-145 kcal/mol and promote electronic transitions which can give rise to luminescence. More energetic photons can cause decomposition of the molecule and less energetic ones lead to vibrational and rotational transitions.

If light is absorbed by a molecule it does so in $\sim 10^{-15}$ s and the molecule undergoes an electronic transition to an excited singlet state. The molecule can spend $\sim 10^{-9}$ s in the excited state, during which time, energy in excess of the lowest vibrational level of the excited singlet state is

dissipated by molecular collisions. On return to the ground state the molecule emits energy (fluorescence) of a longer wavelength than the energy which was absorbed.

All fluorescent molecules have two characteristic spectra. The excitation spectrum, showing the relative efficiency of different wavelengths to cause fluorescence and the emission spectrum which shows the relative intensity of radiation emitted at various wavelengths. The two spectra of pyranine are given in figure 3.

The Stokes Shift of a molecule is given by

$$10^7(1/\lambda_{ex} - 1/\lambda_{em})$$

where wavelengths are in nm. It is a measure of the energy dissipated during the lifetime of the excited state and can be seen to be 1874.4 cm^{-1} for pyranine at pH 11.

The relation between fluorescence intensity and concentration is:

$$F = \phi I_0(1 - e^{\epsilon bC})$$

where ϵ is the molar absorbtivity, b is the light path length through the sample and C is the molar concentration. So there are three major factors which affect fluorescence intensity; ϕ, the fluorescence yield (or quantum yield) which is the ratio of the energy emitted to the energy absorbed. The quantum yield of many compounds is found to be dependent on excitation wavelength. Fluorescence yield also varies with I_0, the intensity of incident light, up to the point where photodecomposition of the molecule may occur. Finally, fluorecsence intensity depends on the molecular absorbtivity ϵ, since a molecule must first absorb radiation before it can fluoresce.

For very dilute solutions the equation reduces to one equivalent to Beer's Law:

$$F = K\phi I_o \epsilon b C$$

this linearity holds over a wide range of concentrations (10^{-8} ppm - 100 ppm). However luminescence quenching, that is the loss of fluorescence by various competing deactivation processes does occur. The linear dependence of fluorescence on concentration falls off once concentration of the fluorescent sample is high enough to absorb significant amounts of exciting light, (>5%) so that fluorescence intensity is no longer constant throughout the sample being measured; this is called the inner cell effect. Non radiative depopulation of excited states occurs primarily as collisions between molecules and so is proportional to the frequency of molecular encounters and consequently depends on temperature and concentration and is inversely proportional to viscosity. The probability of molecular collisions increases with the sixth power of concentration and becomes important at concentrations above 10^{-3} molar. Loss of fluorescence yield due to increased temperature can vary between 1-5%/°C. It is also found that the total fluorescence at normal excitation (fluorescence maximum) is lowered by an increase in temperature, due to dissipation of energy by vibrational energy transitions.

Quenching of fluorescence may also occur in the presence of atoms of high atomic number or of paramagnetic species such as oxygen. The presence of such species allows the possibility of deactivation via an excited triplet state. The life time of such a state is much longer than that of a singlet state (10^{-3}-10^{-2}s) so that delayed deactivation (phosphorescence) may occur instead of fluorescence.

Solvent quenching occurs because solvent interactions with solute molecules are predominantly electrostatic. Light absorption alters the electronic distribution of the solute so the dipole moment of the excited

molecule may be different from that of the ground-state molecule. If the solute molecule becomes more polar in the excited state, there will be greater electrostatic stabilization of the excited state relative to the ground state by interaction with the solvent. If the dipole moment of the solute molecule is lower in the Franck-Condon excited state than in the ground state, then increased solvent polarity produces a shift of the absorption band to longer wavelengths. Increased hydrogen bonding capacity of the solvent is seen as a shift of the absorption band of a solute to either longer or shorter wavelengths depending on the relative stability of of the charge-transfer excited state and charge-transfer ground state of the solute. The effect of pH on fluorescence is similar. If the acidity of the medium is insufficient to protonate non-bonding electron pairs or to abstract a proton from the functional group, the molecules of the medium may form hydrogen bonds with suitable groups on the fluorescent molecule.

The other main problem associated with the measurement of fluorescence intensity is due to the various forms of scattering of light. Rayleigh scatter occurs when non-absorbing particles which are smaller that the wavelength of the incident light, scatter that light with no loss of energy, i.e. at the same wavelength. This phenomenon occurs at all wavelengths but the intensity of reflected light varies with λ^{-4}, and so is minimized by working at longer wavelengths. Raman scatter appears in fluorescent spectra as peaks which occur at frequency differences from the exciting radiation which correspond to vibrational energy levels in the molecule. They are less intense than Rayleigh scatter peaks, but become significant when high intensity sources are used. Tyndall scatter, the scatter of light by larger particles, may also be a problem. This effect is also inversely proportional

to wavelength and the scattered light is polarized.

Fluorescence photography was found to be most successful when illuminating the sample with long ultra-violet light at an angle of 45° to the camera. The use of a normal daylight colour film, Kodacolour Gold 100 or 200 ASA, a Cokin skylight (230) filter to illiminate ultra-violet light from the camera and a Cokin polarizing filter (B160) to remove the majority of the reflected light seemed to give successful results.

APPENDIX III THE BATCH DETERMINATION OF SORPTION COEFFICIENTS

There has been much discussion about the validity of batch sorption tests since the results of such tests are extremely sensitive to experimental conditions (Bradbury and Jefferies, 1985). The sorption coefficient, K_d [cm^3g^{-1}] is defined as

$$\frac{\text{the concentration of a species on the solid phase at equilibrium}}{\text{the concentration of a species in solution at equilibrium}}$$

This was determined here by contacting clay with dilute solutions of pyranine at a constant temperature and for the length of time estimated for the duration of a centrifuge test, to indicate the degree and kinetics of the sorption process.

250mg of E. Grade kaolin was shaken with distilled water in 60cm^3 polyallomer Oak Ridge type centrifuge tubes for 24 hours. They were then centrifuged and the supernatant removed. This was repeated twice before 15cm^3 of either 0.1ppm, 1.0ppm or 10ppm pyranine solutions (adjusted to pH>10 with NaOH) were added to the samples, shaken gently in a water bath at 75rpm for 1, 2 or 3 days and centrifuged. The loss of solution concentration was monitored on a Locarte filter fluorimeter using a zinc low pressure vapour lamp, a primary filter (f11) which transmits the zinc triplet around 470nm and a secondary cut-off filter (f7) which transmits all light of wavelength 510nm and above. A blank determination was carried out at the same time (with no clay in the tubes) to indicate the possible loss of fluorescence intensity in solution during the experiment due to sorption onto the container walls or other reasons. Because it had been reported that the results of batch sorption experiments are sensitive to liquid/solid ratios, the 1ppm runs were

duplicated with only 100mg of clay present. pH was monitored during the experiment, but was found not to vary. The sorption results are given in figure 9.

Further batch experiments were carried out to investigate the sorption of pyranine onto E.Grade kaolin.

a) a study of the contact time,

b) a study of the effect of concentration at pH 7.5,

c) a study of the effect of concentration at pH 11,

d) a further study of the effect of concentration at pH 7.5.

a) The method employed was similar to that given above but using 10ppm pyranine solutions contacted with the clay for 1, 5, 10, 15, 20 and 30 days. The results are given in figure 10 and show a trend of increasing sorption with time. However, it was noted that sorption onto the centrifuge tubes was of a similar order of magnitude and that this might have a significant effect on the results. The pH of the supernatant in all cases was of the order of 11.5.

b) The method was repeated using pyranine solution concentrations of 1, 5, 10, 50 and 100ppm contacted with the clay for 10 days. The initial solution pH was between 7 and 8. Sorption in the blank tubes was found to be of the same order as those containing the clay, so it was concluded that no sorption onto the clay had occurred.

c) Experiment b) above was repeated with similar concentration pyranine solutions at an intial pH of 11. Similar results were obtained in that blank

sorptions were of the same order of magnitude as the tubes containing clay. The pH of the blank solution were consistently higher than those containing clay, indicating that some ion exchange may have occurred.

d) Experiment b) above was repeated again using polycarbonate blood bottles to provide a different container material, to indicate whether this had any effect on sorption characteristics. Again no sorption onto the clay was evident and again the pH was consistently higher than the blank solutions.

The changes in hydrogen ion concentration noted between the clay and blank solutions at pH 11 and pH 7.5 are given in tables A.1 and A.2 and those for pH 11 is given in figure 11.

TABLE A.1 $[H^+]$ CHANGES IN SOLUTION AT pH 11

ppm	$\Delta[H^+]\times10^{-11}$ (mole/dm^3)	$\Delta[H^+]\times10^{-12}$ (mole/g)	$\Delta[H^+]\times10^{-13}$ (mole/m^2)	$\Delta[H^+]\times10^{-7}$ (ion/unit cell
5	0.57	1.38	1.97	0.5
10	1.75	4.92	7.03	1.9
50	9.29	27.36	39.09	10.7
80	27.10	55.70	79.57	21.8

TABLE A.2 $[H^+]$ CHANGES IN SOLUTION AT pH 7.5

ppm	$\Delta[H^+]\times10^{-9}$ (mole/dm^3)	$\Delta[H^+X10^{-10}$ (mole/g)	$\Delta[H^+]\times10^{-10}$ (mole/m^2)	$\Delta[H^+]\times10^{-8}$ (ion/unit cell
1	1.09	5.35	0.76	2.08
5	2.44	15.81	2.26	6.21
10	2.71	11.62	1.66	4.50
50	1.31	7.14	1.02	2.80
90	1.38	7.84	1.13	3.10

The point of zero charge (zpc) of kaolin is approximately 5. 10-20% of the total area is composed of broken bonds which account for the majority of the ion exchange capacity of 3-5 mEq/100g. The mineral is triclinic and has the cell parameters given in table A.3.

TABLE A.3 KAOLIN CELL PARAMETERS (Deer, Howie and Zussman, 1966)

$A = 5.15$ Å	$b = 8.95$ Å	$c = 7.39$ Å
$\beta = 104.8°$	$\alpha = 91.8°$	$\gamma = 90°$
cell volume is $a.b.c.\sin\beta$	$= 329.32$ Å^3	
sheet cell area	$= 46.09$ Å^2	$= 46.09 \times 10^{-20}$ m^2

The [H+] exchange in solution noted at pH 7.5 was three orders of magnitude greater than at pH 11, and the change in [H+] per unit cell at pH 7.5 was ten times larger at higher pyranine concentrations than at pH 11, but the solutions at pH 7.5 showed no concentration dependence. This suggests that the exchange was concentration dependent up to a certain point, and then levelled off. This levelling off does not appear to be related to the cation exchange capacity of the mineral which is several orders of magnitude greater than the highest exchange value of 55.7×10^{-9} mmole/100g.

Since no adsorption of pyranine at 10ppm was noted in experiments b), c), and d), it was concluded that the adsorption observed in experiment a) was due in large part to sorption onto the container walls.

APPENDIX IV. DIFFUSION COEFFICIENTS AND THEIR DETERMINATION

The partial differential equation describing one dimensional transport in a porous medium, when there is no reaction which produces changes in the concentration of the solute other than rapid equilibrium sorption is:

$$\frac{\partial(\phi D\frac{\partial C}{\partial x} - qC)}{\partial x} - \frac{\alpha\partial C}{\partial t} = 0 \qquad [A.8]$$

where ϕD is the dispersion coefficient [L^2T^{-1}], α is the matrix capacity factor = $(\phi + \rho_b k_d)$, where ϕ is the through-transport porosity of the matrix and $\rho_b k_d$ is the volume sorption coefficient, since ρ_b is the bulk density of the matrix and k_d is the sorption coefficient (the ratio of the mass of the component of interest, sorbed onto the matrix per unit mass of matrix to the mass of the component remaining in solution per unit volume of solution) [L^3M^{-1}]. C is the concentration of the component in solution [ML^{-3}] and q is the volumetric flux (the Darcy velocity) [LT^{-1}], t is the time and x the distance from the input.

The flux of the component in solution is given by:

$$F = -\phi D\frac{\partial C}{\partial x} + qC \qquad [A.9]$$

If D_a is the apparent diffusion coefficient for the migration of the solute through the matrix measured under no-flow conditions,

$$D_a = D_s/\alpha \qquad [A.10]$$

where D_s is the the matrix diffusion coefficient for the solute and α is the matrix capacity factor.

$$D_s = D_i \delta / \theta^2 \qquad [A.11]$$

where δ is the ratio of the viscosity of the bulk solution to the average viscosity of the interstitial solution, θ is the geometric tortuosity factor, defined as L_e/L, where L_e is the average length of streamlines in the void space of the matrix between two parallel planes at a distance L apart. D_i is the diffusion coefficient of a component in free solution and is given by the Nernst equation:

$$D_i = \frac{RT\lambda_i}{|z_i| F^2} \qquad [A.12]$$

where λ_i is the equivalent conductivity of i, which is inversely related to the viscosity of the fluid, R is the gas constant, T is the absolute temperature, F is the Faraday constant and $|z_i|$ is the absolute value of the charge on the ion. Equation [A.12] indicates that an increase in relative centrifugal field will have no effect on the molecular diffusion coefficient.

As kaolin has the platey morphology shown in figure 4 the following consolidation process leads to samples in which clay particles lie perpendicular to the direction of principle stress. Samples were prepared from a slurry mixed under vacuum for two hours and consolidated one dimensionally as given in Walker (1965) to produce a 1.5 inch diameter sample, 80 mm in length at an effective vertical stress (σ'_v) of 70 kPa.

For the diffusion measurement samples were trimmed, usually to 3.5 cm and set in a modified triaxial cell (figure A.1) in a temperature controlled room. The perspex body of the cell was comprised of sections so that a sample length not accommodated by the Bellofram seal could be taken up by the addition or removal of sections as necessary(figure A.2). 1.5 inch hollow end caps (also of perspex) were covered by 3 mm thick porous stainless steel discs with a hydraulic conductivity of at least an order of magnitude higher than that of the sediment. Each end cap had two 2 mm internal diameter PVC tubes sealed into the base for fluid inflow and outflow. Each hollow end cap was connected to a reservoir via a peristaltic pump as in figure A.3. The difference in pressure between the two reservoirs was monitored by a differential pressure transducer and retained at zero by adjusting the height of the reservoir connected to the lower end cap (figure A.4).

The system was set up by circulating a solution of distilled water in each reservoir and then by replacing the solution in the lower reservoir with either 0.6M NaCl or 100ppm pyranine (1.907×10^{-4}M) and monitoring the concentration reaching the upper reservoir using an ion-selective electrode for chloride determinations or fluorimetry for pyranine concentration. The solution in the lower reservoir was replaced regularly to maintain a constant concentration input.

Theory

Ideally, for the diffusion experiments there should be no flow across the sample,, so equation [A.8] becomes:

$$\frac{\partial C}{\partial t} = \frac{\phi D}{(\phi + \rho_b k_d)} \frac{\partial^2 C}{\partial x^2} \qquad [A.13]$$

The system may be regarded as a one dimensional diffusion in a medium bounded by two parallel planes at x = 0 and x = L. The concentration of solution at the inlet surface (x = 0) is maintained at C_o and the concentration at the outlet face (x = L) is C_t and the volume of this solution is v. If the initial concentration is zero, then provided that C_t remains considerably less than C_o, C_t may be taken as zero and the solution to equation [A.13] may be given as in Crank 1970) as:-

$$C = \frac{C_o x}{L} + \frac{2}{\pi} \sum_{n=1}^{\infty} C_o \frac{\cos n\pi}{n} . \sin\left(\frac{n\pi x}{L}\right) . \exp\left[\frac{-\phi D n^2 \pi^2 t}{L^2(\phi + \rho_b k_d)}\right] \qquad [A.14]$$

the flux through the sediment is $-\phi D \frac{\partial C}{\partial x}$, so:- [A.15]

$$\text{the flux} = \frac{\phi D C_o}{L} + \frac{2\phi D C_o}{L} \sum_{n=1}^{\infty} \cos n\pi . \exp\left[\frac{-\phi D n^2 \pi^2 t}{L^2(\phi + \rho_b k_d)}\right] \qquad [A.16]$$

The total quantity diffused through the slab in time t is $A \int_o^t F dt$, so

$$\frac{Q}{A} = \frac{\phi D C_o t}{L} + \frac{2\phi D C_o}{L} \sum_{n=1}^{\infty} \frac{-L^2(\phi + \rho_b k_d)}{n^2 \phi D \pi^2} . \cos n\pi . \exp\left[\frac{-\phi D n^2 \pi^2 t}{L^2(\phi + \rho_b k_d)}\right]$$

$$= \frac{\phi D C_o t}{L} + \frac{2C_o L(\phi + \rho_b k_d)}{\pi^2} \sum_{n=1}^{\infty} \frac{(-1)^n}{n^2} \left[1 - \exp\left[\frac{-\phi D n^2 \pi^2 t}{L^2(\phi + \rho_b k_d)}\right]\right]$$

as $\frac{(-1)^n}{n^2} = \frac{-\pi^2}{12}$ and $Q = C_t v$ and as $t \to \infty$ the exponential term disappears

$$\frac{C_t}{A} v = \frac{\phi D C_o t}{L} - \frac{L C_o(\phi + \rho_b k_d)}{6} \qquad [A.17]$$

so as $t \to \infty$ the slope of the plot of C_t, the concentration of the outlet cell against time gives a value for the intrinsic diffusion coefficient, ϕD and has an intercept on the time axis of:

$$\frac{L^2(\phi + \rho_b k_d)}{6\phi D} \qquad [A.18]$$

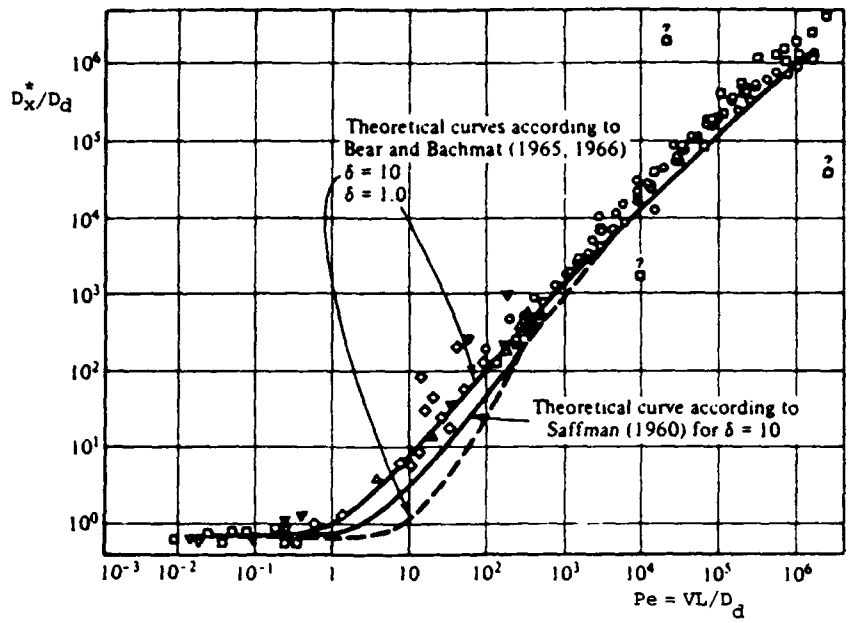

figure 1 the dependence of Peclet number on velocity

(from Bear and Verrjuit, 1987)

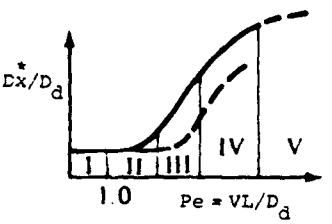

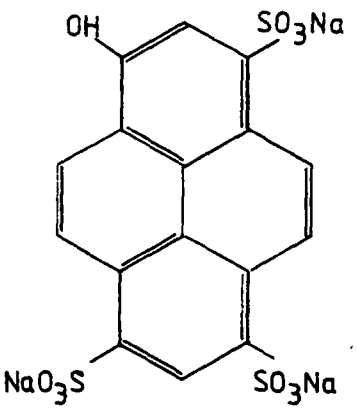

figure 2 pyranine

figure 3 the fluorescence spectra of pyranine

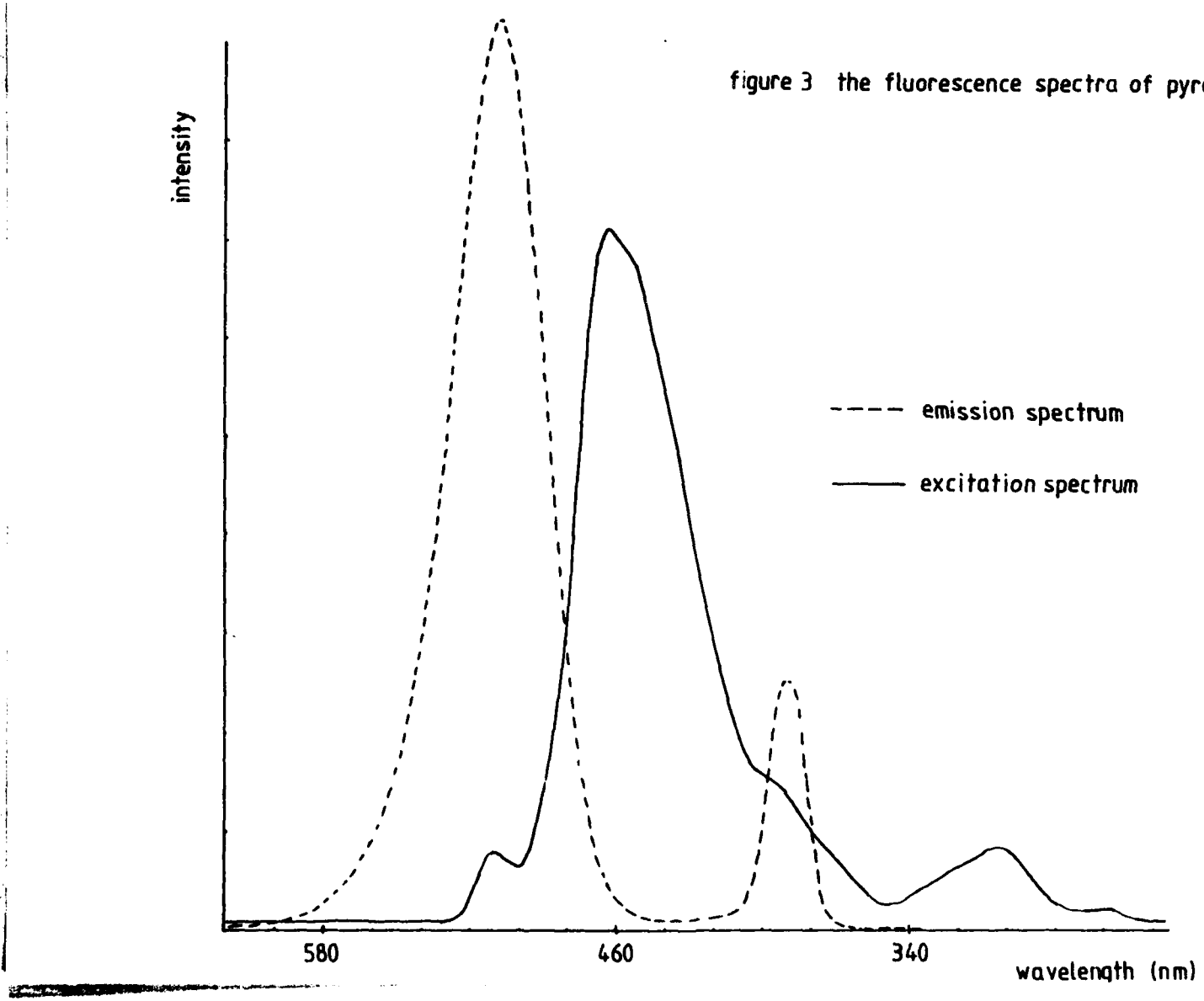

figure 4 Electron micrograph of kaolin

2µm

figure 5 The structure of kaolin
(from Lambe and Whitman, 1979)
a) atomic structure
b) symbolic structure

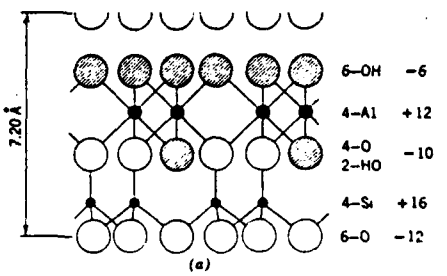

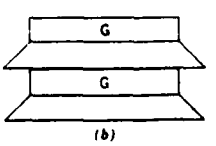

figure 6 particle size distribution of E Grade kaolin

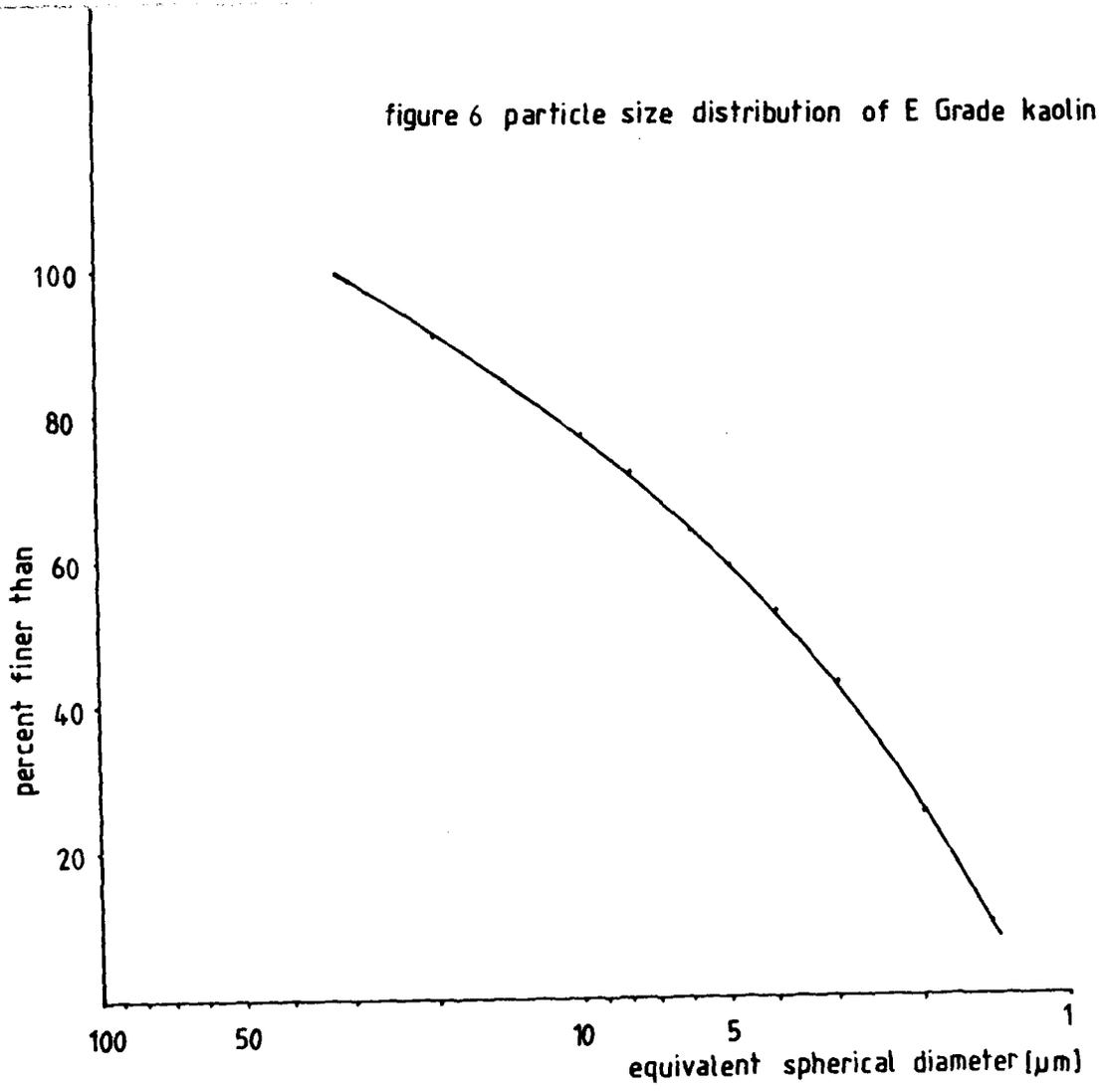

figure 7 hydraulic conductivity of E Grade kaolin

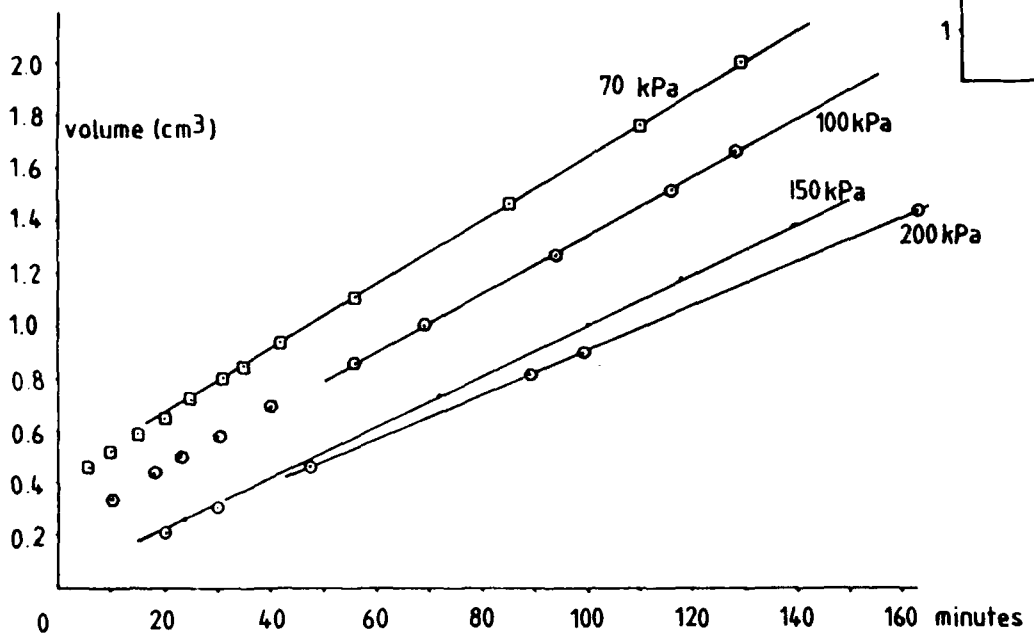

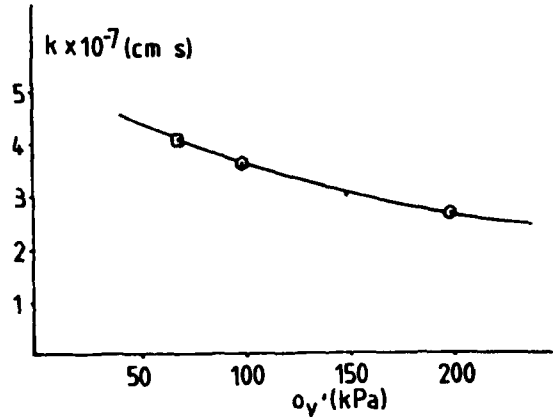

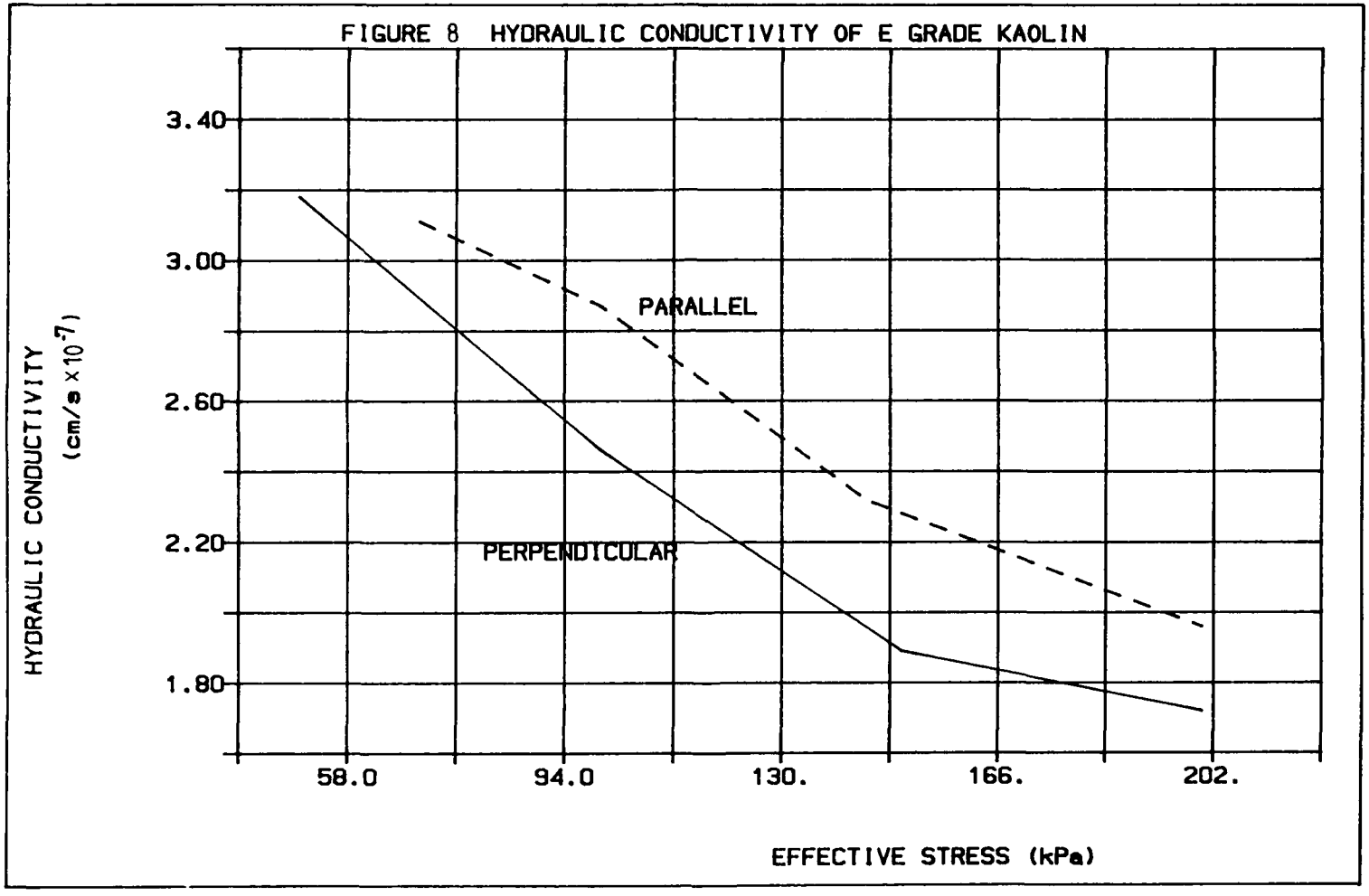
FIGURE 8 HYDRAULIC CONDUCTIVITY OF E GRADE KAOLIN
HYDRAULIC CONDUCTIVITY (cm/s x 10^-7)
3.40
3.00
2.60
2.20
1.80
PARALLEL
PERPENDICULAR
58.0
94.0
130.
166.
202.
EFFECTIVE STRESS (kPa)

figure 9 the sorption of pyranine onto E Grade kaolin

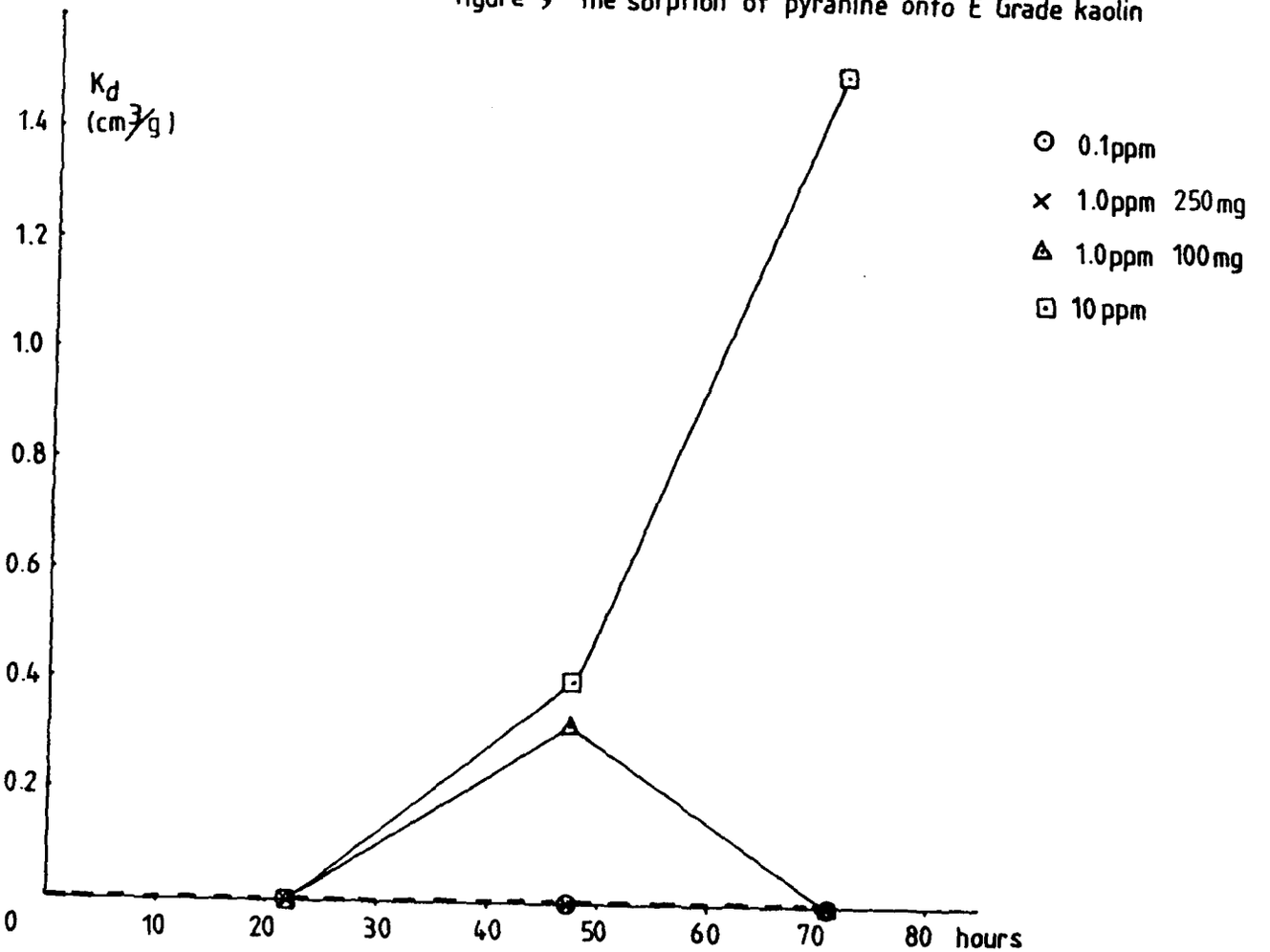

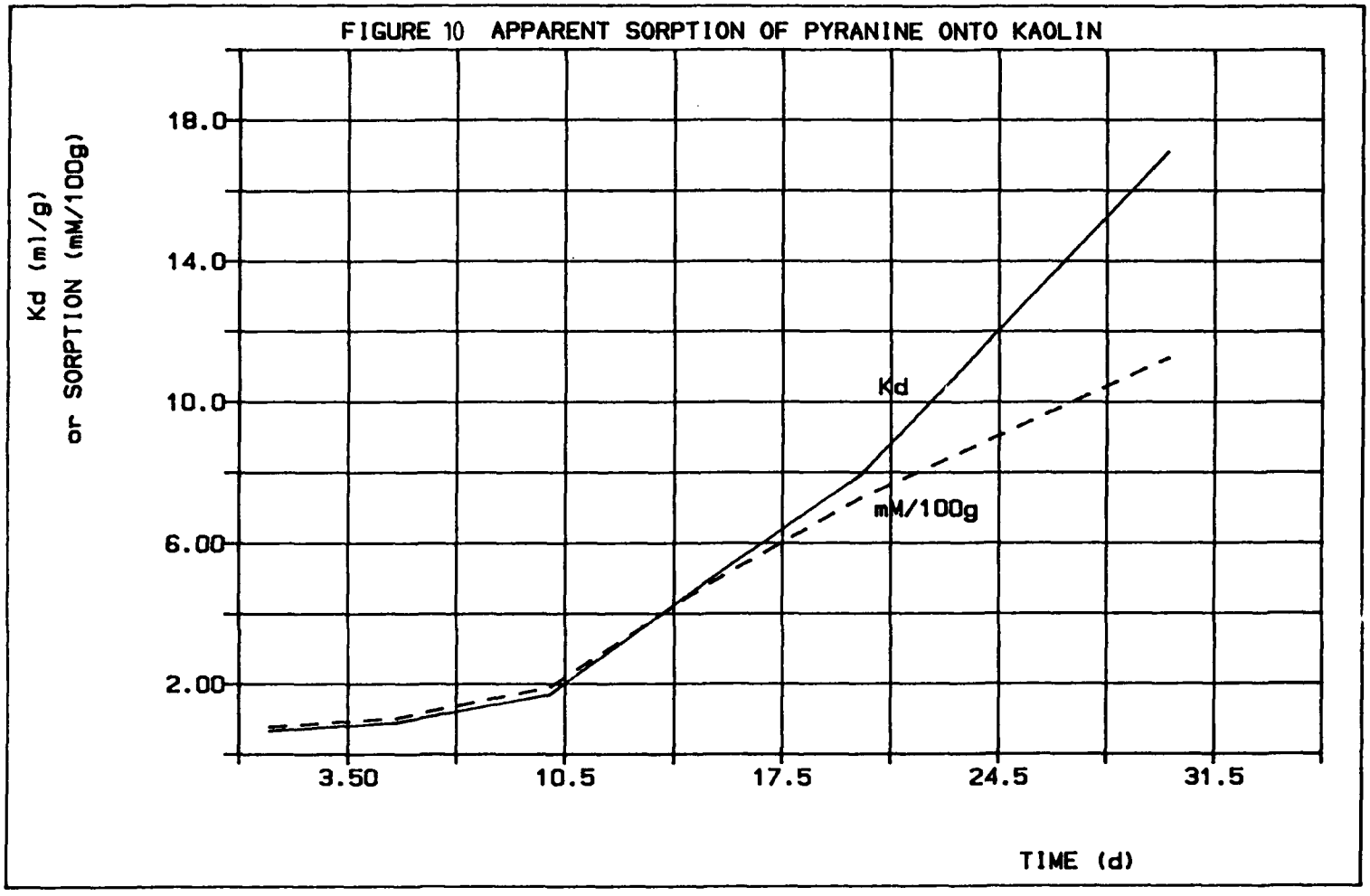
FIGURE 10 APPARENT SORPTION OF PYRANINE ONTO KAOLIN
Kd (ml/g)
or SORPTION (mM/100g)
18.0
14.0
10.0
6.00
2.00
Kd
mM/100g
3.50
10.5
17.5
24.5
31.5
TIME (d)

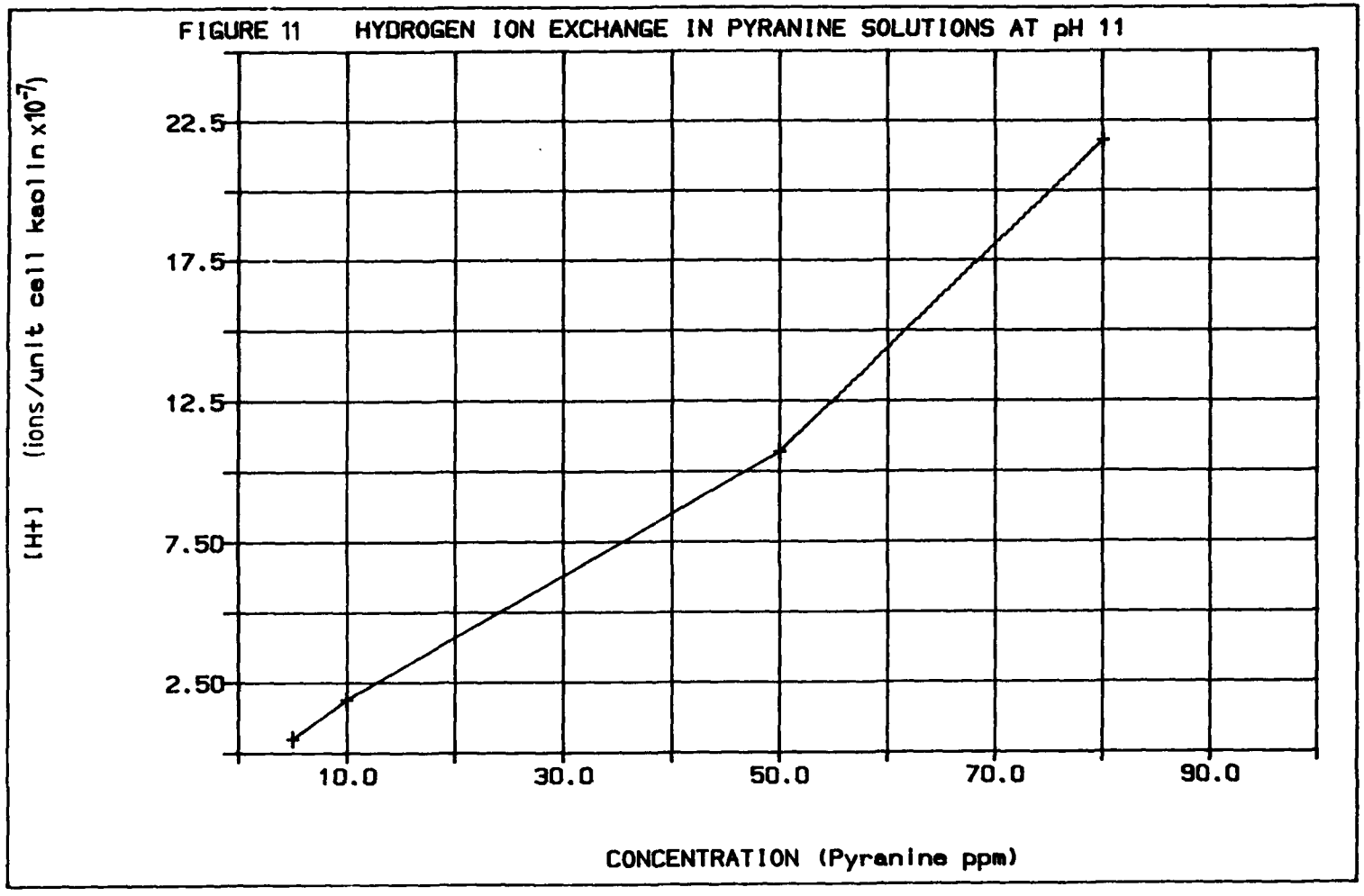
FIGURE 11 HYDROGEN ION EXCHANGE IN PYRANINE SOLUTIONS AT pH 11
[H+] (ions/unit cell kaolin x10⁻⁷)
22.5
17.5
12.5
7.50
2.50
10.0
30.0
50.0
70.0
90.0
CONCENTRATION (Pyranine ppm)

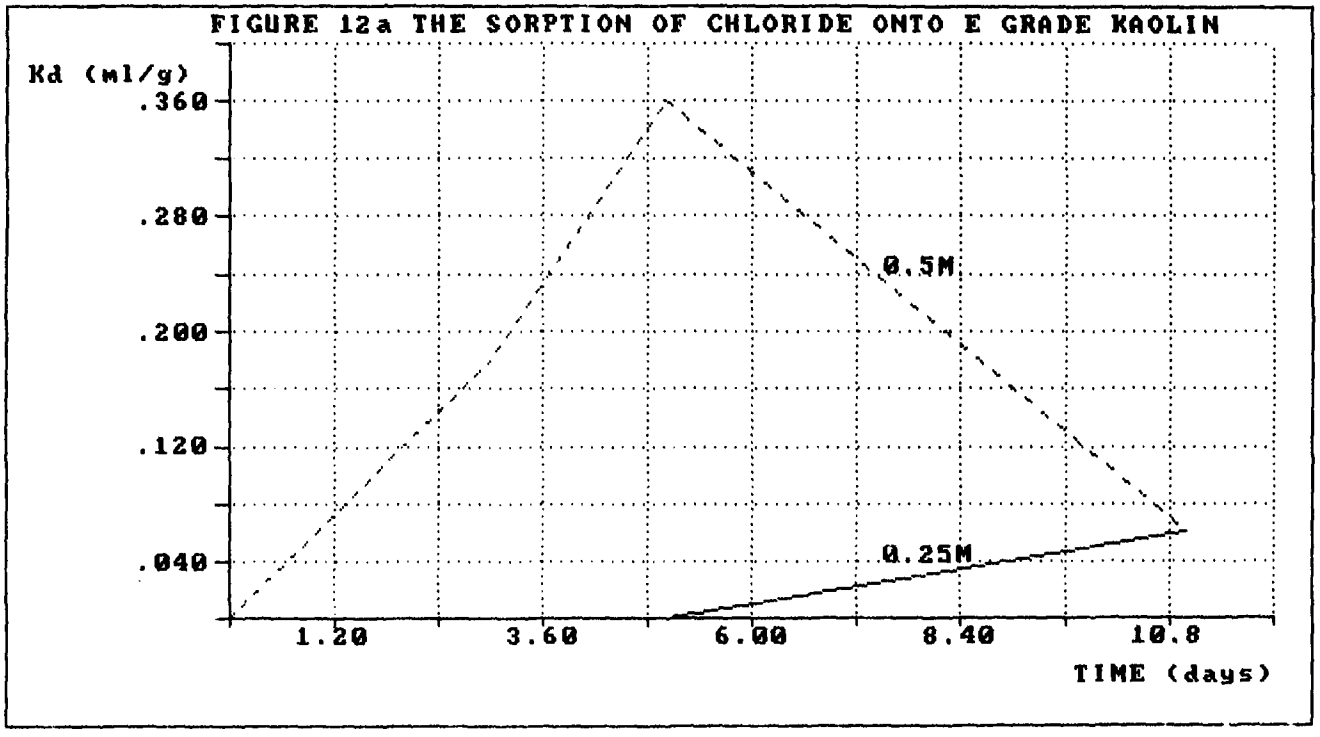
FIGURE 12a THE SORPTION OF CHLORIDE ONTO E GRADE KAOLIN
Kd (ml/g)
.360
.280
.200
.120
.040
0.5M
0.25M
1.20
3.60
6.00
8.40
10.8
TIME (days)

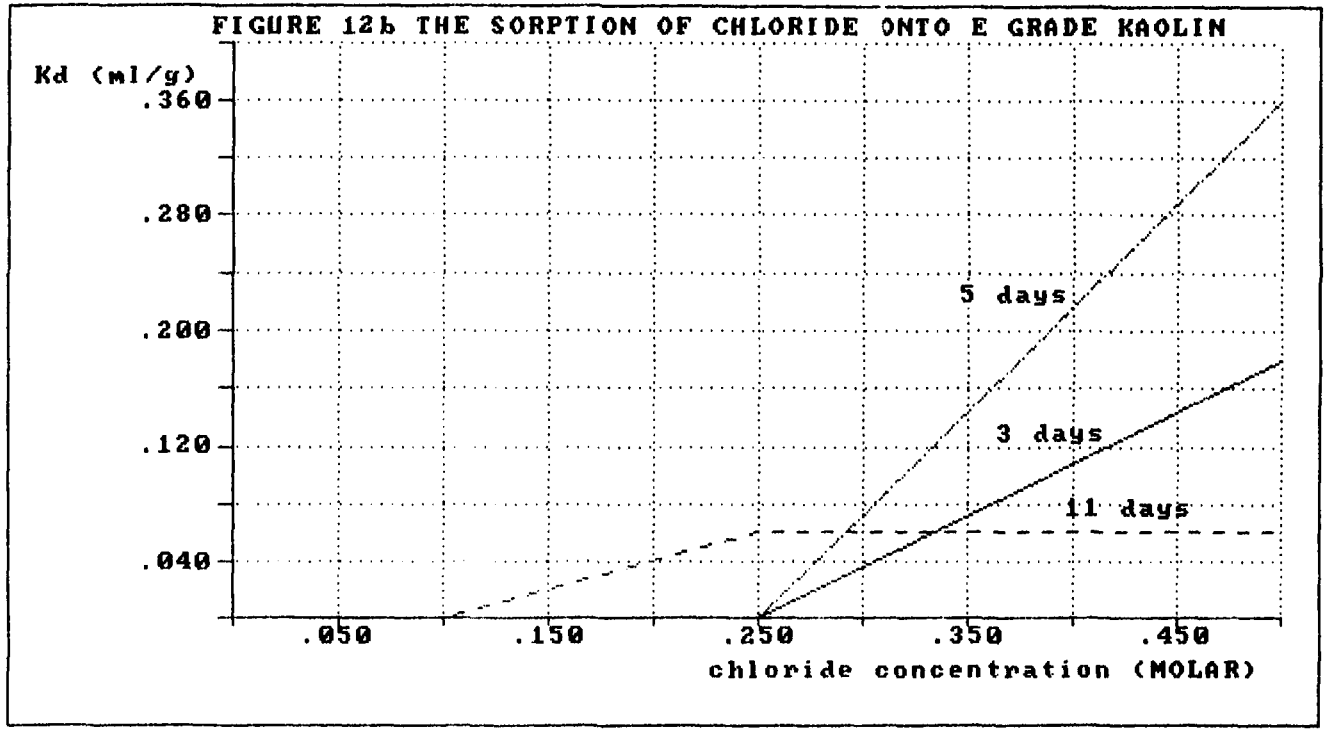
FIGURE 12b THE SORPTION OF CHLORIDE ONTO E GRADE KAOLIN
Kd (ml/g)
.360
.280
.200
.120
.040
5 days
3 days
11 days
.050
.150
.250
.350
.450
chloride concentration (MOLAR)

figure 13 The diffusion of chloride through E Grade kaolin

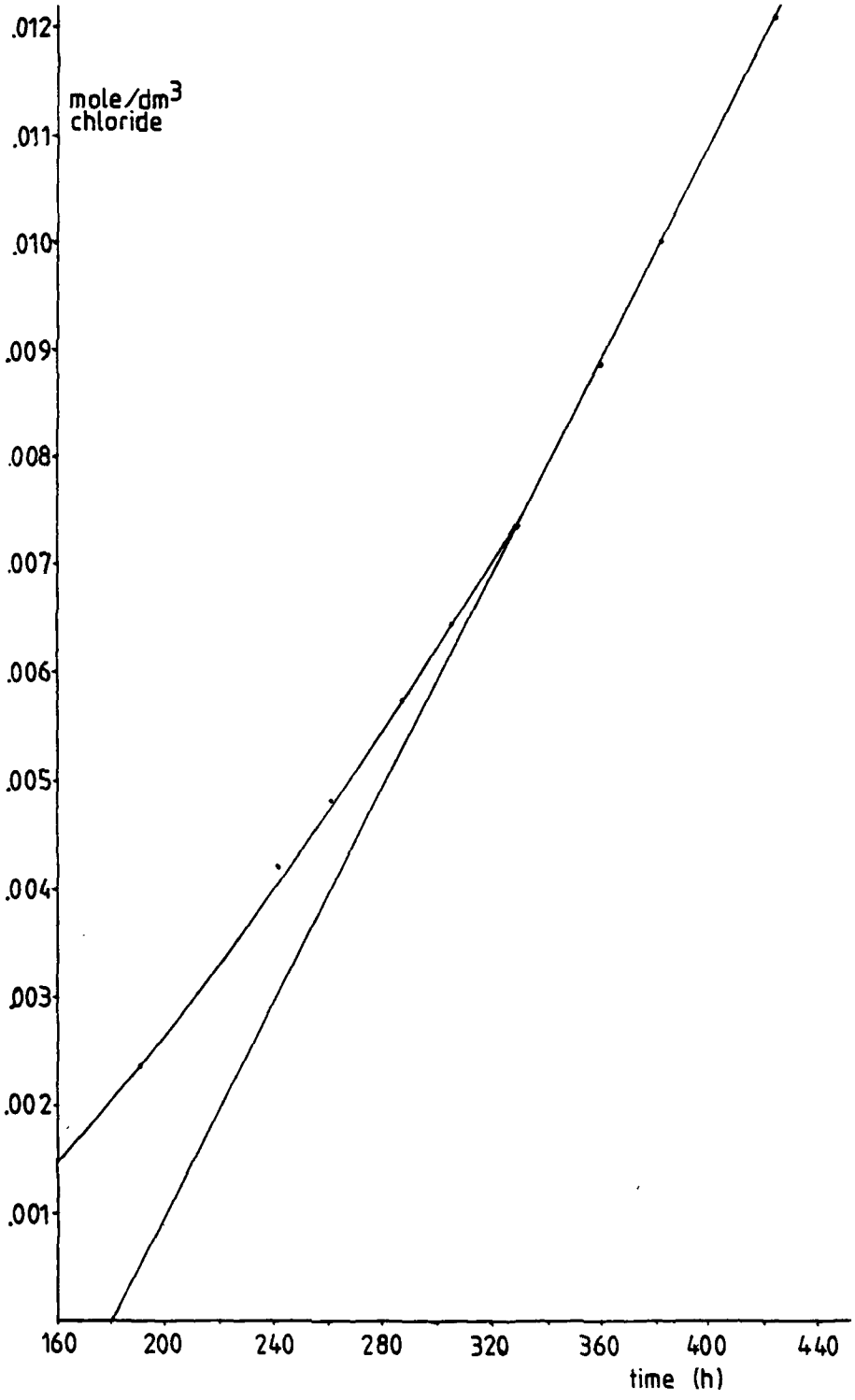

figure 14a The flux of pyranine through E grade kaolin

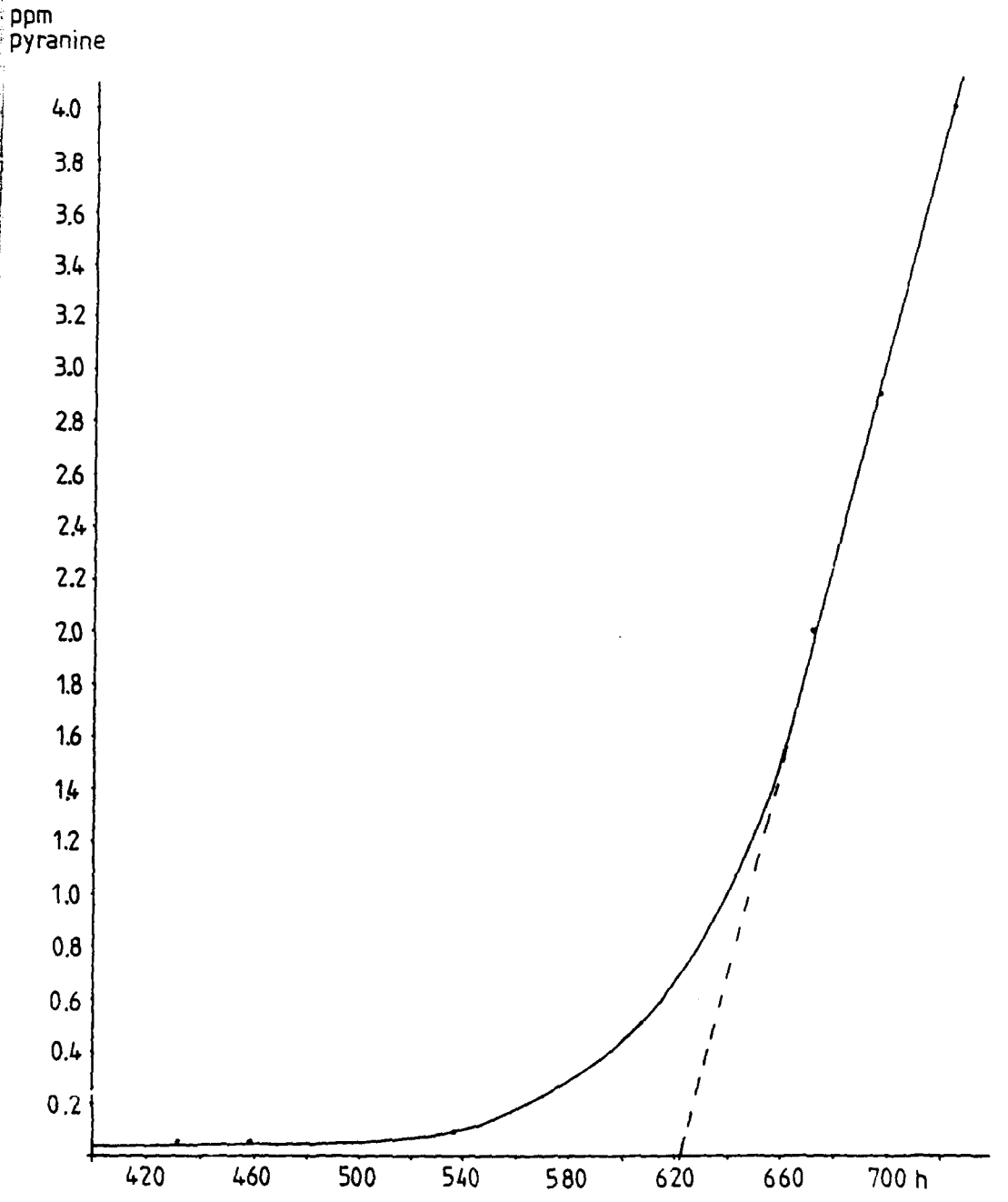

figure 14b The flux of pyranine through E Grade kaolin

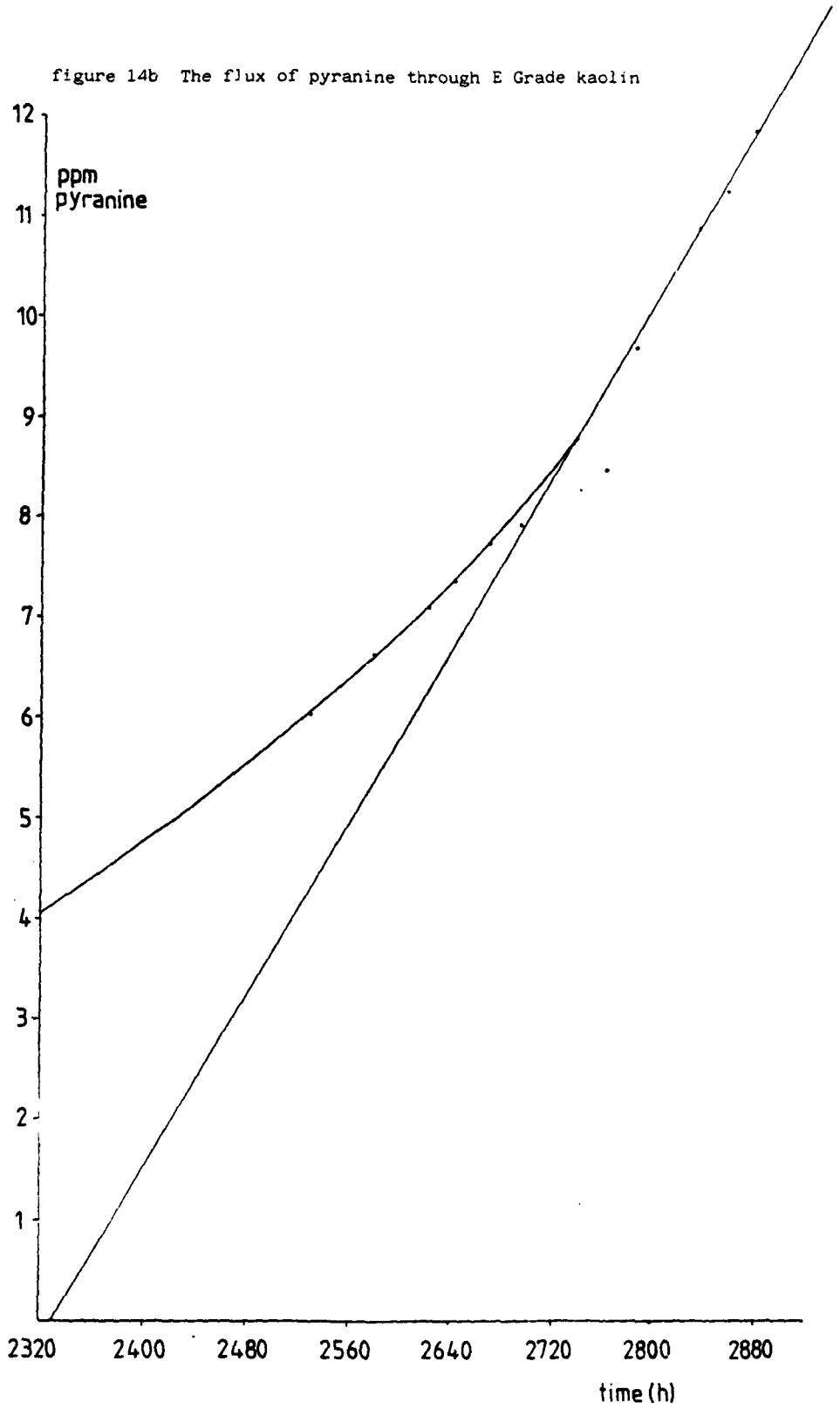

figure 15 Filtram laminated filter drain

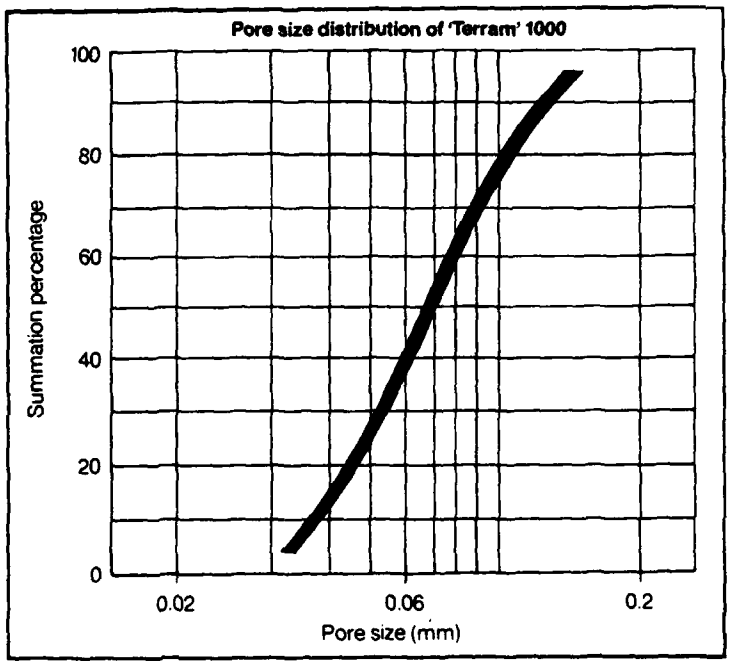

figure 16 Terram pore size distribution

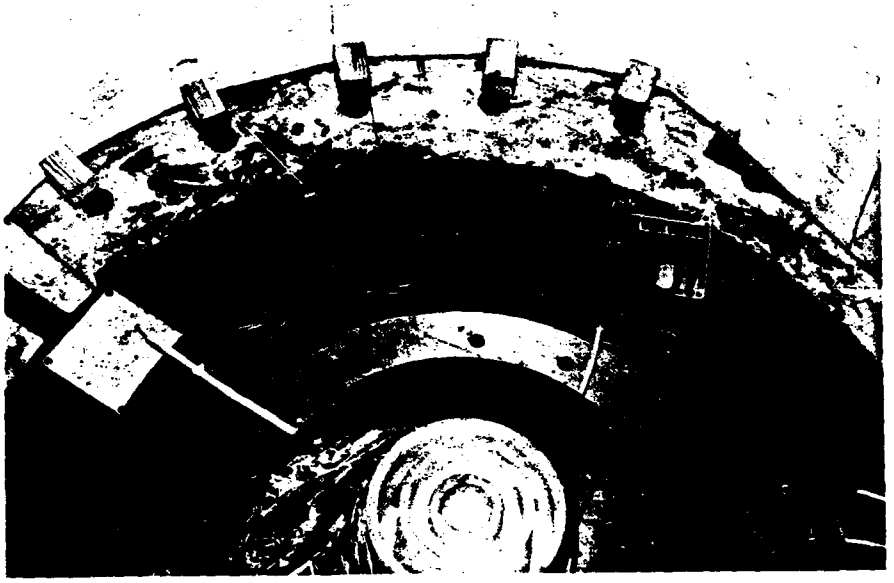

figure 17 The permeable base layer

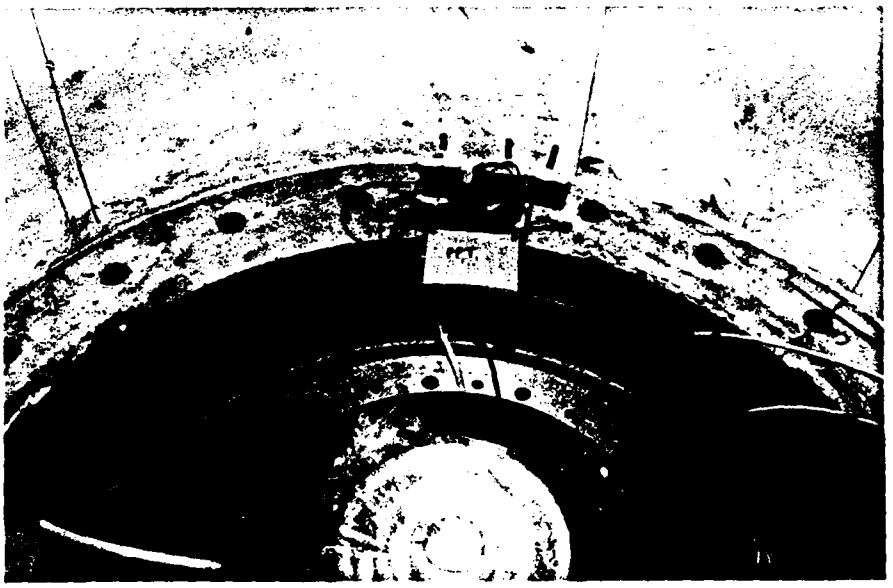

figure 18a The drum centrifuge

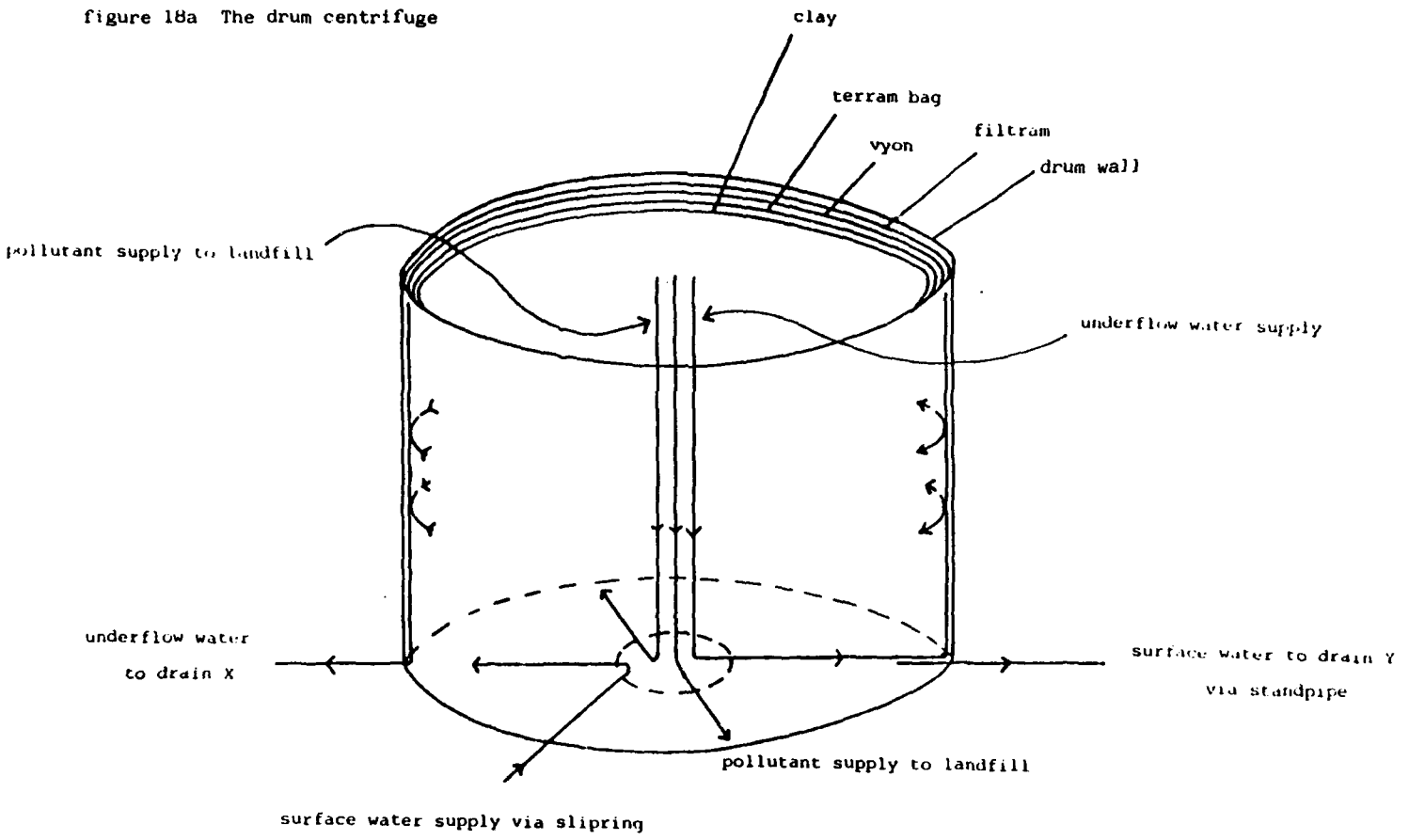

figure 18b sections through drum centrifuge models

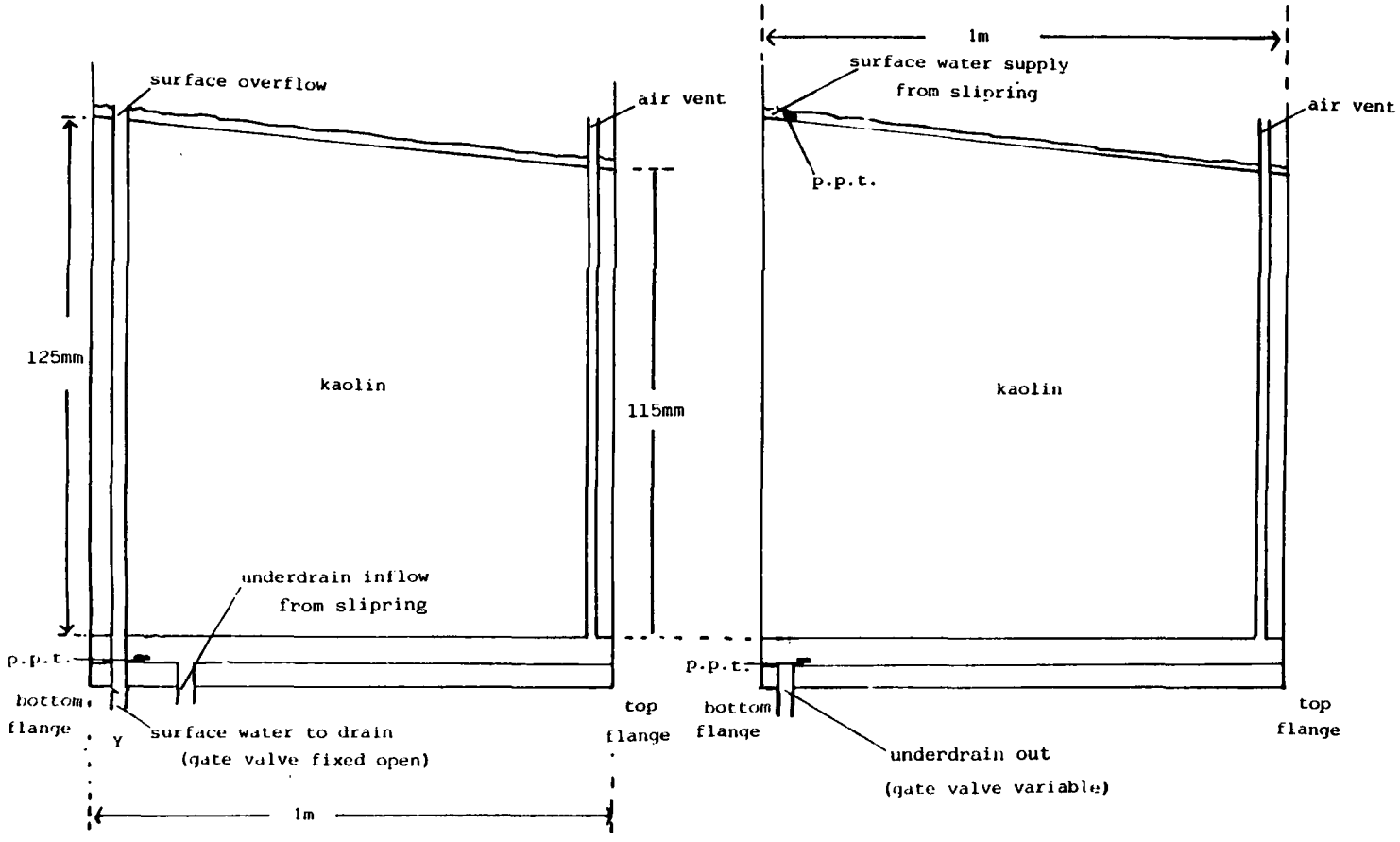

figure 18c sections through drum centrifuge models

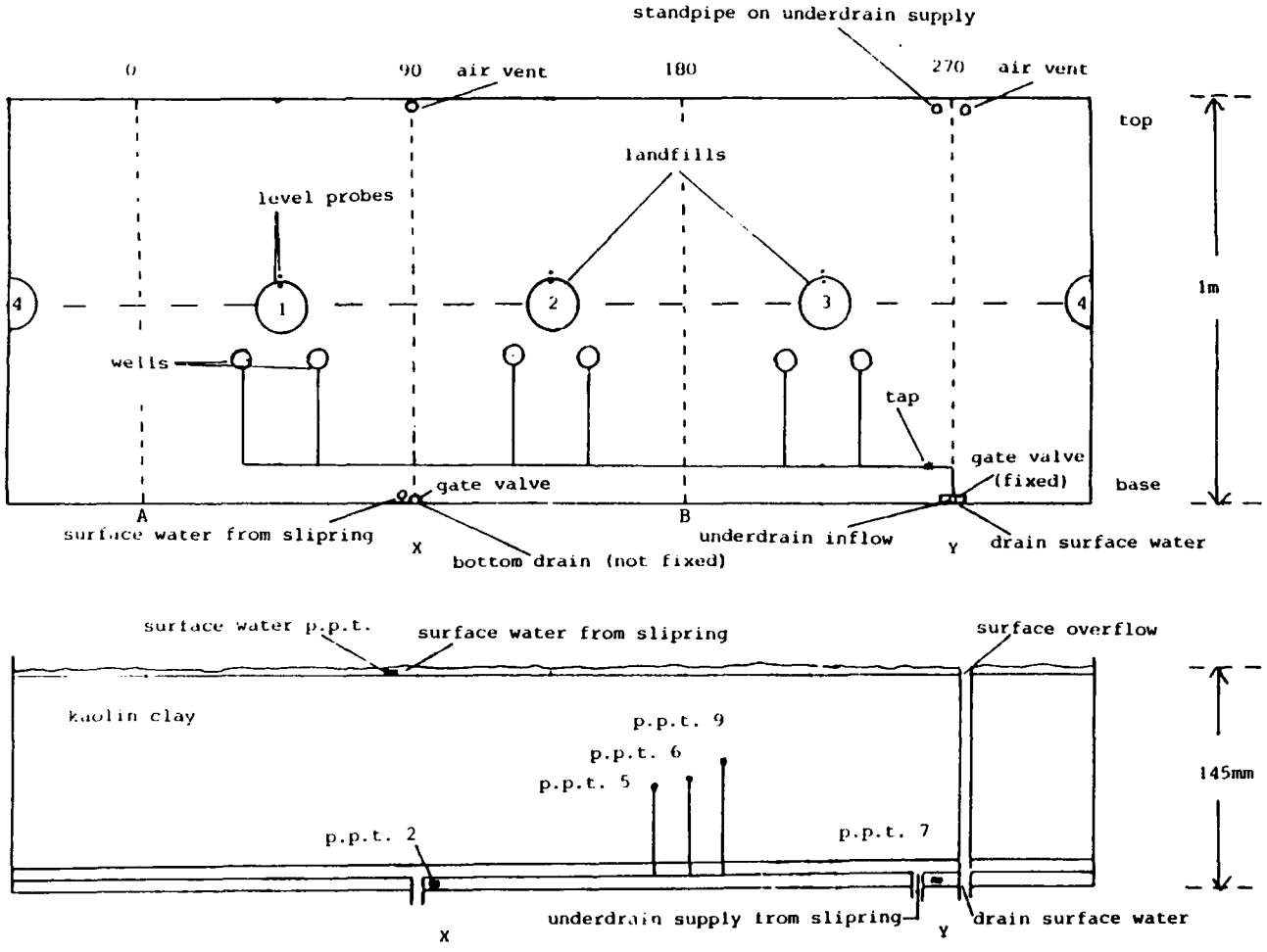

Figure 18d

Plan of the drum centrifuge

(not to scale)

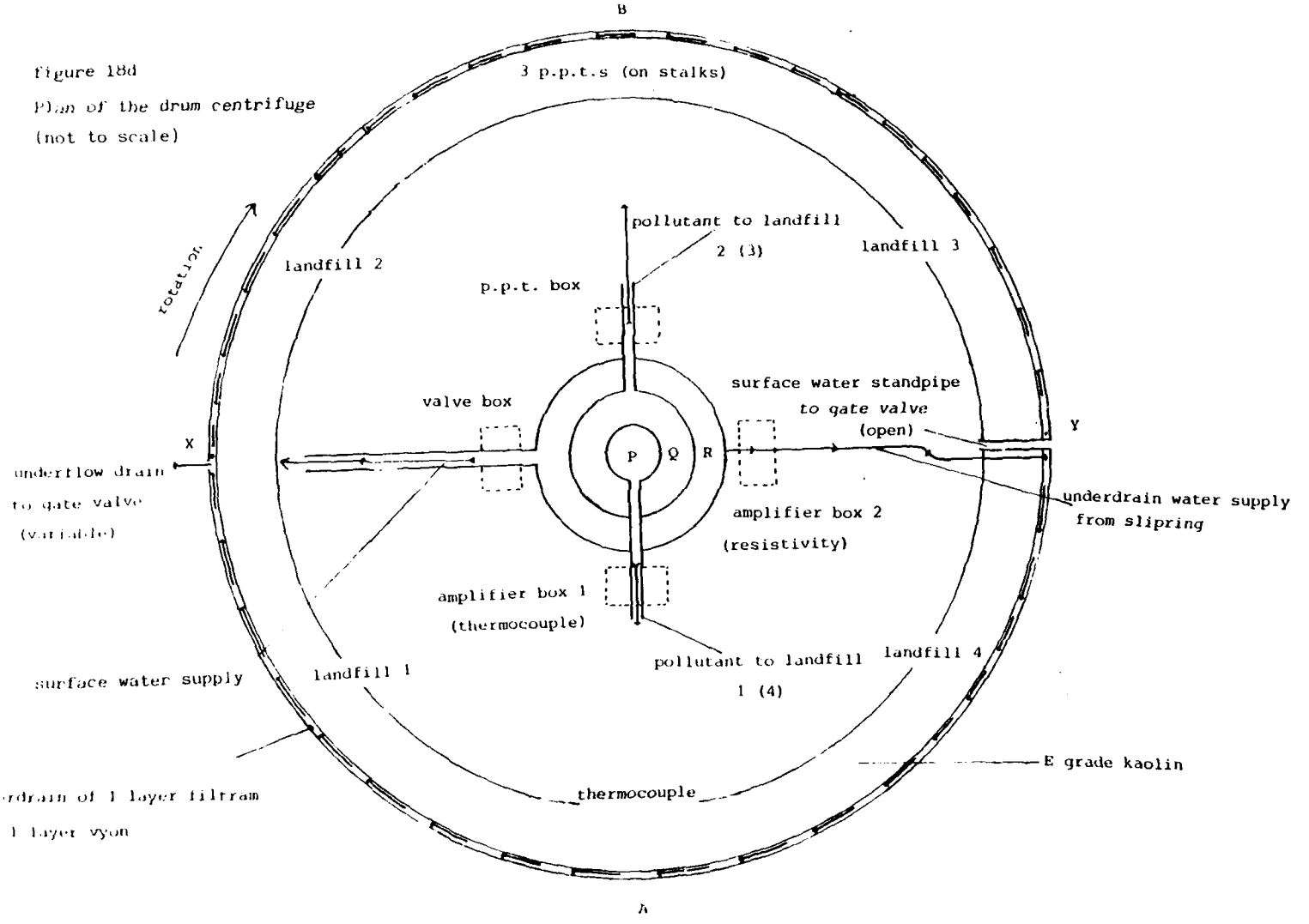

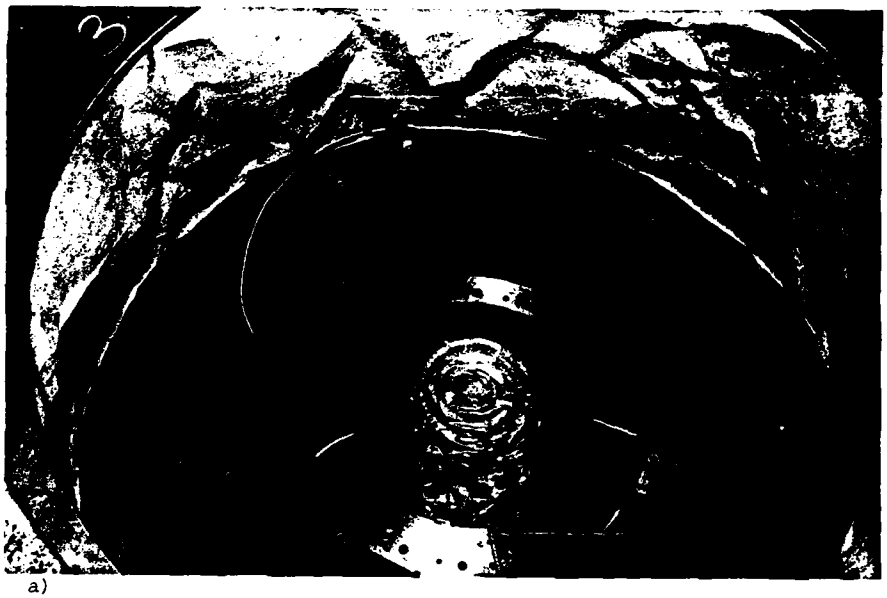

a)

figure 19 The bag in place
a) The standpipe
b) The pore pressure transducer stalks.

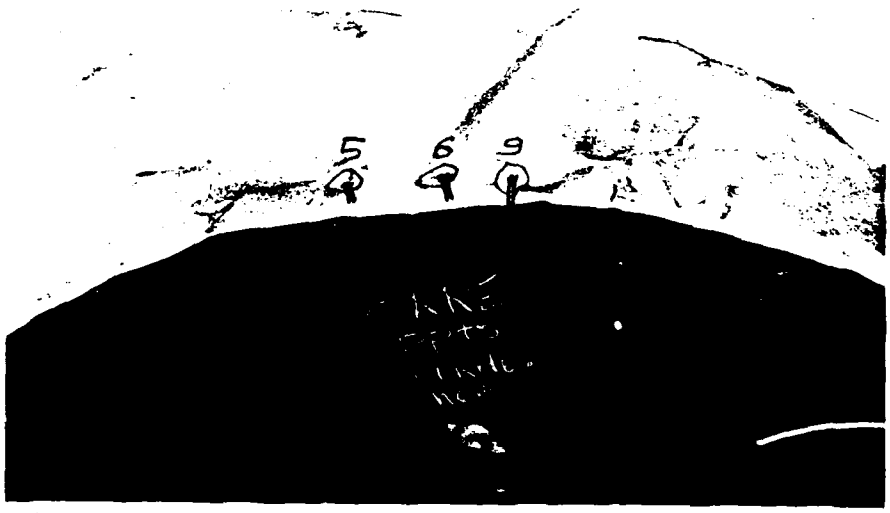

b)

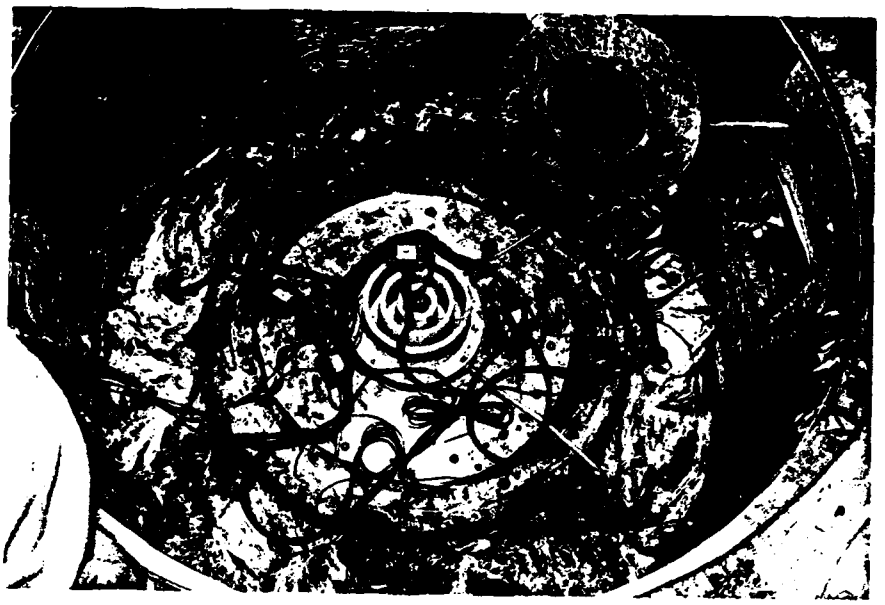

figure 20 Drum wiring

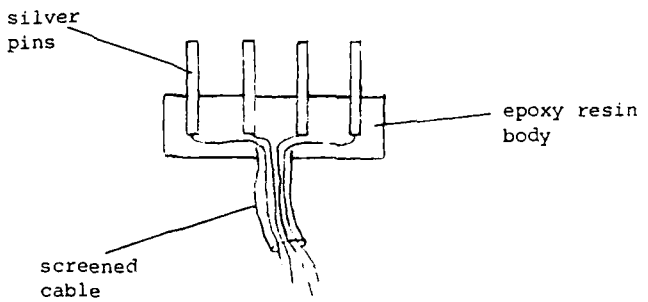

figure 21a A resistivity probe
(scale x2)

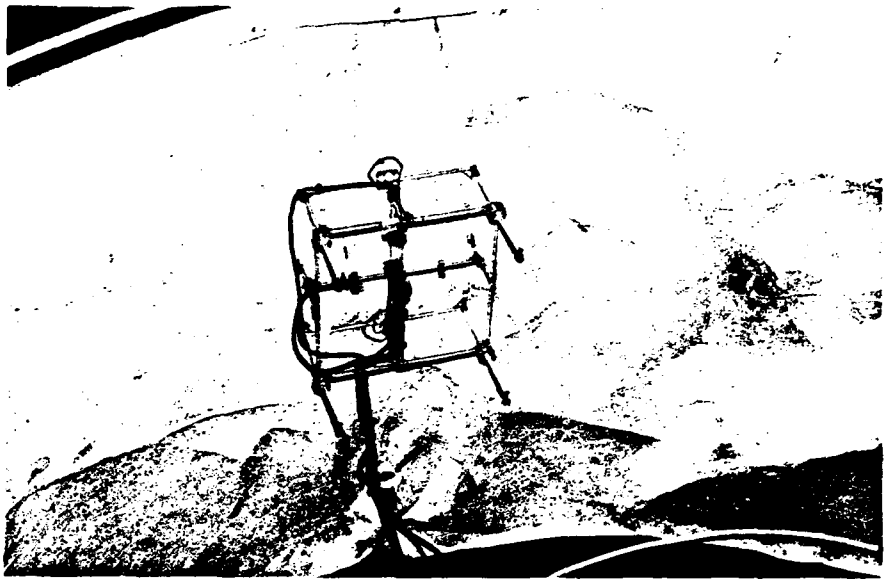

figure 21b The resistivity probe framework

figure 21c The resistivity probe array

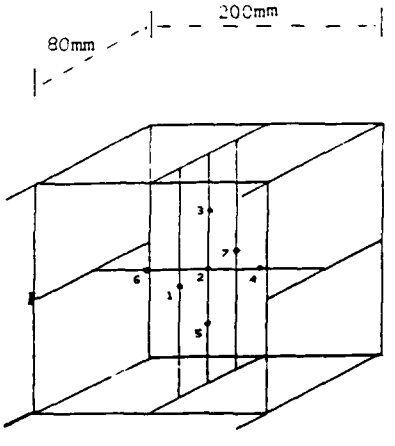

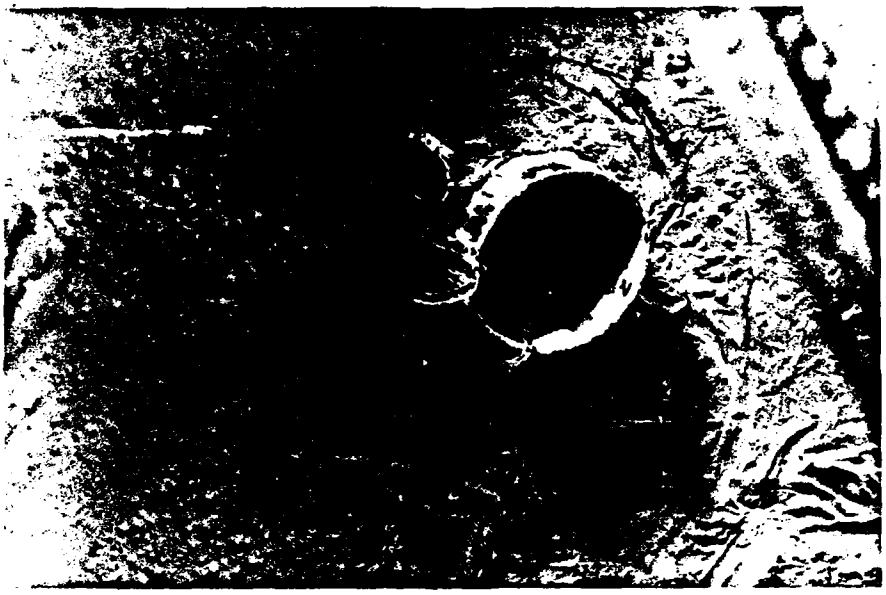

figure 22c Landfill construction

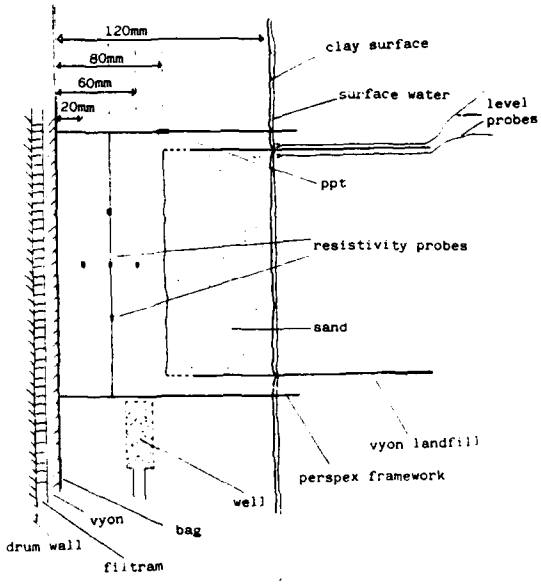

figure 23 A landfill site

figure 24 Surface fissures

figure 25 Deep cutting channel

figure 26 Flow regime in run 3

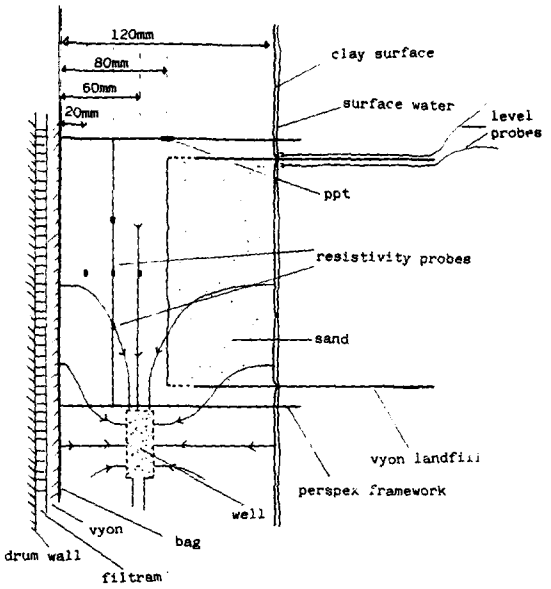

figure 27 Landfill core positions

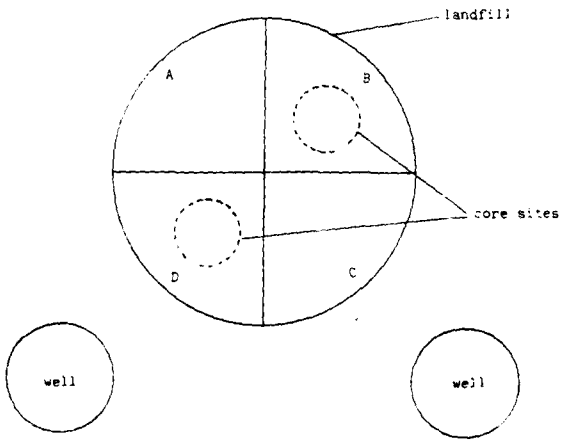

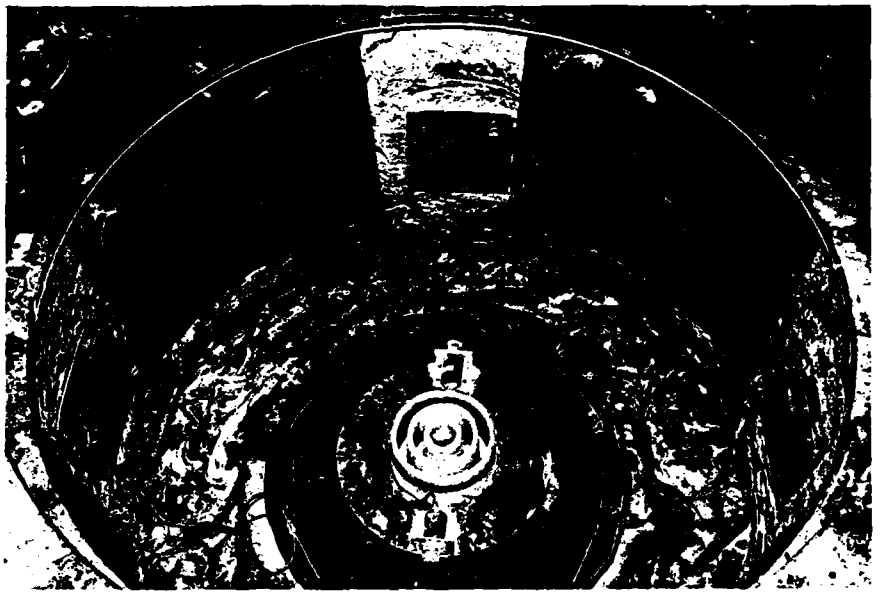

a)

figure 28 Calibration boxes

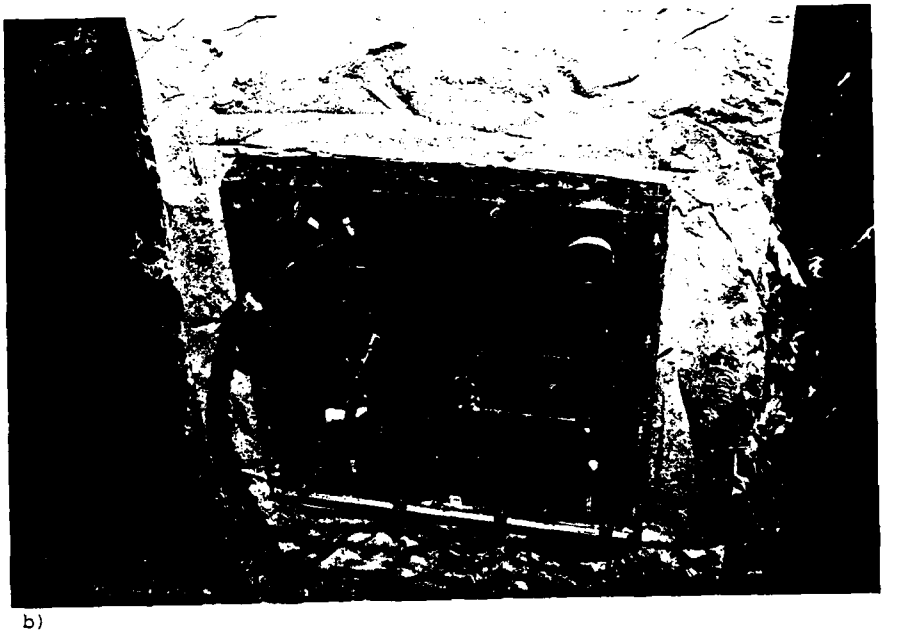

b)

c)

figure 28 Calibration boxes

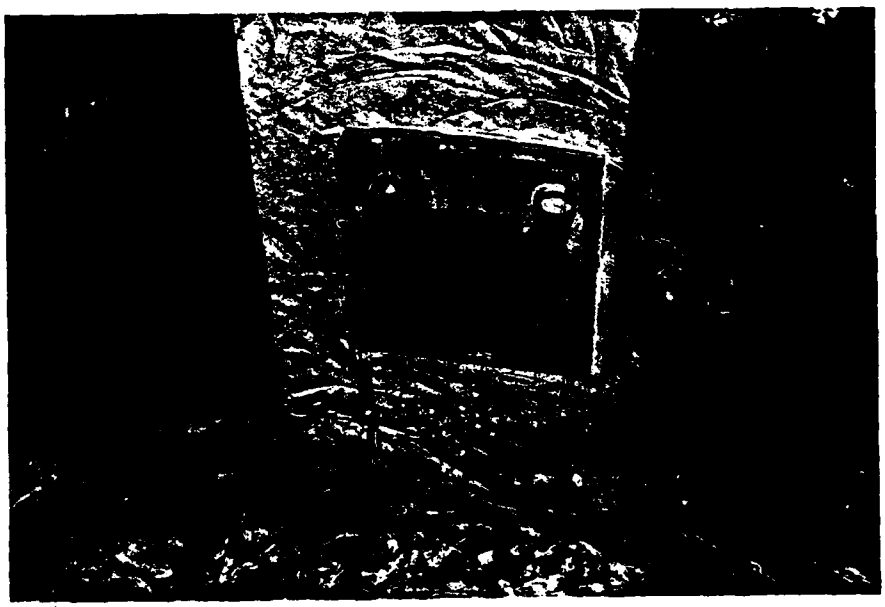

d)

FIGURE 29a

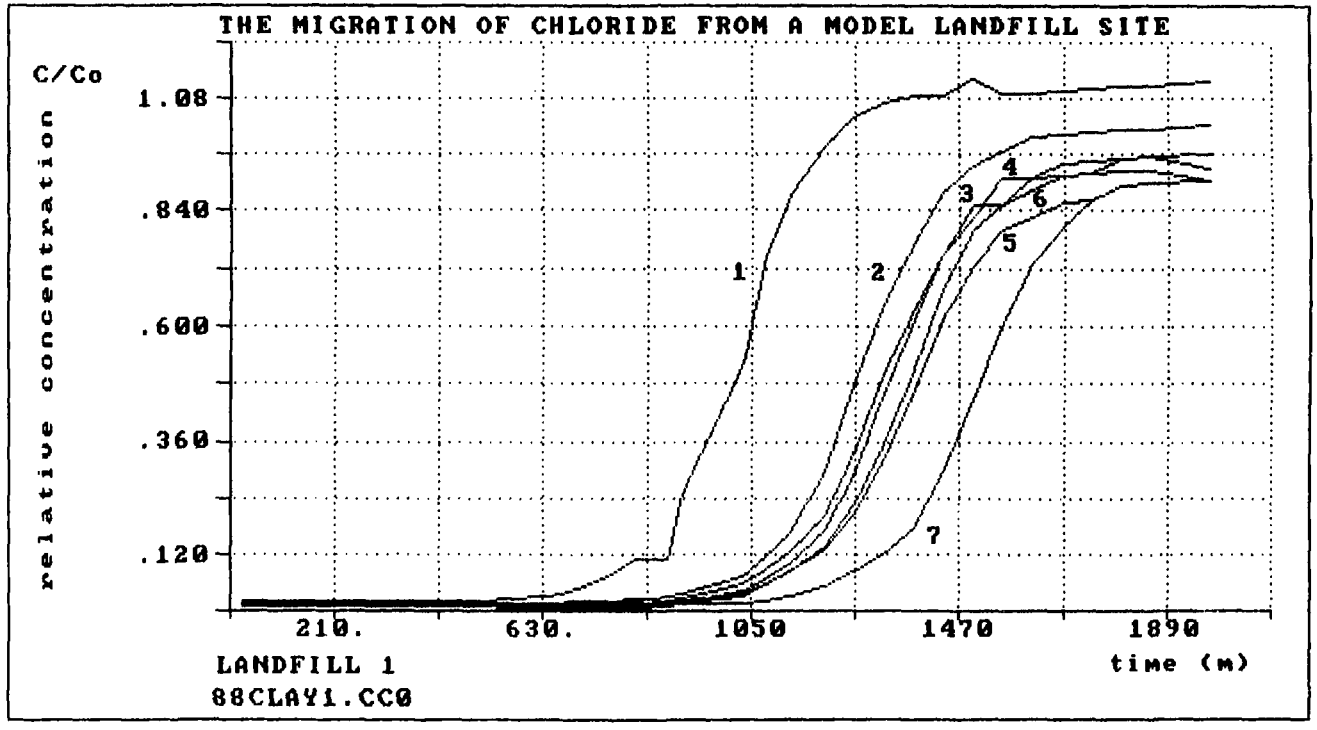
THE MIGRATION OF CHLORIDE FROM A MODEL LANDFILL SITE
C/Co
relative concentration
1.08
.840
.600
.360
.120
1
2
3
4
5
6
7
210.
630.
1050
1470
1890
time (m)
LANDFILL 1
88CLAY1.CC0

FIGURE 29b

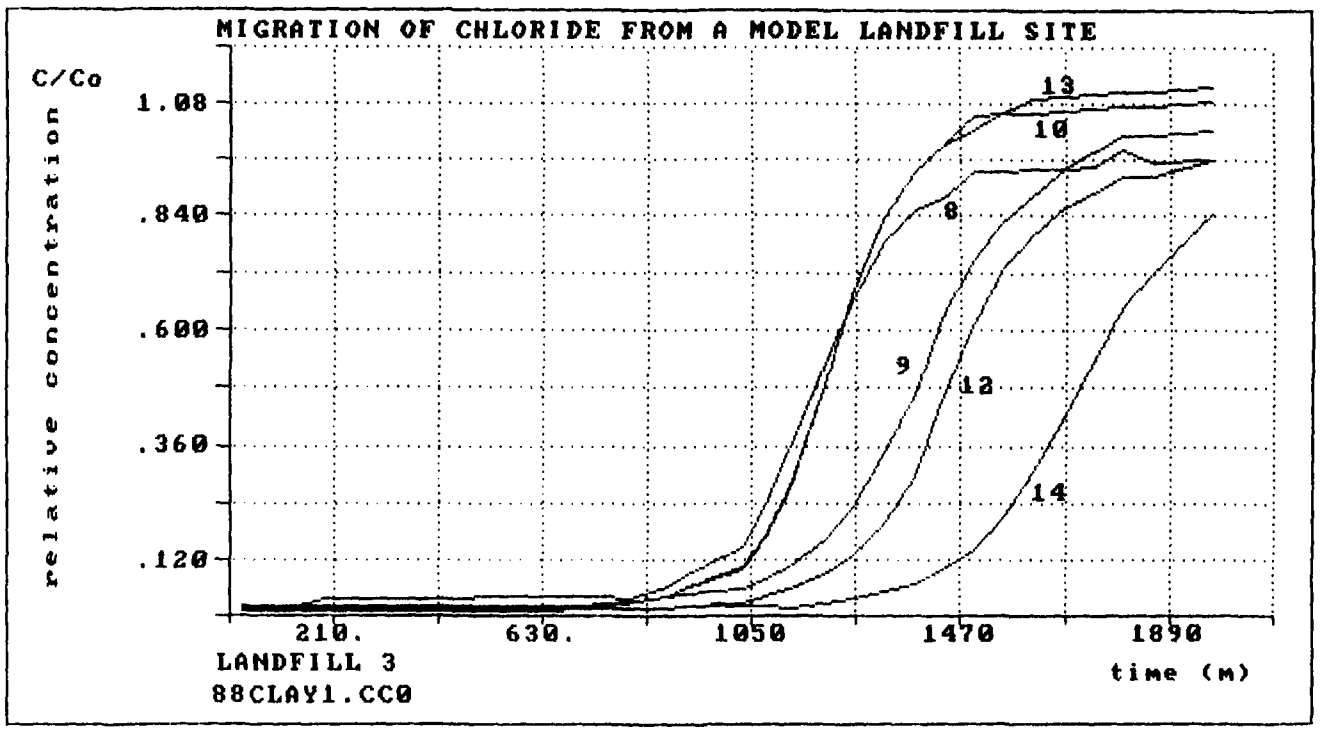
MIGRATION OF CHLORIDE FROM A MODEL LANDFILL SITE
C/Co
relative concentration
1.08
.840
.600
.360
.120
13
10
8
9
12
14
210.
630.
1050
1470
1890
time (m)
LANDFILL 3
88CLAY1.CC0

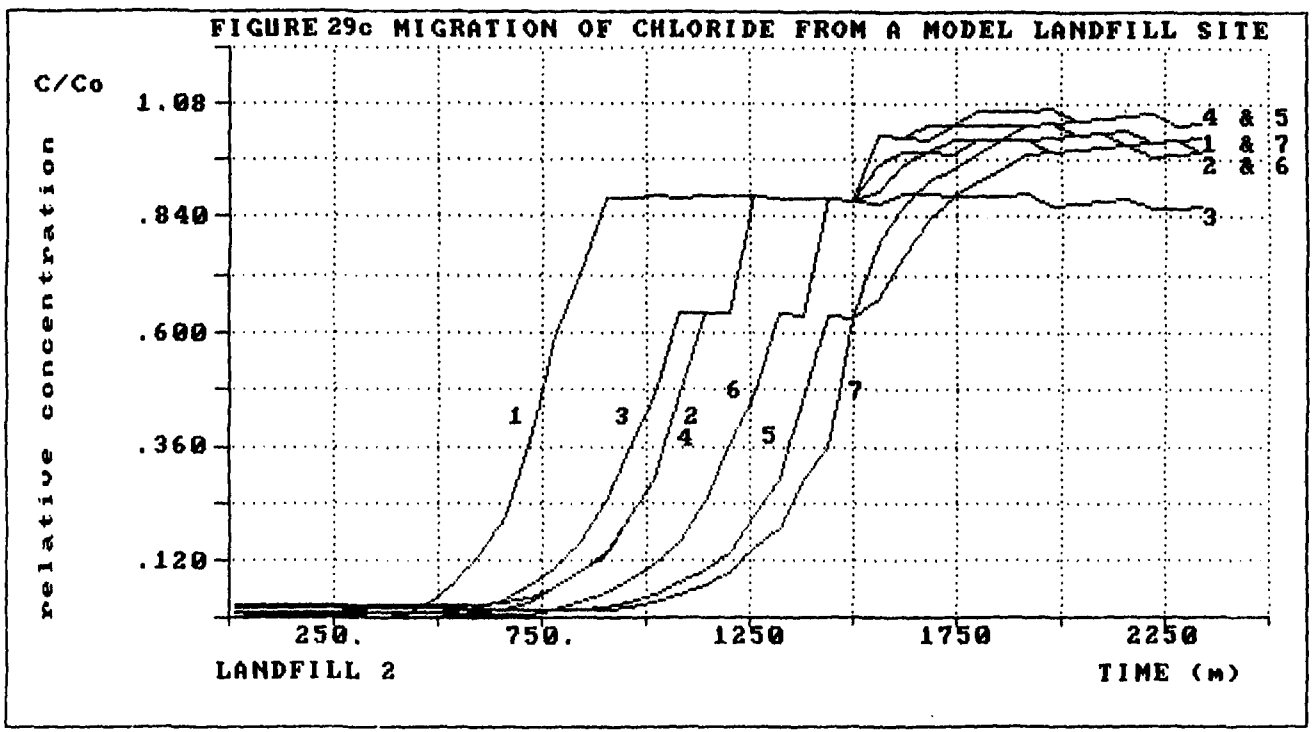
FIGURE 29c MIGRATION OF CHLORIDE FROM A MODEL LANDFILL SITE
C/Co
relative concentration
1.00
.840
.600
.360
.120
250.
750.
1250
1750
2250
LANDFILL 2
TIME (m)
1
3
2
4
6
5
7
4 & 5
1 & 7
2 & 6
3

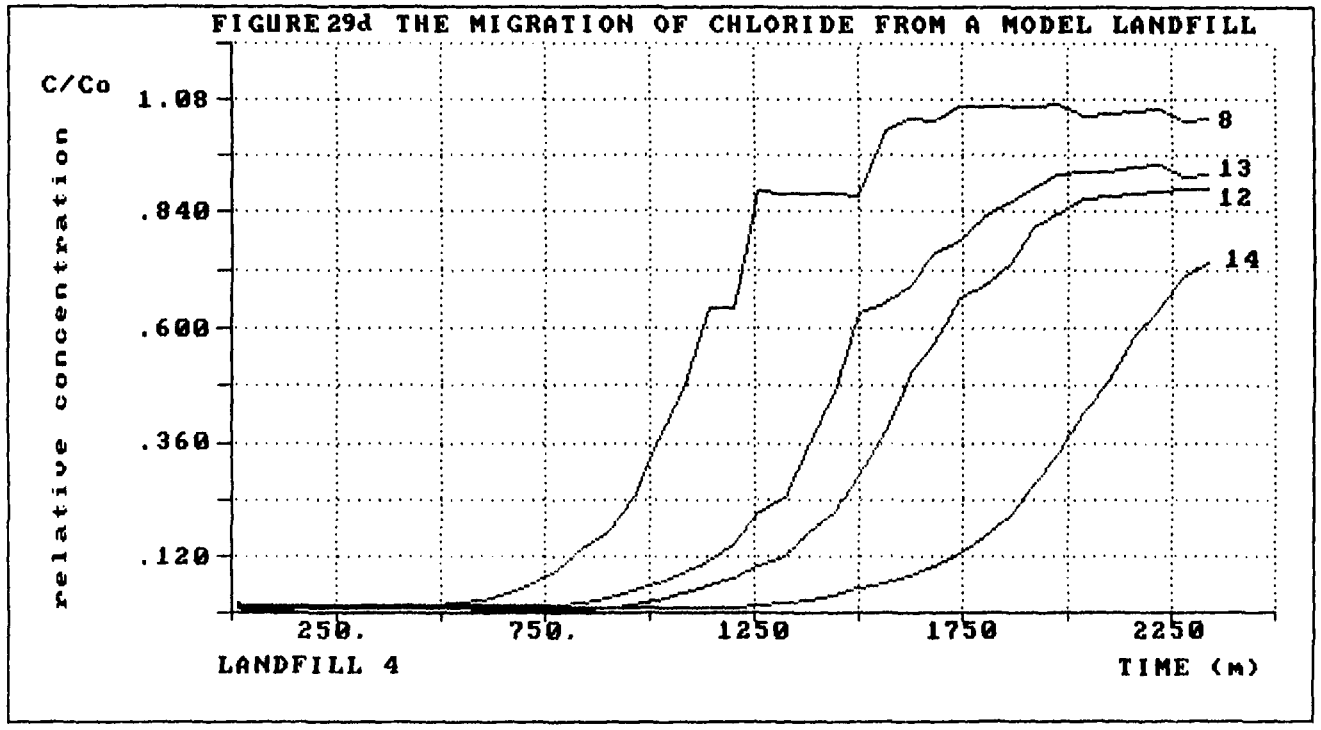
FIGURE 29d THE MIGRATION OF CHLORIDE FROM A MODEL LANDFILL
C/Co
relative concentration
1.08
.840
.600
.360
.120
8
13
12
14
250.
750.
1250
1750
2250
LANDFILL 4
TIME (m)

figure 30 surface flaws

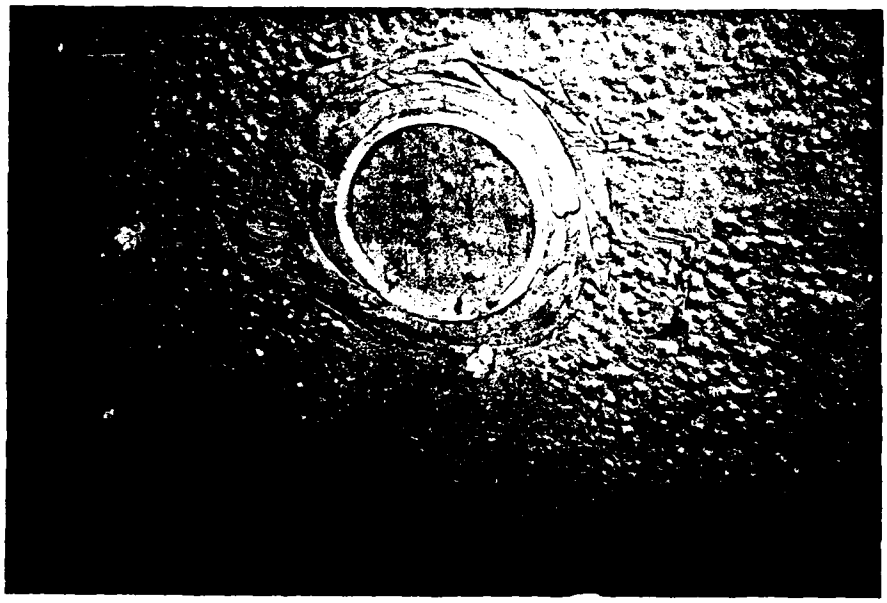

AD-A195 334 DRUM CENTRIFUGE STUDY OF THE TRANSPORT OF LEACHATES FROM LANDFILL SITES(U) CAMBRIDGE UNIV (ENGLAND) DEPT OF ENGINEERING J R CROWDON ET AL. 05 MAY 88 2/2

UNCLASSIFIED CUED/D-SOILS/TR214 DAJA45-86-C-0021 F/G 24/3 NL

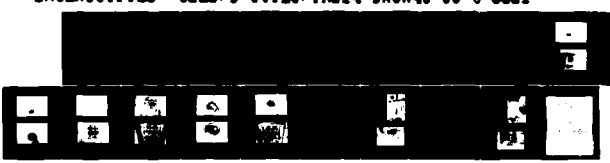

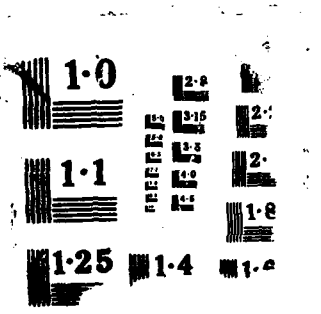
1·0
1·1
1·25
1·4
1·8

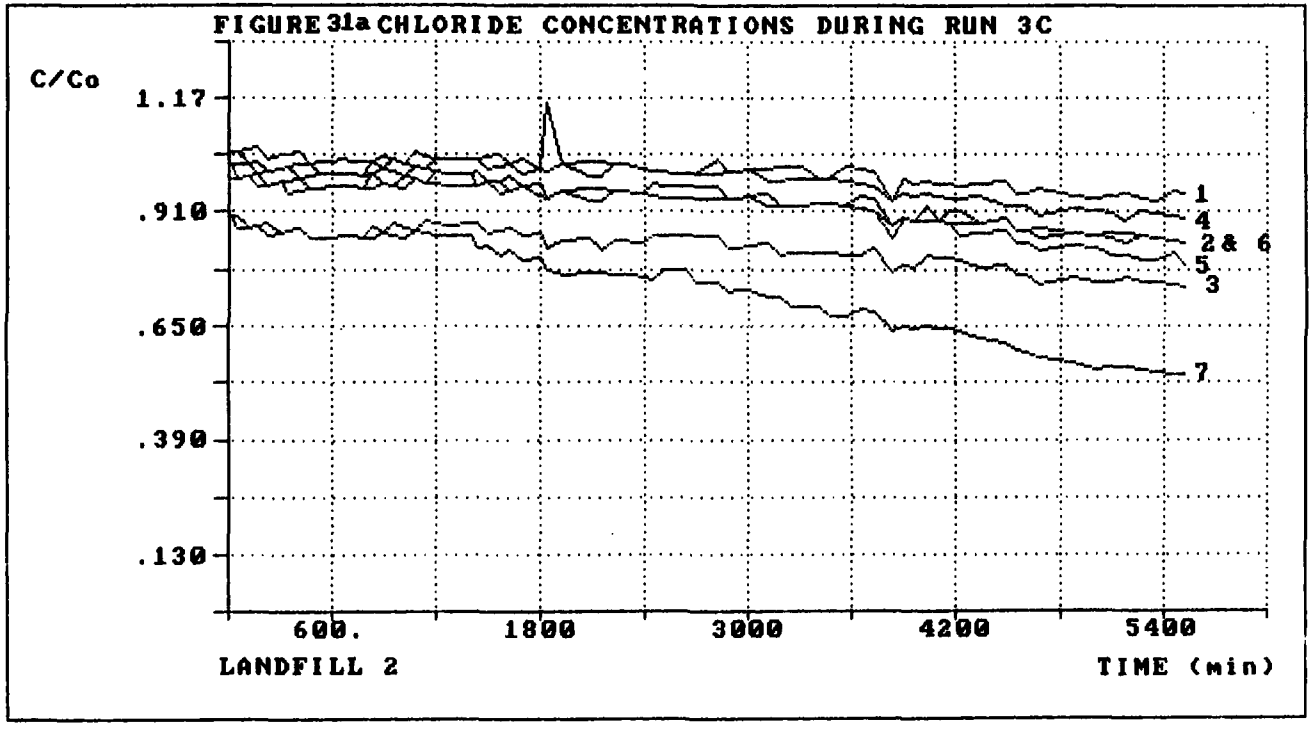
FIGURE 31a CHLORIDE CONCENTRATIONS DURING RUN 3C
C/Co
1.17
.910
.650
.390
.130
600.
1800
3000
4200
5400
LANDFILL 2
TIME (min)
1
4
2 & 6
5
3
7

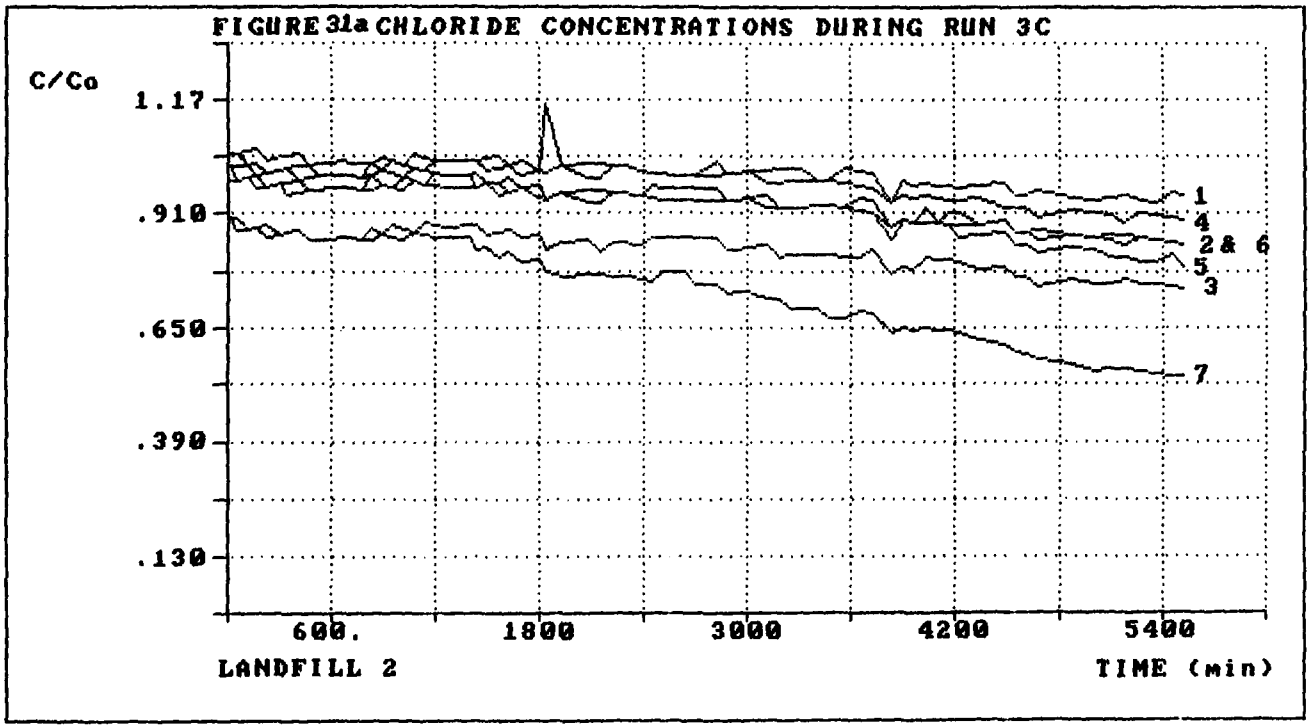
FIGURE 31a CHLORIDE CONCENTRATIONS DURING RUN 3C
C/Co
1.17
.910
.650
.390
.130
600.
1800
3000
4200
5400
LANDFILL 2
TIME (min)
1
4
2& 6
5
3
7

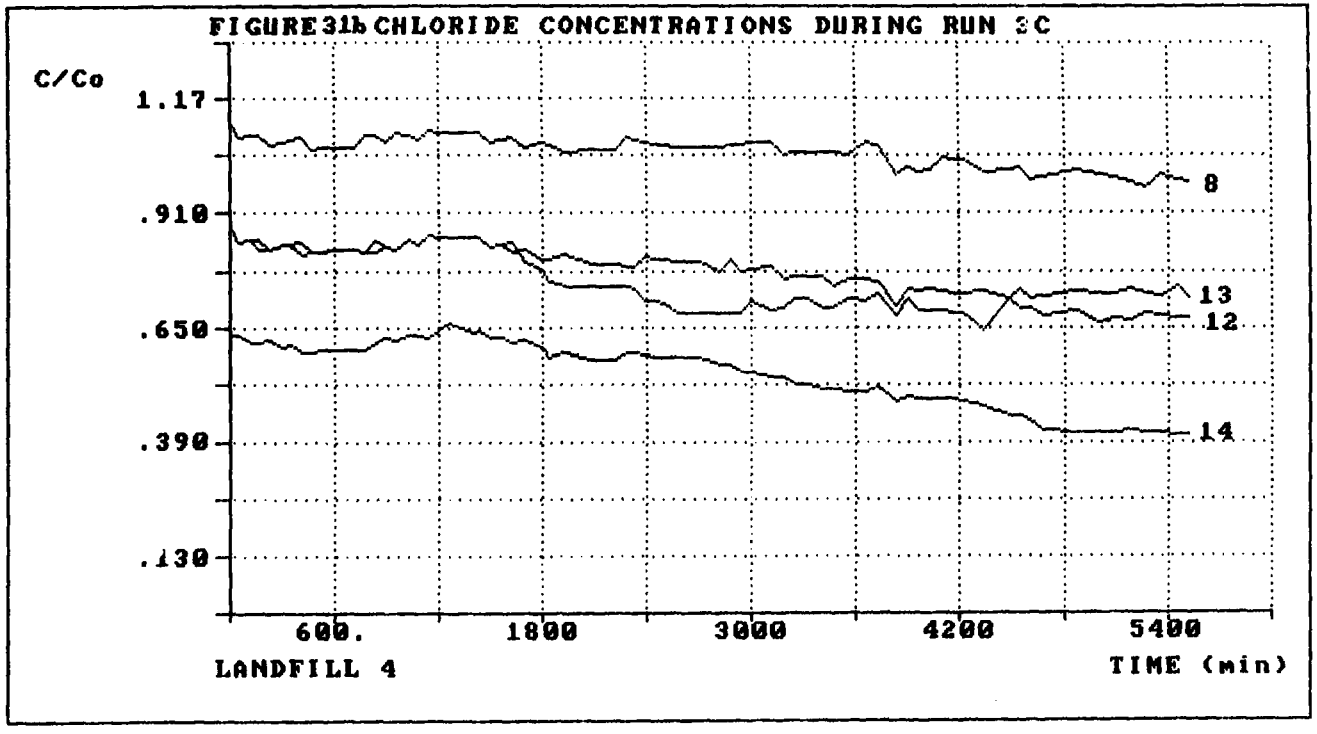
FIGURE 31b CHLORIDE CONCENTRATIONS DURING RUN 3C
C/Co
1.17
.910
.650
.390
.130
8
13
12
14
600.
1800
3000
4200
5400
LANDFILL 4
TIME (min)

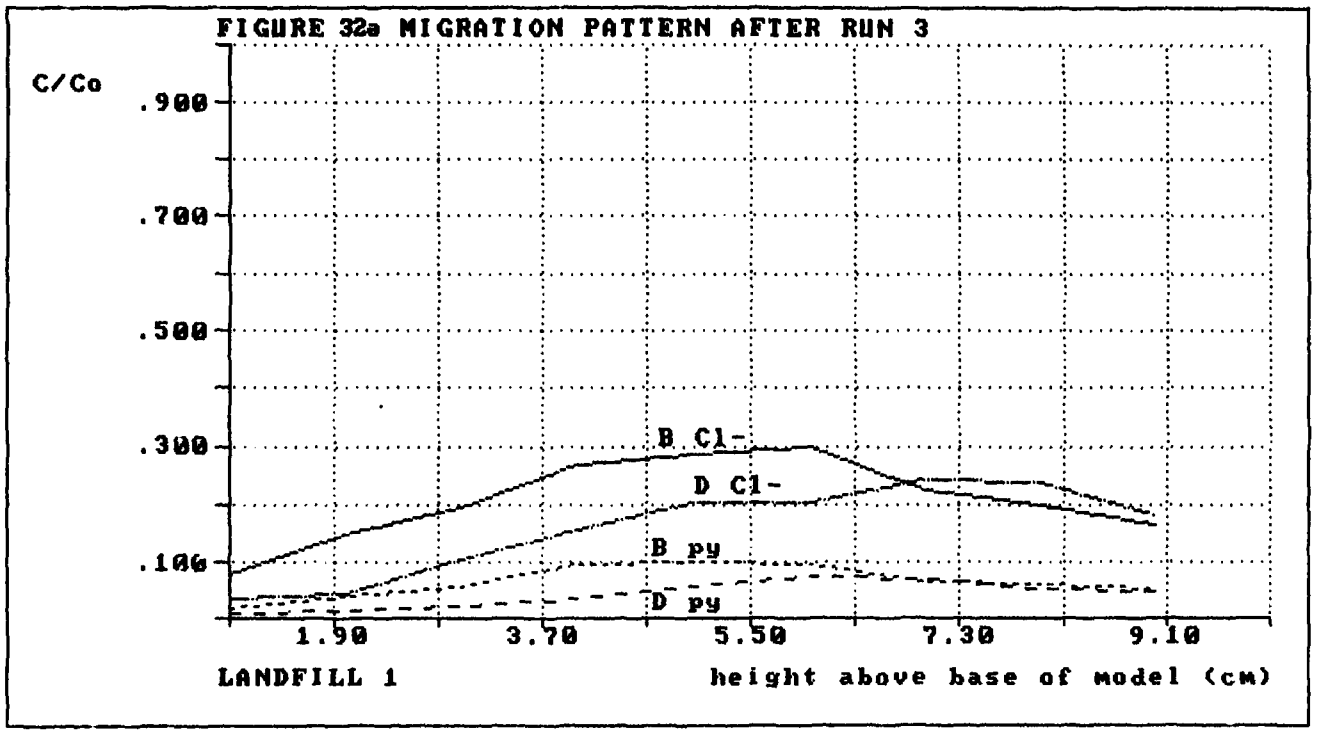
FIGURE 32a MIGRATION PATTERN AFTER RUN 3
C/Co
.900
.700
.500
.300
.100
B Cl-
D Cl-
B py
D py
1.90
3.70
5.50
7.30
9.10
LANDFILL 1
height above base of model (cm)

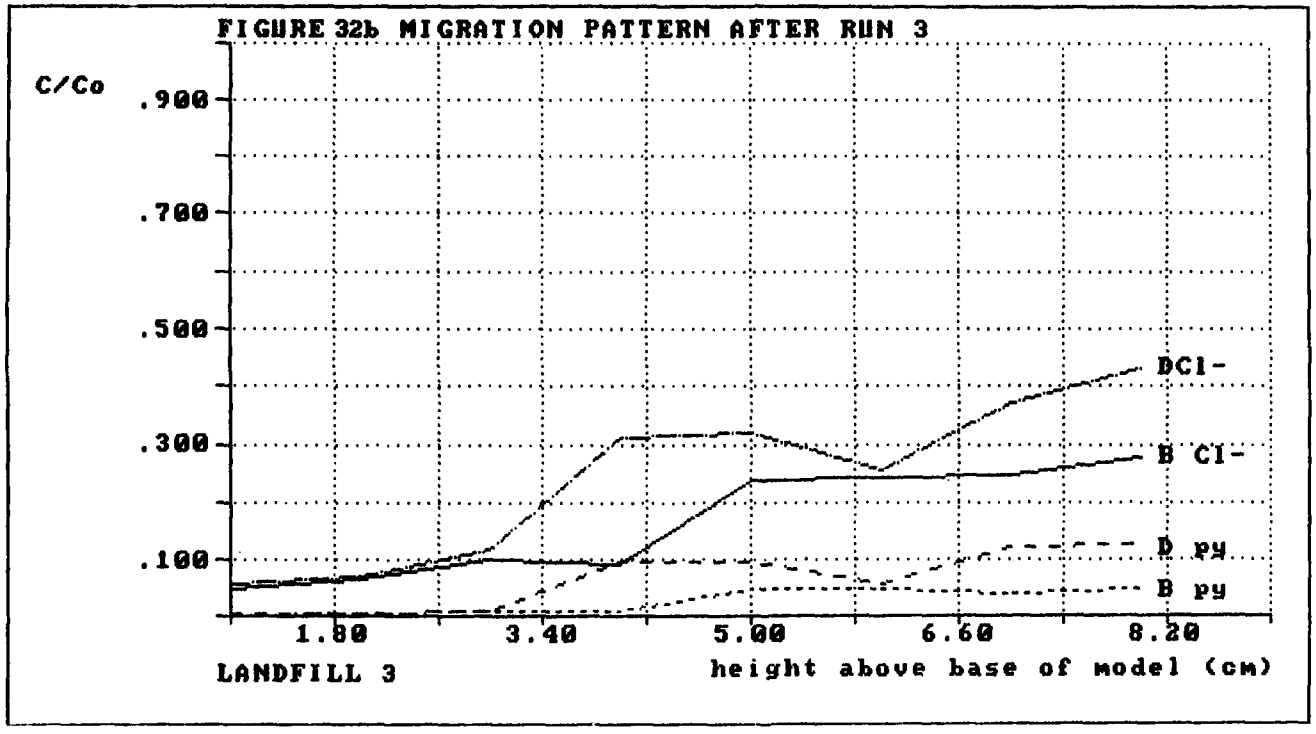
FIGURE 32b MIGRATION PATTERN AFTER RUN 3
C/Co
.900
.700
.500
.300
.100
D Cl-
B Cl-
D py
B py
1.80
3.40
5.00
6.60
8.20
LANDFILL 3
height above base of model (cm)

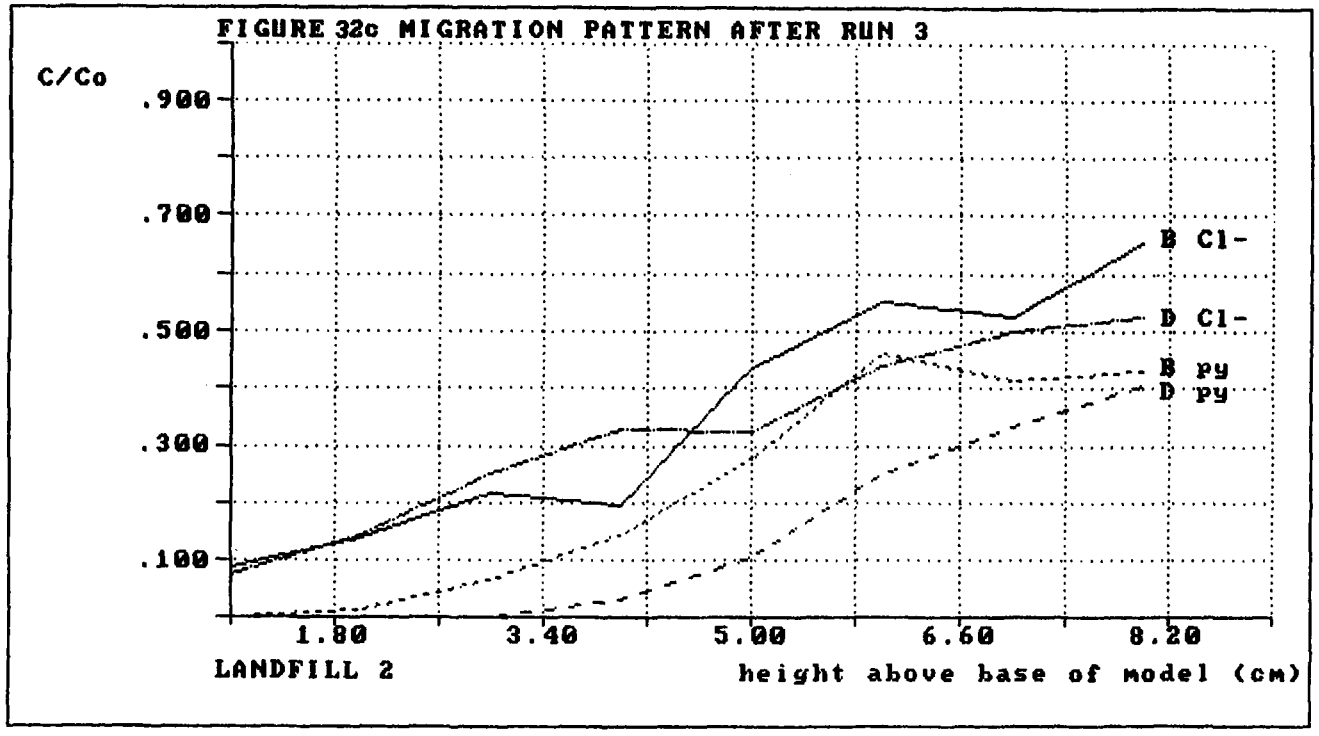
FIGURE 32c MIGRATION PATTERN AFTER RUN 3
C/Co
.900
.700
.500
.300
.100
B Cl-
D Cl-
B py
D py
1.80
3.40
5.00
6.60
8.20
LANDFILL 2
height above base of model (cm)

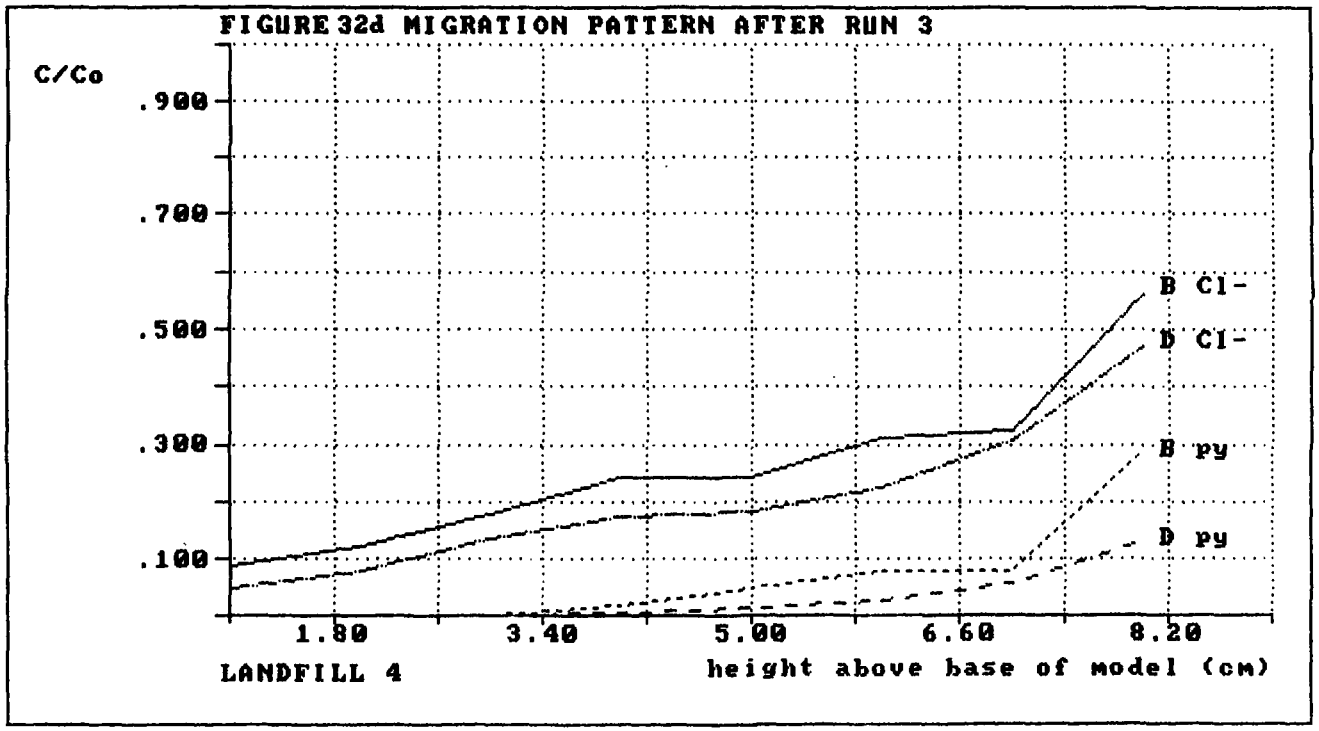
FIGURE 32d MIGRATION PATTERN AFTER RUN 3
C/Co
.900
.700
.500
.300
.100
B Cl-
D Cl-
B py
D py
1.80
3.40
5.00
6.60
8.20
LANDFILL 4
height above base of model (cm)

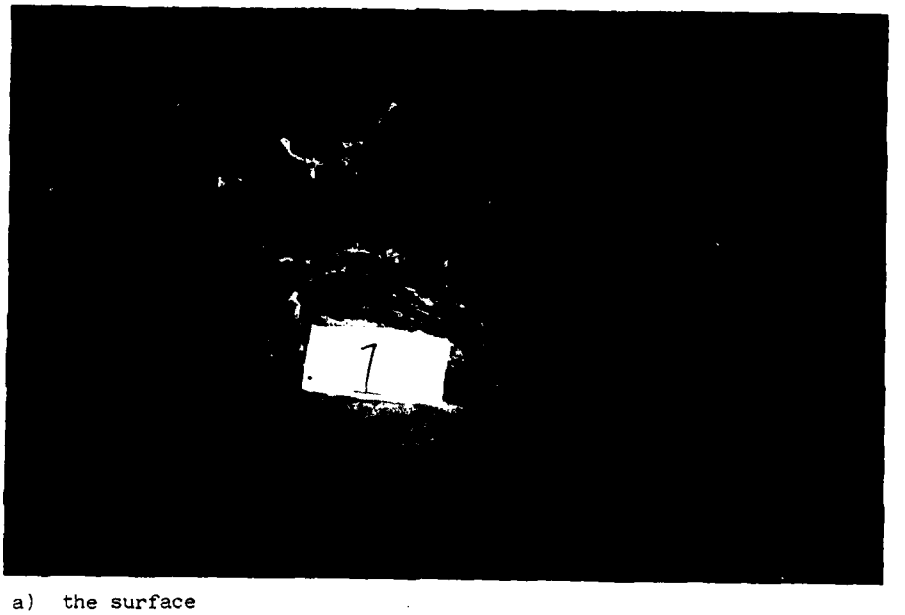

a) the surface

figure 33 Ultra-violet photos of landfill 1

b) 80mm from the base

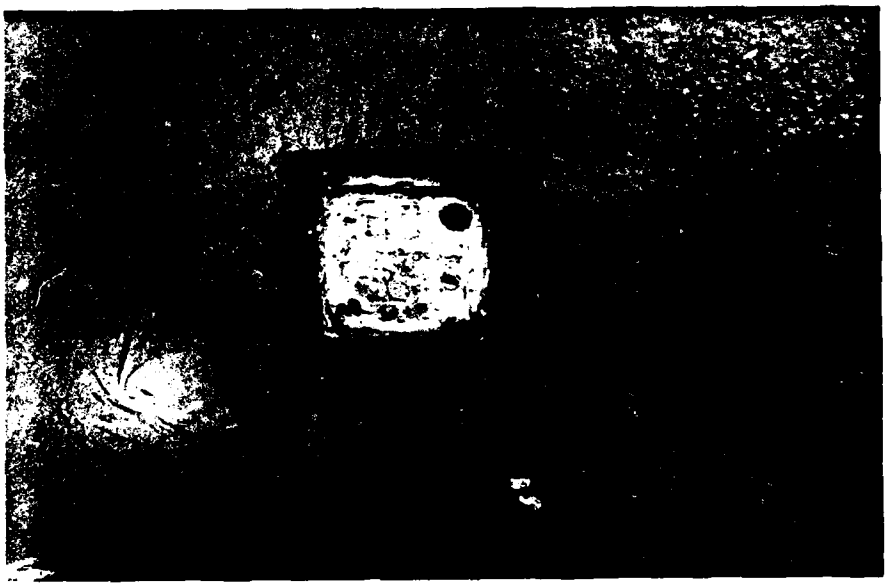

c) 60mm from the base

figure 33 Ultra-violet photos of landfill 1

d) 40mm from the base

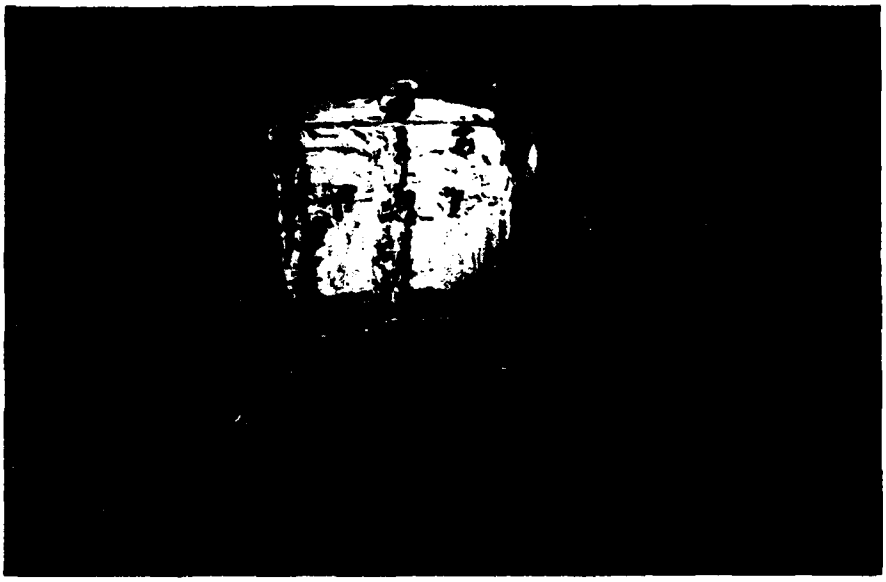

e) 20mm from the base

figure 33 Ultra-violet photos of landfill 1

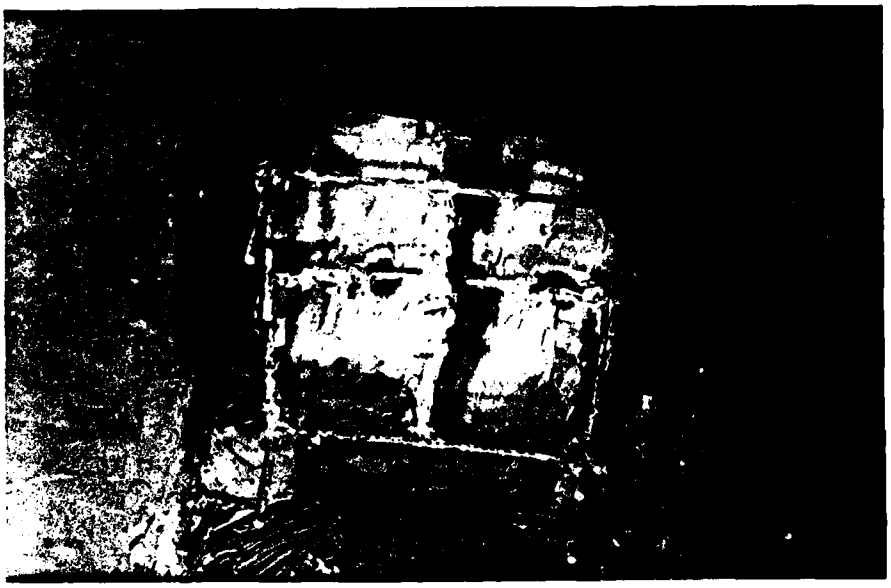

f) at the base

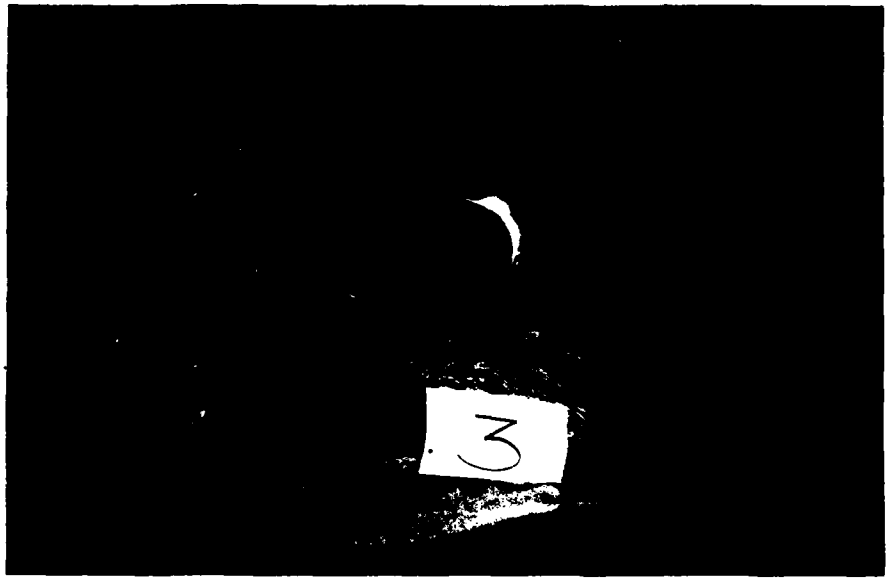

a) the surface

figure 34 Ultra-violet photos of landfill 3

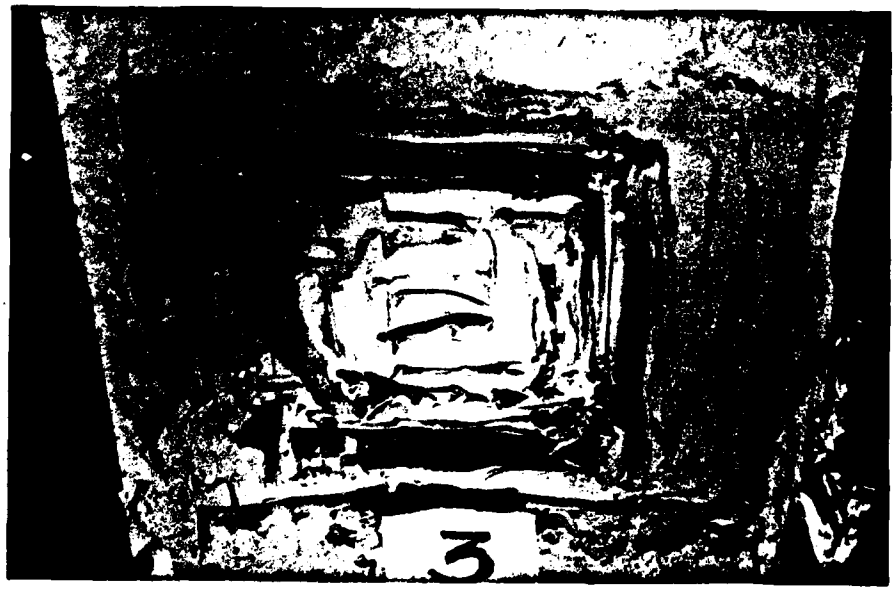

b) 60mm from the base

c) 40mm from the base

figure 34 Ultra-violet photos of landfill 3

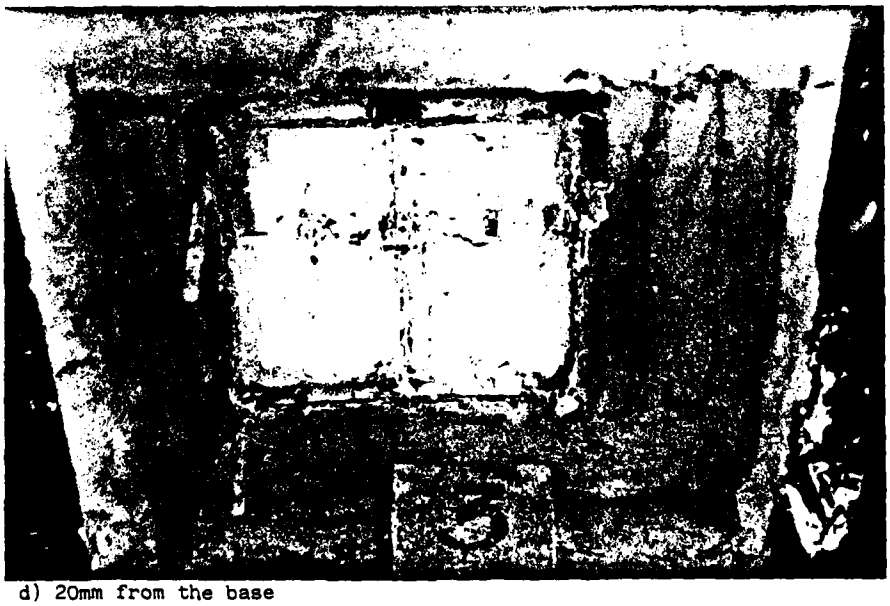

d) 20mm from the base

a) the surface

figure 35 Ultra-violet photos of landfill 2

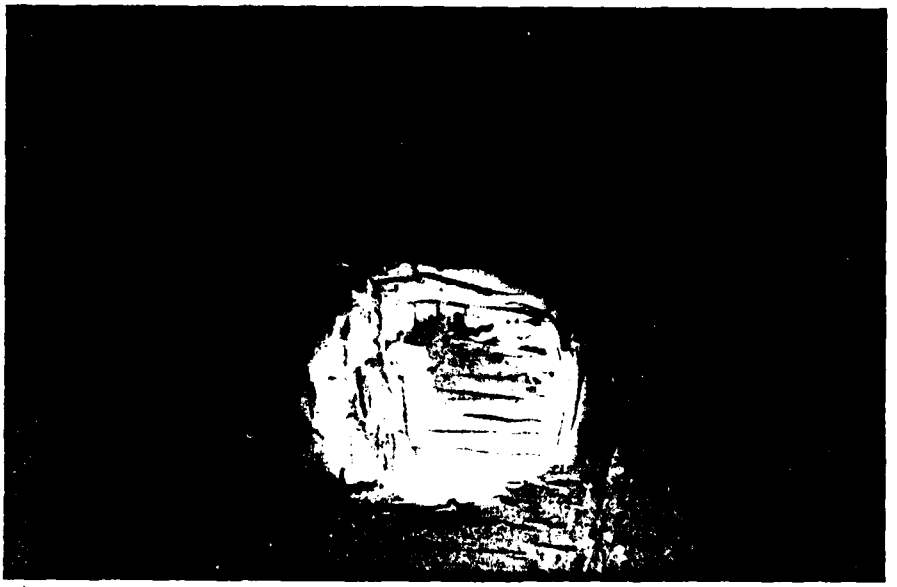

b) 80mm from the base

c) 60mm from the base

figure 35 Ultra-violet photos of landfill 2

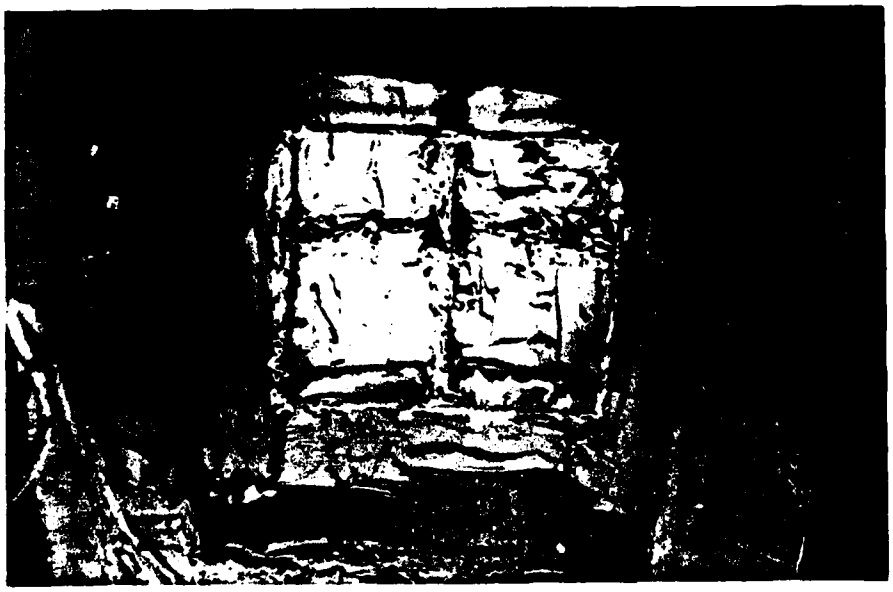

d) 40mm from the base

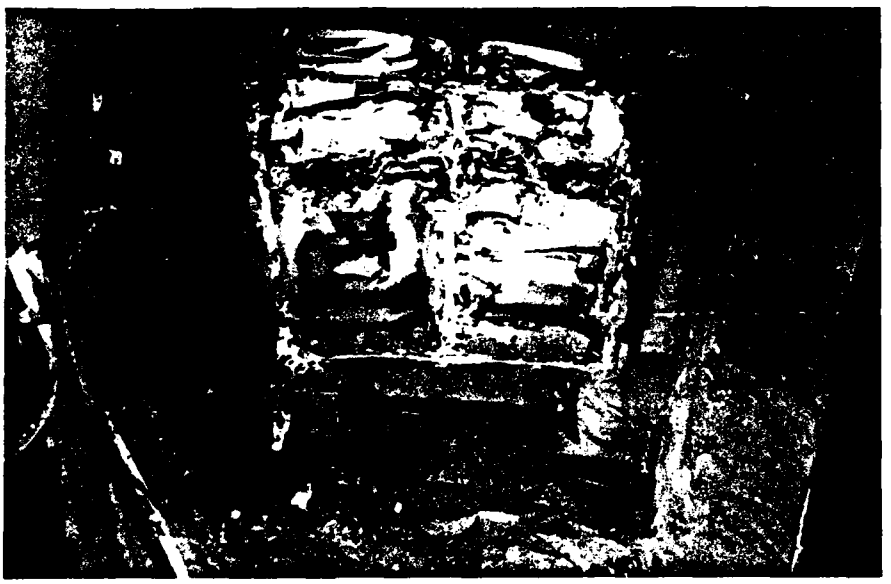

e) 20mm from the base

figure 35 Ultra-violet photos of landfill 2

f) at the base

a) the surface

figure 36 Ultra-violet photos of landfill 4

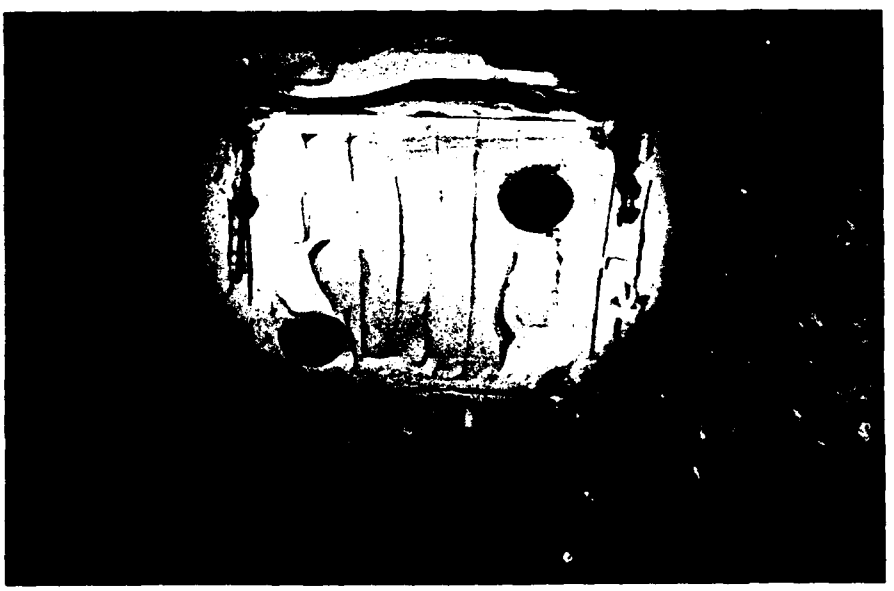

b) 80mm from the base

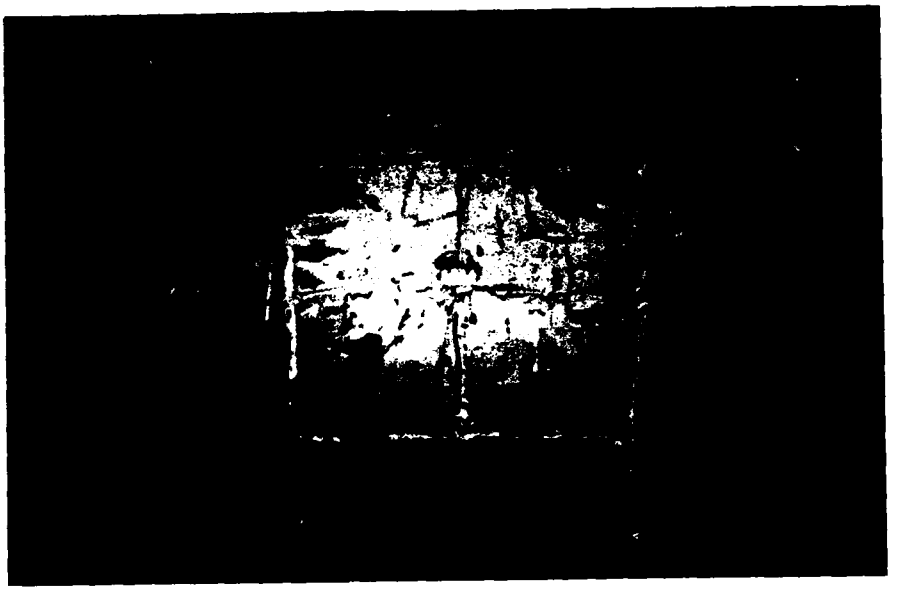

c) 40mm from the base

figure 36 Ultra-violet photos of landfill 4

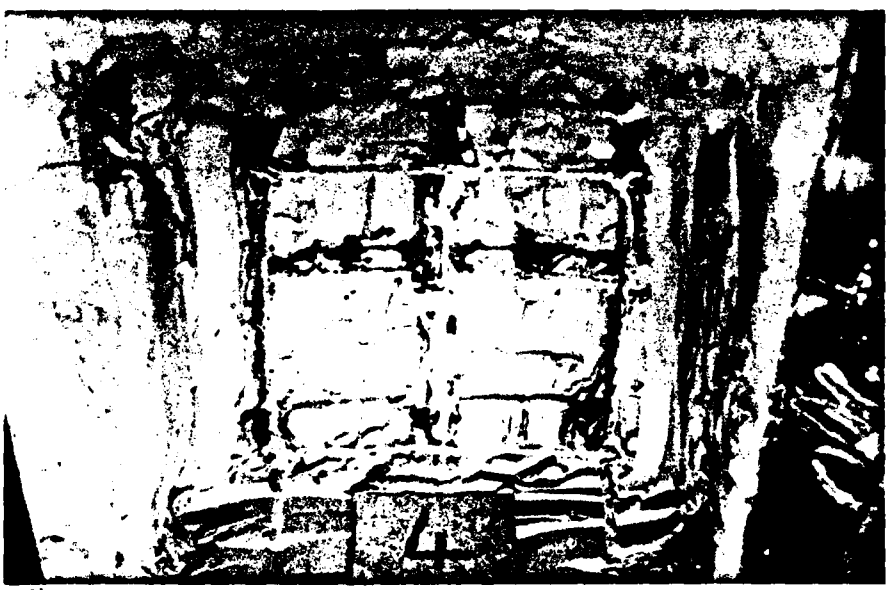

d) at the base

figure A.1 The diffusion cell

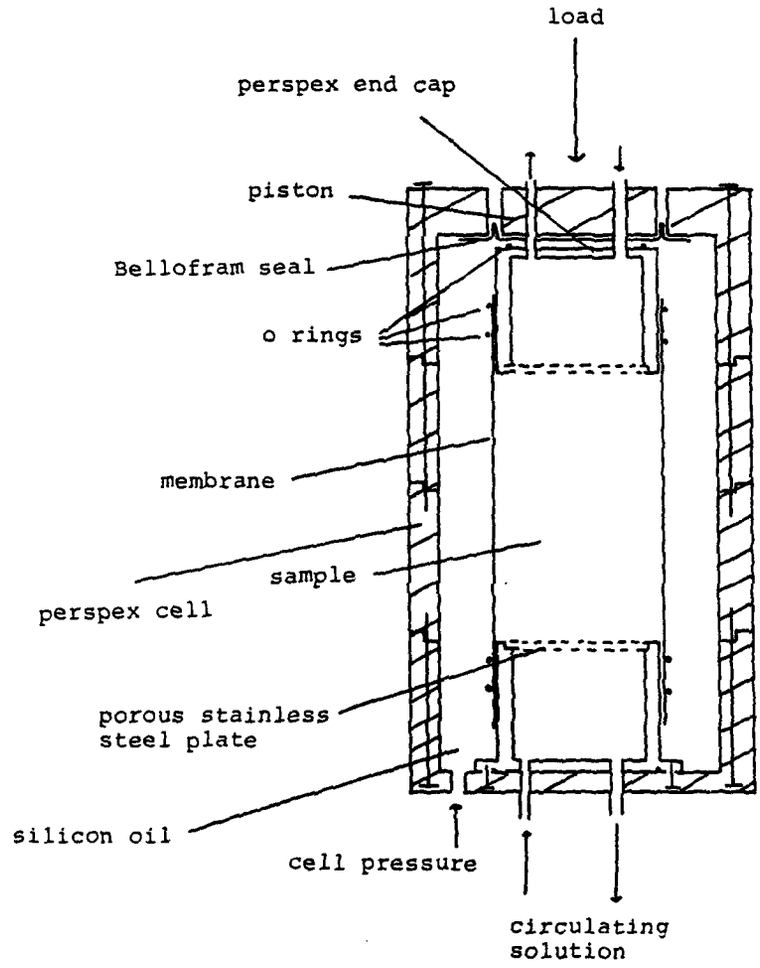

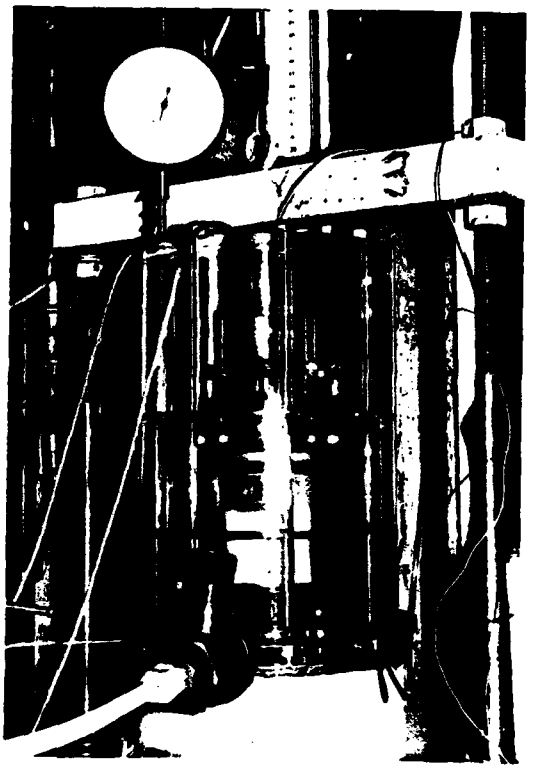

figure A.2
The diffusion cell

figure A.3a The diffusion system

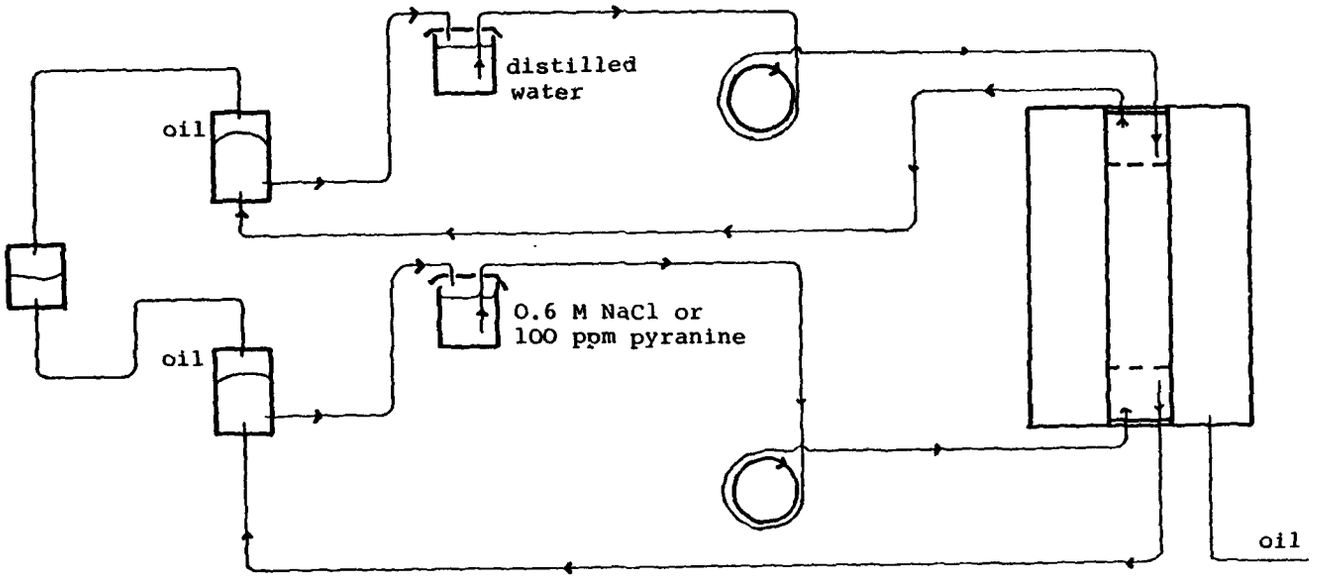

differential pressure transducer | interface | reservoir | pump | diffusion cell

figure A.3b
The differential
transducer
system

figure A.4 The diffusion system

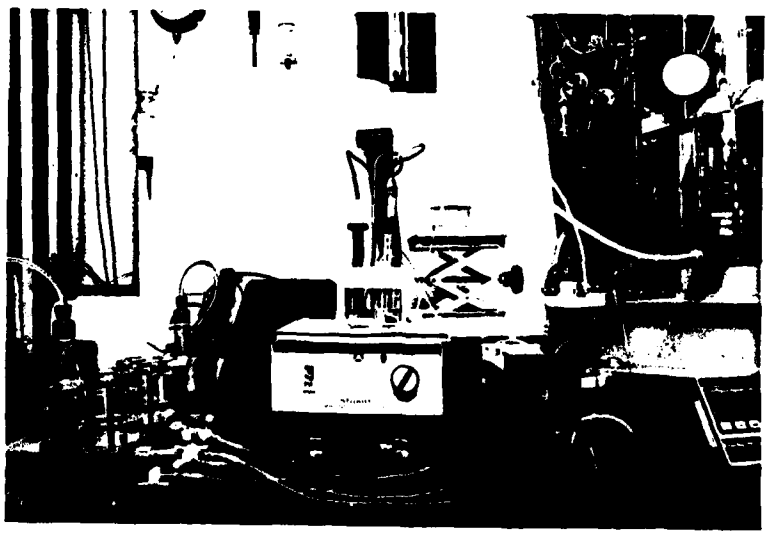

END

DATE
FILMED

9-88